Indoor Radio Channel Propagation Modelling by Ray Tracing Techniques

David I. Laurenson

A thesis submitted for the degree of *Doctor of Philosophy* at The University of Edinburgh

— 1994 —

Declaration of Originality

I hereby declare that this thesis and the work reported herein was composed and originated entirely by myself, in the Department of Electrical Engineering at The University of Edinburgh.

David I. Laurenson

Abstract

In a response to the requirement for a more detailed channel model based on the physical characteristics of the environment within which indoor radio communications operate, this thesis presents a channel model based on ray tracing techniques. The mathematical basis for the model is presented in terms of the electromagnetic properties of simple objects. The resulting model is coded into a simulation system which takes a description of a building in terms of the structure of internal walls, floors and ceilings. Through repeated application of the reflection process, a description of the channel impulse response is created for a given transmitter and receiver position from the multipath components generated.

This model is applied, in progressing degrees of complexity, to two buildings for which narrowband physical measurements are available. Comparison is made between the measured results and the narrowband simulation results which leads to an analysis of the various propagation mechanisms involved in in-building communications. It is found that the model, while not accurately predicting the measured results, does produce a model that, considering the unknown parameters of the environment and experimental procedure, relates well to the channel experienced by a communication system.

Wideband channel characteristics are determined from the simulation model, and found to give access to more detailed information on the channel than is obtainable through physical measurement. The results of the wideband simulations are compared with published material containing measurement results, and the relationship to the narrowband results already presented is shown.

Table of Contents

List of Figures

List of Tables

List of Abbreviations and Acronyms

AR	autoregressive
ARMA	autoregressive moving average
AWGN	additive white Gaussian noise
CW	continuous wave
DAC	digital to analogue converter
EM	electromagnetic
FAF	floor attenuation factor
GTD	geometrical theory of diffraction
IR	infra-red
ISI	inter-symbol interference
kbps	kilobits per second
LMS	least mean square
LOS	line of sight
mbps	megabits per second
MIMD	multiple instruction, multiple data
MoMSE	modified mean square error
NDT	non-destructive testing
OBS	obstructed line of sight
PCN	personal communication network
pdf	probability density function
PN	pseudorandom noise
radio	radiotelegraphy
rms.	root mean square
SAW	surface acoustic wave
SE	square error

SVDP	singular value decomposition prony
TDL	tapped delay line
UHF	ultra high frequency
US	uncorrelated scattering
UTD	unified theory of diffraction
WSS	wide sense stationary

List of Principal Symbols

$*$	The complex conjugation operator
$\lvert\cdot\rvert$	The modulus operator
$A_i, A_i(t)$	Amplitude of a multipath component of a channel impulse response
c	Propagation velocity
D	Diffraction coefficient
$(\Delta f)_c$	Coherence bandwidth
$\delta(\cdot)$	The delta function where $\delta(x) = 1$ iff $x = 0$, otherwise $\delta(x) = 0$
$\underline{E}$	Electric field
$E(\cdot)$	An expectation operator
ϵ	Permittivity
η	Intrinsic impedance
$F(\cdot)$	An infinite series based on the Fresnel integral
f_c	Modulation frequency
f_D	Doppler frequency
$\hat{G}$	Multipath power gain
$\Gamma(\alpha)$	The gamma function
$\gamma(\alpha, \beta), \Gamma(\alpha, \beta)$	The incomplete gamma functions
$H(j\omega)$	Fourier transform of the channel impulse response
$\underline{H}$	Magnetic field
$h(\tau), h(t, \tau)$	The channel impulse response
I, I_0	Current
$I_0(\cdot)$	The modified Bessel function of order zero
j	A solution of $x = \sqrt{-1}$

$L_n(\cdot)$	A Laguerre function
λ	Wavelength
μ	Permeability
n'^2	A parameter defined by the electromagnetic properties of a surface
$n(t)$	A Gaussian distributed noise process
P, P_1	Powers
P_a, P_d, P_t	Phase delays
$P_J(a, d)$	The joint probability function
$\underline{\hat{\phi}}$	A unit vector in spherical coordinates
$\phi_i, \phi_i(t)$	The phase of a multipath component of a channel impulse response
ψ	Grazing angle of incidence
R	A reflection coefficient
$\underline{\hat{r}}$	A unit vector in spherical coordinates
$\mathbb{R}$	The set of real numbers
ρ_s	A scattering coefficient
$\hat{\sigma_\tau}$	rms. delay spread
T_m	Range of nonzero delay power spectrum
τ	A delay
$\underline{\hat{\theta}}$	A unit vector in spherical coordinates
u_e, u_i	Fields
V_m	Mobile velocity
ω_0	Modulation frequency expressed in radians

Acknowledgements

1 I will lift up mine eyes unto the hills, from whence
cometh my help.
2 My help cometh from the LORD, which made heaven
and earth.

Psalm 121:1-2

I would like to thank Steve McLaughlin and Asrar Sheikh for providing me with guidance and supervision over the past three years. I would also like to extend special thanks and deep gratitude to my parents and John, my brother, who have encouraged me and always believed that I could stay the course.

So many others should be thanked for their encouragement and support. There are too many to name them all, but I would mention the support of Dave, Anne, Simon, Chris, Norm, Aun, Nichole, Pete, Elias, Daniel, Tracey, Steve M., Sandra D., Sandra M., David, Gary, Ed, John, Steve R. and Andrew.

Special thanks go to Peter and Bernie who took the time to review the thesis and give constructive advice.

Thanks are also due to the Royal Academy of Engineering without whose fellowship, under the Athlone-Vanier Fellowships plan, the most useful year spent in Canada would not have happened, the Science and Engineering Research Council for funding the three years of study, and the Edinburgh Parallel Computing Centre for the use of a parallel machine.

Chapter 1

Introduction

An explosion in growth of the communications industry has prompted the utilisation of radio based systems for in-building communications. As the number of communicating devices, and the amount of information being transferred, are potentially very high, detailed investigation of the mechanism by which the transmitted signals are modified by the environment needs to be conducted. Such investigation facilitates the development of more efficient communication strategies, as well as design parameters for the layout of buildings that better support radio communication systems. This thesis addresses the investigation through the development of a model of the environment based on a ray tracing technique. The ray tracing technique used models the channel in terms of the physical structure of the environment. This leads to a detailed description of the propagation mechanisms involved in in-building communications.

1.1 Communication Systems

Since the development of equations to describe the electromagnetic medium by James Clerk Maxwell, and the subsequent invention of radio communications, the electromagnetic spectrum has been widely used for many diverse applications. Much work has been carried out in analysing how communication between two entities takes place, and how the information being received can be characterised. The aim of such studies is to maximise the rate at which information can be transferred between the two communicating entities, and

to minimise the error with which the data is received. Any communication system can be viewed as a link between a source and a destination where information is sent from the source and received at the destination. The intervening stages are shown in Figure 1–1. The transmitter takes the information from the source and codes it in a form suitable for transfer over the channel such that the cost of transmission is minimal. In this context, cost is a function of the bandwidth used, the time taken to perform the communication, the degree to which the transmission interferes with other transmissions occurring simultaneously and the amount of information that is lost in the communication process. The channel is a description of how the communications medium alters the signal that is being transmitted. Finally the receiver takes the signals that have been altered by the channel, and attempts to recover the information that was sent by the source. The estimate of this information is passed to the destination as the received information.

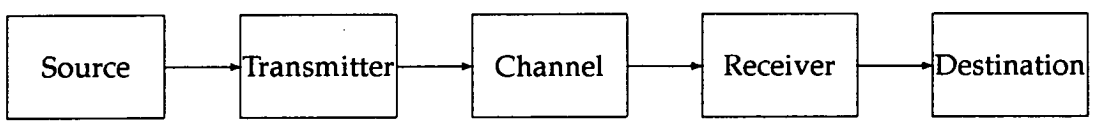

Figure 1–1: Basic communication system

For a radio communication system, the channel describes how the electromagnetic propagation of a transmitted signal induces a signal at the receiver. It is possible to express the channel in terms of an impulse response, that is the signal that would be received were an impulse to be transmitted. Where communication takes place in an environment that has a number of distinct propagation paths from the transmitter to the receiver, the channel impulse response can be described by a summation of weighted phasors,

$$h(\tau) = \sum_{i=0}^{\infty} A_i e^{j\phi_i} \delta(\tau - \tau_i) \tag{1.1}$$

where A_i is the magnitude of the impulse response at delay τ_i with associated phase angle ϕ_i and j satisfies $j^2 = -1$. The received signal, $x(t)$ can be described

in terms of the transmitted signal, $y(t)$ and the channel impulse response as

$$x(t) = y(t) * h(\tau) + n(t) = \sum_{i=0}^{\infty} \left(A_i y(t - \tau_i) e^{j\phi_i} \right) + n(t) \tag{1.2}$$

where $*$ represents the convolution operation and $n(t)$ is a noise function, often assumed to be a zero mean Gaussian process.

In a mobile communication system, the channel changes according to the movement of the communicating entities and other objects that have an effect on the electromagnetic fields at the receiver. This results in a time varying channel impulse response, thus $h(\tau)$ is a function of time and delay and can be represented as

$$h(t, \tau) = \sum_{i=0}^{\infty} A_i(t) e^{j\phi_i(t)} \delta(\tau - \tau_i) \, . \tag{1.3}$$

$A_i(t)$ and $\phi_i(t)$ are dependent on the distance from the transmitter to the receiver via the associated propagation path, and are described statistically in many channel models. As the wavelength of radio communications is small compared to typical path lengths, a small change in the path length is reflected in a large change in $\phi_i(t)$. Thus $\phi_i(t)$ may be modelled as a uniformly distributed random variable. $A_i(t)$ is often assumed to be a Rayleigh distributed variable in a communications link where there is no direct line of sight between the transmitter and receiver; often termed an obstructed line of sight (OBS) path [1]. Figure 1–2 shows a set of Rayleigh distributed probability density functions with various values of σ which controls the variance of the distribution. In the case of a line of sight (LOS) path, A_i is assumed to be a Ricean distributed random variable [1,2]. Appendix C gives expressions for the Ricean distribution, and Figure 1–3 shows the probability density function for various values of s which describes the amplitude of the LOS component.

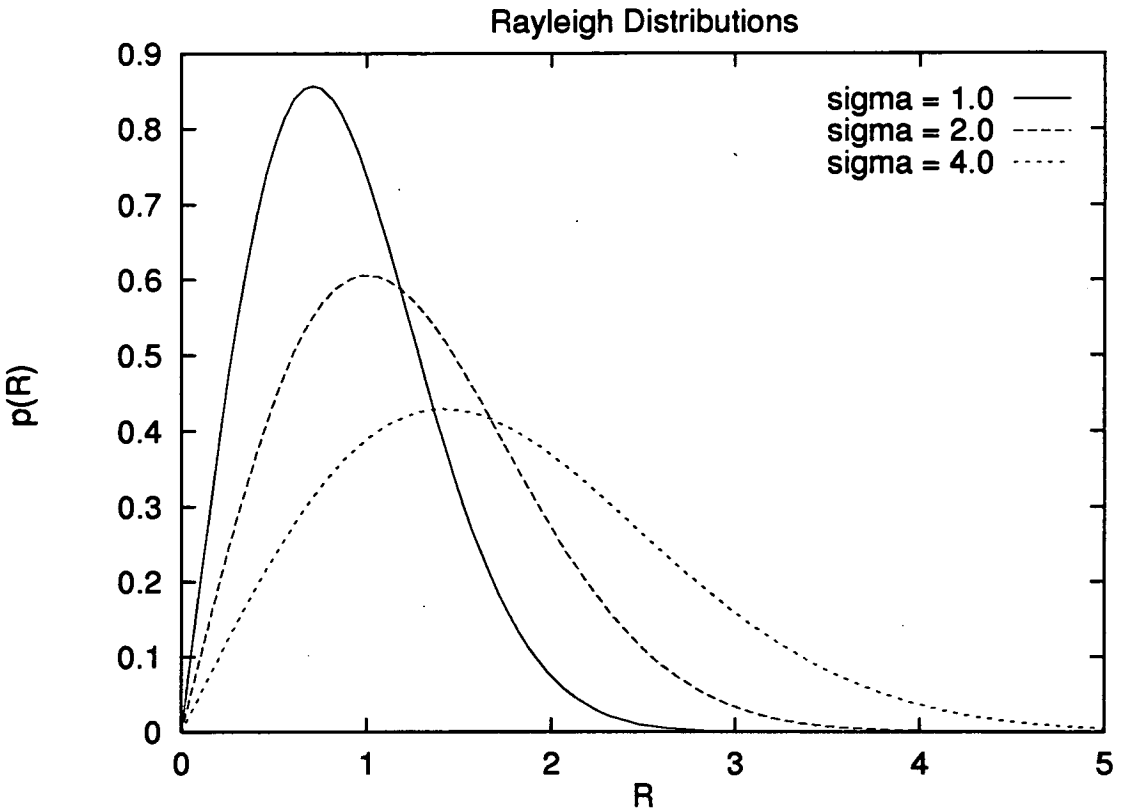

Figure 1–2: Rayleigh distribution probability density functions

1.2 In-building Communications

An explosion in the number of radio communication devices has been experienced in recent years with $\frac{3}{4}$ million UK customers accessing the telephone network via cellular radio in 1990 [3] growing to $1\frac{3}{4}$ million UK customers at the present time [4], and a drive towards a globally accessible network for contacting people regardless of location. This, plus the desire to extend cellular telephony to the mass market via the DCS 1800 standard, a wideband communication standard operating at 1.8GHz, will put further demand on the scarce electromagnetic spectral resource. Such a network, by its very nature, must be a hybrid system of all the communication techniques, one of them involving radio communications within office buildings. Due to the high number of communicating devices that personal communicators would introduce

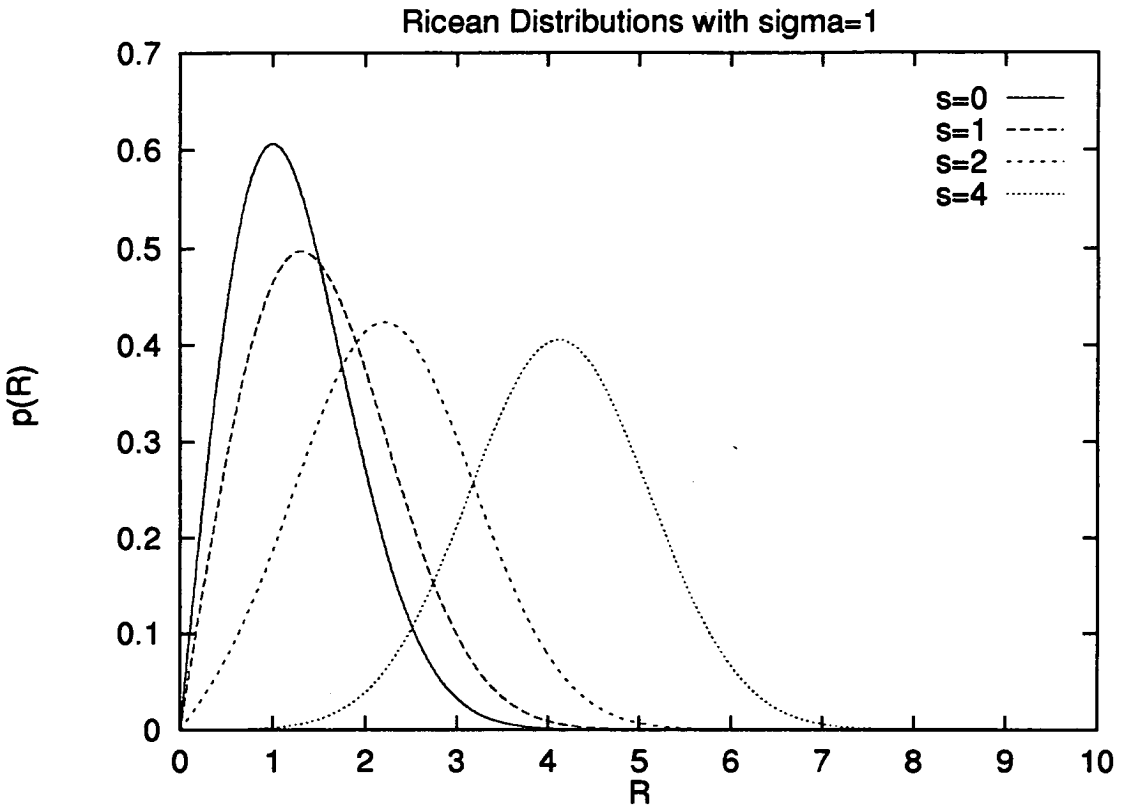

Figure 1–3: Ricean distribution probability density functions

into the average office, some method of supporting the high bandwidth of communications that would be generated must be developed.

The outdoor environment has for many years been supporting mobile communications for private and public users, and has seen a great deal of work in characterising the environment in order to utilise the potential bandwidth to its maximum capability [5–15]. In the outdoor environment one of the communicating entities is usually located at a fixed position above building height, so the majority of scatterers are in close proximity to the mobile. The indoor scenario, by contrast, has both of the communicating entities in close proximity to scattering and diffracting objects. The indoor environment is characterised by a large number of propagation paths from the transmitter to receiver, and is hence classed as a multipath environment.

The average office already contains a large number of communicating de-

vices, ranging from computer terminals connected to computers at some other location and shared peripherals like printers, to telephones, paging systems and cellular telephones. These devices, except for the last two examples, are typically connected together by a wire based interconnection system, with data rates ranging from ten kilobits per second (kbps) to tens of megabits per second (mbps) [16]. The cost of wiring a building to support the wide variety of interconnection technologies supplied by different vendors can rapidly become prohibitive, particularly in the situation where the communicating devices are to be relocated at some point in the future, requiring costly re-wiring.

Unfortunately the radio spectrum is already supporting a large number of incompatible systems, each requiring a unique allocation of the radio spectrum. As Obuchowski [17] points out, there is a requirement for system designers to make efficient use of the remaining available bandwidth. Thus, to achieve the aim of an indoor radio communication system, the details of how the channel affects a transmitted signal need to be known, allowing system designers to take advantage of the channel characteristics to maximise usage of the available bandwidth. Evaluation of coding, and reception schemes designed for the indoor communications environment can then be performed, showing the performance of various methods. By examining these issues, a set of requirements for an office communication system can be evolved.

1.2.1 The requirement

A radio based communication system for an indoor network requires to deal with the problems that are caused by a large number of communicating devices operating at the same, and at similar operating frequencies. Where two devices are transmitting on the same frequency, the receiver experiences co-channel interference if both of the transmitters are within a certain range of the receiver. The interference caused here can be controlled by restricting the separation of the two transmitters to be greater than some defined reuse distance or using some means of dividing the transmission time between the two transmitters so that only one is operational at any one time. In the case of

two transmitters operating within adjacent frequency bands, adjacent channel interference may occur. This can be minimised by judicious design of the modulation scheme.

One possible connection scheme involves dividing up a building into a number of local radio communication sites, or cells. Typically each cell is assigned a set of frequencies that differ from all adjacent cells. These frequencies may be reused in another cell that is separated from the first by at least the reuse distance. These cells could be connected either by a point to point radio link, or by high capacity wire based connections. As the number of cell sites is significantly smaller than the number of communicating devices, the additional cost of forming the backbone connection out of a wire based technology is not unreasonable. Different types of communications will have different requirements of the network, each requiring specialised functions. For voice based communications, redundancy can be exploited, and accurate information transferral is not essential. For data communications, the communication can be slow, but must be accurate. In a multiple base system using a packet based system where computer communications take place using a set of communication blocks, it is possible for the packets of communication to arrive at the receiver out of sequence. This situation can be dealt with using communication protocols to reconstruct the transmitted signal.

1.2.2 Wireless advantages and disadvantages

One of the major problems that presents itself is the already limited spectrum available for communications. The remaining free spectrum has to be used to its maximum potential, spread spectrum technology presenting itself as a suitable means of increasing performance. Splitting up of the environment into a number of small cells also increases the overall accessible bandwidth of the communication system, but also increases the cost as more cell sites are required. Techniques such as diversity combining can also be used to increase the available bandwidth through improved reception capabilities.

Where a large number of devices, each being of a low power, are transmitting, a sizable amount of radio power is being generated. The effects of radio communication on human health are being examined [18], however much more work is required in this area before large scale communication systems are developed.

The unconstrained nature of the communication medium of radio requires the issue of network security to be addressed. Verification of communication entities must also be performed to ensure that only registered devices may communicate using the network, and that only registered devices may receive the data. Some form of encryption may be required for communications to avoid interception of data transmitted over the network by devices not taking part in the communications.

In addition to security considerations from external devices accessing the network, interfering signals can be generated by other devices in the office environment, for example printers and other electromechanical devices. These devices can temporarily disrupt a communication link through the noise that they generate.

A wireless communication system has a number of advantages, not least the mobility of the devices within the environment. It is a simple matter to relocate a communicating device, and no additional cost of rewiring and excessive downtime is associated with such a move. It is also a simple matter to add in a communication device to the system or remove one from the system without any disruption to the remainder of the system. Other than the initial outlay on setting up the cell sites, the cost of running and maintaining a radio based communications solution is minimal. These, and other factors, show the appeal that a radio communication system has for the office environment.

1.2.3 Interconnection technology

Two areas of the electromagnetic spectrum are potential candidates for supporting high capacity radio communication systems, namely the infra-red (IR) band, and the ultra high frequency (UHF) band. The IR band is extensively

used in the home for remotely controlled devices. In such applications the data rate is low, and a direct line of sight between the transmitter and the receiver is not difficult to achieve. IR communications will operate if no direct line of sight is available, but a reflected path is. As IR communications are close to visible light in frequency, and warm bodies emit IR radiation, communication links are subject to large amounts of noise from the environment. Obviously such a medium is not conducive to the development of a dynamic network that must support a high bandwidth of communication as envisaged for office communications.

UHF communication links differ from IR links in a number of respects. Many of the surfaces in an office environment will appear as opaque objects for IR communications, but as transmissive objects for UHF communications. This has an advantage in that groups of offices in a building requiring separate IR transceivers for each office can be served by one cell site operating in the UHF band.

1.3 Channel Modelling

In order to evaluate the effectiveness of a given channel coding and processing technique before construction, some model of the channel must be developed that adequately describes the environment. Such analysis reduces the cost of developing a complex system by reducing the amount of hardware that has to be developed for evaluation of performance. Theoretical models have a second advantage in their ability to reproduce a channel for comparison between various communication strategies, resulting in an accurate measure of relative performance.

Indoor channels are highly dependent upon the placement of walls and partitions within the building. In such cases, a model of the environment is a useful design tool in constructing a layout that leads to efficient communication strategies. To achieve this aim, a channel model of an indoor environment must be applied to various layout plans of offices which will lead to the characteri-

sation of design methodologies. Much work has been carried out in measuring the channel in buildings of various layouts, and structural compositions. In order to combine these results, some unified model of an indoor channel must be developed.

A channel model is useful in determining the mechanisms by which propagation in the indoor environment occurs, which in turn is useful in the development of a communication system. By examining the details of how a signal is propagated from the transmitter to the receiver for a number of experimental locations, a generic model may be developed that highlights the important characteristics of a given indoor environment. Generic models of indoor communications can then be applied to specific situations to describe the operation of a radio system, and may also be used to generate building designs that are particularly well-disposed to supporting radio communication systems.

1.4 Ray Tracing for Channel Modelling

The use of ray tracing in computer graphics for modelling in the visible light spectrum is well known. The technique is based on casting a series of "rays" of light from a source, and tracing the rays as they reflect off objects in some scene. To produce an image from this series of rays, the surfaces of the lit scene are projected towards a point through an observation plane. The image created on this plane is then displayed on a screen, or other medium, to the user of the system.

A similar technique may be used for radio propagation, where the rays are normal to the surfaces of equal signal power, and lie in the direction of propagation. By creating a number of images that are the result of reflections and diffractions of the electromagnetic waves off surfaces in the environment, and using ray based techniques, the effect of a transmitted signal on a receiver may be determined.

Due to the complexities of modelling a dynamic environment using a ray tracing technique, it is only practical to simulate the fading channel of a mobile

system by moving either the transmitter or the receiver around the environment. The results of this process may be presented in terms of the signal power that would be experienced by a receiver moving through this environment, or in a more detailed form showing the multipath nature of the environment, and the changing channel impulse response as the receiver moves around the environment.

1.5 Organisation

This thesis describes an attempt to create a model of a general indoor channel from the physical layout and construction of the structures found in the building using a ray tracing technique. The remainder of this thesis consists of the following chapters:

Chapter 2 reviews the published work that has been conducted in the field of channel measurement and modelling. Measurements and models that relate to indoor radio channels are examined, and reference made to selected models of the outdoor counterpart. This examination will lead to the conclusion that a physically based modelling system is required in order to combine the modelling results obtained for a number of different environments.

Chapter 3 describes the physical considerations that affect the propagation of an electromagnetic wave from a transmitter to a receiver. The chapter also introduces the basis of the ray tracing model developed here.

Chapter 4 uses a limited set of the model features described in Chapter 3 in an attempt to recreate results obtained from narrowband measurement experiments. The model is used as a tool to determine the significance of diffraction as a propagation mechanism to the channel impulse response.

Chapter 5 presents the results of an electromagnetic simulation of one of the sets of narrowband measurement experiments conducted. Analysis based on the physical construction of the building is presented on

each simulation result for the various experimental locations used in the set of measurements.

Chapter 6 presents two sets of wideband simulation experiments, with comparison being made to measured results available in the current literature.

Chapter 7 concludes the thesis by reviewing the results of the previous chapters, and indicating the possible direction of future work in this field.

Chapter 2

Channel Measurement and Modelling

2.1 Introduction

In order to evaluate the performance of a given signal processing or array processing technique in a practical communication system, before the system has been constructed, a model of the channel is required. Such a model is desirable as it reduces both the cost and time of system evaluation as well as highlighting the important characteristics of the channel. Detailed information on how the channel affects the transmitted signal is crucial in the calculation of how systems such as antenna arrays perform when the received signal at each antenna is related to that received at the other antennae by a non-trivial relationship. Prior to development of a suitable model, the characteristics of that type of environment have to be determined through experimental measurements. Once these have been performed, a mathematical model can then be constructed to describe the measured results in a form suitable for evaluating the performance of a proposed system.

In this chapter we describe some of the literature relating to channel measurements, and models that are based on these results. These models are divided into two types; narrowband models and wideband models. Narrowband models are often presented in terms of the statistical distribution of the received signal amplitude, with information on how rapidly the channel characteristics change. Wideband models may be represented by temporal models, or parametric models. Through performing this review, the need for a detailed

model of the channel based on the physical layout of the environment which can more thoroughly describe the channel will be shown.

2.2 Previous Work in Channel Modelling and Measurement

Communication systems can be broadly categorised into narrowband and broadband systems. A narrowband signal can be defined as one whose band of frequencies over which the signal is represented is small compared to the carrier, or modulation frequency, f_c [2, chapter 3]. For a communication system a more rigorous definition relates the band of frequencies over which the transmitted signal ranges to the modulation imposed by the channel on those frequencies. Where a channel has an impulse response with an essentially nonzero delay power spectrum over a range defined by T_m, then a coherence bandwidth, $(\Delta f)_c$, is defined to be the reciprocal of T_m [2, chapter 7], which is known as the multipath spread of the channel. Where the signal to be transmitted over this channel has a bandwidth of less than the coherence bandwidth, then it is said to be narrowband. That is all of the frequencies in the transmitted signal are subjected to the same attenuations, leading to the definition of the channel as being frequency non-selective. Such channels can be adequately described by a memoryless model, and are characterised by their average attenuation and the statistics of the variations around this average. The corollary of this is that a wideband channel is one where the signal to be transmitted has a bandwidth greater than the coherence bandwidth so that the component frequencies of the communication are subject to different attenuations by the environment.

2.2.1 Narrowband models and measurements

In order to construct efficient communication systems for indoor radio networks and personal communication network (PCN) systems, a great deal of effort has been expended and considerable quantities of information obtained

on the propagation of radio transmissions, mostly in the form of experimental measurements [19]. Statistics relating solely to narrowband channels consist of power level measurements over some geographical area with, very often, separate results for large scale, or global, variations and small scale, or local, variations. Due to the relative simplicity of the measuring equipment required to perform these measurements, the majority of characterisation work has been carried out for narrowband channels [20–31].

Lecours *et al.* [20] describe the results of a narrowband experiment to measure the average power received by a mobile in a moderately dense urban environment. They show that the received power can be characterised by a slowly changing mean value and a rapidly changing signal power. The experimental system that they use removes the slow fading by passing the received signal through a low-pass filter to give an estimate of the local mean for a given time period. It was found that the slowly varying mean value can be statistically described by a log-normal distribution, and the rapidly varying component by a Ricean or Rayleigh distribution.

Unfortunately in the indoor environment the slowly varying and rapidly varying components of the received signal power are affected by many other processes giving rise to other statistical distributions. Experiments have been performed to measure the signal attenuation for communication between one device inside a building and a second outside [21–23]. They show that the propagation is dependent on the frequency of operation, the presence or absence of a line of sight path, the type of construction material used in the building and the number of floors through which the signal must propagate. One interesting result from [21] is that penetration loss, that is the loss incurred from transmission through the outer wall of the building, decreases with frequency. This characteristic had also been observed by Rice in previous experiments operating at lower frequencies [32]. The median signal strength for the rapid signal variations is shown to decrease as d^n where d is the distance over which the propagation is occurring, and n is a constant which assumes different values, depending upon the type of environment, in the range -3.0 to -4.5 for

propagation within a building and outdoor propagation [23]. Values for n have been reported ranging from as high as -1.2 to as low as -6.5 by Alexander [26]. Dempsey [33] shows that at a certain transmitter to receiver distance, the received signal strength decrease becomes more rapid, that is the value of n increases and the signal strength is therefore not adequately modelled by a power law with a fixed n.

Measurements dealing with communications between two entities in the same building can be considered according to the following categories:-

- Large-scale signal variations
- Small-scale statistics
- Dependence on transmitter frequency
- Correlation of diversity signals
- Rapidity, duration, and frequency of occurrence of fades

Large-scale signal characterisation

Through measurements made at 850MHz, 1.7GHz and 4.0GHz, Devasirvatham *et al.* [24] suggest a model for signal power variations where the received power can be described by a free-space loss with a linear path attenuation. The linear path attenuation was found to be between 0.23 and 0.62 dB per metre. Alexander [26] and Seidel and Rappaport [28] use a relationship where signal power, s, is related to the distance between the transmitter and receiver, D, as

$$s(\mathrm{dB}) = -n \log \mathrm{D} \; . \tag{2.1}$$

Alexander gives a set of n values for various types of building with different construction materials, and Seidel derives a second model that incorporates a floor attenuation factor (FAF) to take account of communication between floors without altering the value of n. Owen and Pudney [29] note that a better fit to this model can be obtained, especially for short distances, if only the horizontal distance is used as opposed to the actual distance between the transmitter and the receiver. Two possible reasons for this effect are proposed;

lack of attenuating objects other than the floor losses already incorporated into the model; and the ducting effects of stairwells and lift shafts.

Rappaport and McGillem [34], after performing measurements at 1.3GHz, take this form of analysis further by calculating the shadowing effects of various objects found in the indoor environment. This data, coupled with a diffraction model, can be used to estimate the large scale path loss for a given transmitter and receiver location. In their measurements, path loss factors between 1.5 and 2.8 are found to characterise their measurements.

The dependence of large scale signal variations on the physical layout of the environment has been shown by a number of experimental measurements, both in the outdoor and the indoor environment. One recent study of radio coverage in New York City was performed by Goldsmith and Greenstein [35] where they showed that the optimal cell shape was not hexagonal, as is commonly used, but a diamond shape aligned to the layout of the streets which are in a regular grid pattern as in most North American cities. The indoor environment is often constructed in a regular manner, and similar patterns may be expected to be developed by this structure.

Small-scale signal characterisation

Models for the rapidly varying component of a mobile channel often use a Rayleigh or Ricean distribution to describe the probability of occurrence of a particular signal amplitude. In general the Rayleigh model is applied to channels where no LOS path exists between the transmitter and the receiver, the Ricean model describing those channels where one does exist [25,27]. Other measurements have shown that the distinction is not well defined, and that the Ricean model can apply to non-LOS channels [31]. Todd *et al.* [30] have shown that the envelope of a set of measured small scale statistics conforms to a Rayleigh distribution, but the statistics of the data sets may deviate significantly from this distribution. Suzuki [36] showed, through a series of wideband measurements, that the channel for mobile communications can often be better modelled by a Nakagami distribution [37] than by Rayleigh or Ricean distri-

butions. Through other measurements this has been found to be the case for indoor communications as well [38, 39]. Assuming a Nakagami distribution as a model for communications, a number of authors have been studying the effect that it has on the error rate of communication systems [40–42].

Frequency dependency of models

Alexander [27] showed that the large scale variations are highly dependent on the frequency of operation. Systems operating at 60GHz are restricted to single offices for point to point communications, whereas systems operating at 900MHz can cover a set of offices, or an entire floor. This difference is due to the different free-space losses and to the number of potential reflectors at the two frequencies. Due to the shorter wavelength at 60GHz the free-space loss is greater at a specific distance from the transmitter than it is for 900MHz. At 60GHz most surfaces found in buildings reflect radio waves more than they allow transmission of the waves.

Correlation between multiply received signals

Using only one received version of the transmitted signal as an estimate of that signal poses a problem for reliable estimation during periods of severe channel fading. In practical systems, the fading may cause errors in the estimation process, causing the received signal to be mis-interpreted. One means of mitigating this problem is to use a set of signals that fade independently in the estimation process. Such a technique is referred to as diversity combining. Lee [43, chapter 9] lists four forms of combining: selective combining, switched combining, maximal ratio combining, and equal gain combining. The effectiveness of these techniques are limited by the degree of independence of fading within the set of signals. A measure of this can be obtained from calculating correlations between pairs of signals.

For narrowband communications where there is no natural time diversity caused by multipath propagation, diversity can be sought through the use of coding techniques, the use of multiple frequency bands, and through the use

of multiple antennae. One interesting form of antenna diversity, that is using more than one antenna, consists of utilising the polarization of received signals to obtain two independently fading signals without the requirement to space the antennae [44]. This form of diversity has received relatively little attention in the literature [45]. Lee and Yeh [46] present results for outdoor mobile systems where there is little cross-polarization between horizontal and vertical polarizations. Cox *et al.* [47] show that unlike the outdoor environment, the indoor scenario exhibits a large degree of cross-polarization. This suggests that polarization diversity should be used in the process of signal estimation, if only to make best use of the signal power impinging on the receiver.

To measure the potential gains of using diversity, the correlation between the multiple signals being combined must be determined. If the correlation of signal strengths between the signals is low then the gains may be high. Todd *et al.* [30] display results for frequency and space diversity at 1.7GHz in the form of correlation curves for an office environment.

Rapidity, duration and frequency of occurrence of fades

The speed with which the channel impulse response and the statistics vary are important parameters in the calculation of the efficiency of a particular coding strategy as well as the transmitter and the receiver structure. The indoor mobile environment is classed as a non-stationary one as the statistics of the channel vary with time, but is often treated as a locally stationary one [2]. Bultitude [31] describes the nature of this non-stationarity in terms of bursts of fading occurring on a channel between two fixed antennae. Obviously, for a communication system to operate effectively at all times, the design must accommodate the worst fading that is present on the channel. This involves using the statistics of the periods of fading for performance evaluation, ignoring the periods of non-fading in the manner of Bultitude [31].

Lee and Yeh [48] develop a measure of the duration for which a received signal is above a particular threshold and contrast this with the commonly used measure of the level crossing rate. The former measure may be simpler to

relate directly to the error rate associated with the channel than the latter which is more prone to the effects of noise on the received signal. Similar information can be obtained through the use of an autocorrelation of the channel impulse response with time. This indicates the rapidity of change in the channel, an important parameter for predicting the performance of estimation algorithms.

Doppler spread

As path lengths between the transmitter and receiver change, due to movement of the communicating devices or other objects in the environment, a Doppler frequency shift is induced on the signal. The maximum value of this frequency shift is given by

$$f_D = \frac{2V_m f_c}{c} \tag{2.2}$$

where f_D is the maximum Doppler shift, V_m is the velocity of the mobile, f_c is the communication frequency, and c is the velocity of propagation [49]. Howard and Pahlavan [50] show a Doppler spread of 0.3–6.1Hz for indoor mobile channels. These measurements were performed at a carrier frequency of 910MHz.

Simulation systems

On assuming a Rayleigh fading channel, it is straightforward to construct a channel simulation for narrowband communications by generating a Rayleigh distributed signal. The commonly used approach is shown in Figure 2–1. Arredondo, Chriss and Walker [51] constructed such a Rayleigh fading signal that incorporates the effects of Doppler shifts due to vehicle motion through the application of noise shaping filters. The simulator was constructed in hardware using a zener diode as the source of Gaussian noise, and shown to give good conformance to the theoretical functions for power spectrum, level crossing rate, and fade duration. Smith extended this work using a computer simulation of the technique [52].

Casas and Leung [53] construct a similar form of narrowband simulator using a microprocessor to generate the Gaussian distributed random signals.

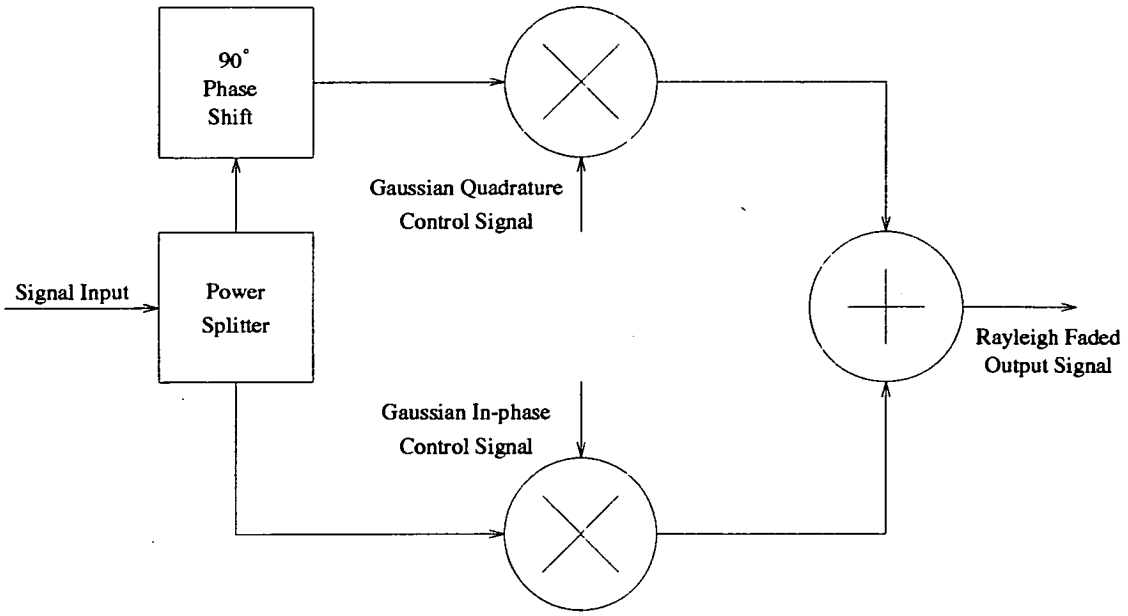

Figure 2–1: Rayleigh fading simulator

The filtered signals are then fed to a digital to analogue converter (DAC) before being mixed with an input signal which represents the transmitted signal. The resulting signal was compared with theoretical channels using cumulative probability distribution functions and level crossing rates for various Doppler frequencies and found to model a Rayleigh fading channel well. The simulator deviates from the theoretical distribution only at low Doppler frequencies for low signal powers [53, figure 14].

Ball [54] describes a hardware implementation, similar in form to Arredondo's work, using a binary pseudo-random sequence to generate a Gaussian distributed signal. Specific sequence generators were chosen to give amplitude distributions that have little skew, and were chosen to be different generators for the in-phase and quadrature components used to generate the faded signal. Other authors, for example [55], use this form of narrowband simulator, either directly, or as a building block for a wideband simulation.

2.2.2 Wideband models and measurements

Proakis, Stein, Bello and Parsons and Bajawa [2,10,49,56] represent a channel as a locally stationary system, simplifying the analysis, and allowing a number of equivalent relationships to be derived. The direct representation of a channel in terms of time and delay is the commonly used impulse response, $h(t,\tau)$. From this the delay-Doppler, or the frequency-time representation can be obtained by applying the Fourier transform to the time-delay impulse response with respect to the time and delay variables respectively. On a subsequent application of the Fourier transform with respect to the remaining variable, the frequency-Doppler representation of the system can be obtained. The delay-Doppler representation of the channel can be used to determine the multipath spread of the channel. Likewise, four representations of the channel correlation functions, and power spectra can be obtained through the use of double Fourier transforms.

Having defined the representations of the channel, the process of channel modelling is concerned with defining the parameters for these representations. This is commonly done using statistical methods, but can also be performed using physical modelling methods which will be discussed later. One commonly used model assumes that the direction of arrival at the receiver is uniformly distributed between $(-\pi,\pi)$ [57] and that the multiple waves arriving at the receiver have equal signal amplitudes [1]. For the outdoor radio environment where the path lengths between the transmitter and the receiver are approximately equal for all significant paths between the transmitter and receiver this assumption is acceptable. However, for the indoor radio case where the transmitter and receiver are in close proximity, small differences in path lengths give rise to substantial differences in signal amplitude between the multiple waves arriving at the receiver. In addition, as the communicating devices move, the reflection coefficients that alter the attenuation of each path arriving at the receiver change as the angle of incidence at the reflecting surfaces is altered.

The multiple waves arriving at the receiver at different times give rise to an effect called frequency selective fading. This occurs when the bandwidth

of the communications is greater than the coherence bandwidth of the channel as defined by Proakis [2, chapter 7]. This is manifest in the received signal as ISI where symbols are corrupted by the preceding symbol or symbols. Lorenz and Gelbrich [7] describe measurement results where this occurs for a communication rate of only 5 kbps due to a long delay path.

Perhaps the best known multipath model for radio communications is the three ray model developed by Rummler [58] to model microwave LOS channels. The simplified model has two parameters with a delay, τ, which is fixed at 6.3ns. It is shown that the fixed delay does not reduce the flexibility of the model. The equation governing the simplified model is given as

$$H(j\omega) = a[1 - b\exp(-j(\omega - \omega_0)\tau)] , \tag{2.3}$$

where a and b control the attenuation of the transmission paths. ω_0 controls the frequency of the position of the minimum, or notch, of a simulated fade which may or may not be within the bandwidth of the channel.

Temporal measurements and models

Most experimental data for wideband channel measurements of the indoor environment are in the form of temporal measurements, that is measurement of the channel impulse response with respect to time. The impulse response of a channel, $h(t,\tau)$, can be represented as

$$h(t,\tau) = \sum_i A_i(t)\exp(j\phi_i(t))\delta(\tau - \tau_i(t)) , \tag{2.4}$$

where A_i is the amplitude of the i^{th} path from the transmitter to the receiver which has a phase ϕ_i and time delay τ_i. The values of A_i, ϕ_i and τ_i are all dependent on time.

In order to determine the channel impulse response for a given environment, experiments to sound the channel can be performed. Such experiments are generally conducted using either a transmitted pulse [59], or a spread spectrum signal [8]. Davies *et al.* [60] demonstrate the use of both forms of experimental sounding systems, the pulse transmission system being used for experiments

conducted at lower frequencies. Tholl *et al.* [61] show through experiments conducted at the same frequency that both methods give similar results.

Consider an experiment where a very short pulse is transmitted and the received signal is observed over time. For a pulse transmitted at time t_0, the received signal will be the transmitted pulse convolved with $h(t, t - t_0)$, the channel impulse response beginning at time t_0. Thus the measured result is not the channel impulse response for a given time, t_0, but a sample of the impulse response as it is changing with time. However, if the channel is locally stationary, that is $A_i(t)$, $\phi_i(t)$ and $\tau_i(t)$ do not change significantly over the period $(t_0, t_0 + \tau_N(t_0))$ where $\tau_N(t_0)$ is the longest delay of all the multipath signals, then the received signal can be used to obtain an estimate of the impulse response at time t_0.

Saleh and Valenzuela [59] describe the results of channel sounding for the indoor environment in terms of a distance-power law, and root mean square (rms.) delay spread. A multipath power gain is calculated for each sounding as the sum of all the contributing powers, that is $\hat{G} = \sum_i \hat{A}_i^2(t)$, and the rms. delay spread is defined as $\hat{\sigma}_\tau = \sqrt{E(\hat{\tau}^2) - (E(\hat{\tau}))^2}$ where $\hat{}$ denotes the estimate of that parameter, and E() is defined as

$$E(\hat{\tau}^n) = \frac{\sum_i \hat{\tau}_i^n \hat{A}_i^2}{\sum_i \hat{A}_i^2} . \tag{2.5}$$

Using measured data, obtained at a frequency of 900MHz, a power law as defined in (2.1) is fitted to the data, with an n value of 3 modelling the data well—that is an inverse cubic power law. For the rms. delay spread, the median value was found to be 25ns with a maximum of 50ns for most cases.

Zollinger [62] performed similar measurements using a spread spectrum system operating on a 900MHz carrier. In some cases it was found that the LOS path did not give rise to the strongest component in the measured impulse response due to constructive interference of delayed multipath components. It was also noted that characteristics changed rapidly with only small movement in the transmitter or receiver positions.

Temporal wideband models are based on the principle of summing multiple copies of the transmitted signal at differing time delays to generate the received signal. This is often achieved using a tapped delay line (TDL) with a constant delay between tap positions and multiplicative weightings on each tap prior to the outputs being summed. If independent fading on each of the paths is assumed, that is the channel has uncorrelated scattering (US) and is often taken to be Gaussian wide sense stationary (WSS), then the TDL simulator can be constructed with Rayleigh distributed weights on each delay, those processes being generated independently.

One of the first wideband channel simulators constructed in accordance with these assumptions was produced by Walker [63] for modelling underwater sonar channels. It is an electromechanical device with shaped cams being used to generate a Rayleigh distributed weight through the movement of a variable resistor tap. This design was found to produce a reasonable approximation of the measured channel. Daniel *et al.* [64] describe a completely electrical system that uses pseudorandom noise (PN) sequences to generate Gaussian noise sources from which Rayleigh distributed weights are obtained. These weighs modify the output of nine taps off a surface acoustic wave (SAW) device to simulate a Rayleigh distributed wideband channel. The position of the 9 taps is selectable from 16 possible positions, save for the first which is preselected to be the input to the SAW device.

An alternative approach to this problem involves characterising the path arrival times as well as the amplitudes of such paths [65]. Suzuki [36] proposed that a modified Poisson process would model the arrival times of multipath components as these exhibited clustering which is not well modelled by a classical Poisson process as used in [65]. The modified Poisson process, as outlined by Suzuki, selects one of two Poisson distributions depending on a state variable. The state variable indicates whether or not a path has occurred in the last Δ seconds. If one has, then the Poisson model used for determining the arrival rate of subsequent paths is increased by a factor K for the duration of the interval Δ after the last path in the cluster. Hashemi [66] modified the discrete

model by selecting different values of K for each decision step, and making the path selection also conditional on the presence or absence of a path at the same delay in the previous time step. Conditional log-normal probabilities are used to generate the amplitudes of the impulse response at the various delays. Ganesh and Pahlavan [67–69] use this model for comparison with measured data from two sites and find the modified Poisson process to fit the data well when a log-normal distribution is used to model the signal amplitudes [67].

Yegani and McGillem [70] characterise the arrival times of various multipath components of the received signal in terms of the interarrival time between those components. The information is collected in the form of a probability function which is then compared with known probability functions to find the best fit. For the measured data that they collected, the Weibull pdf (Appendix C) was found to model the arrival times more closely than the other distributions tested. It should be noted that signals arriving within a small period of time, for example 1ns, will not be considered as distinct paths by a measuring system, and the results must therefore be examined in this light. A comparison of these measured results to a simulated environment is carried out in Section 6.2, highlighting this distinction.

Parametric models

Comparatively little work has been performed on modelling wideband channels in the frequency domain as opposed to the time domain. This is probably due to the intuitive nature of time domain modelling when compared to the same models in the frequency domain. Pahlavan and Howard [71] introduce an autoregressive (AR) model in the frequency domain of a channel, and a corresponding time domain model. It was shown that with relatively few parameters the AR model could approximate the measured data well. When compared with a more complicated time domain model, the AR model could not match the measured data as well as the time domain counterpart. However this may be a feature of the more complex time domain model which uses the modified Poisson distribution described above. The authors further show

in [72] that the poles of the AR model represent the clustering of arrival paths with the phase representing delay and amplitude representing path strength. Four different statistical methods were used to generate the pole location, the models once again showing close modelling of the measured data. Lau *et al.* [73] use the singular value decomposition prony (SVDP) algorithm to determine the poles and zeros of an AR moving average (ARMA) model of the radio channel.

Other modelling techniques

The methods of channel modelling outlined earlier in this section are based on characterising the channel in terms of statistical distributions and finding the controlling parameters of these distributions to describe the effect of the channel on a received signal. Some of the models incorporate information on the structure of particular environments in order to increase the accuracy of a model, especially in determining the slow fading component of a signal. It is possible to extend this technique by using a more complete description of the environment to derive the channel response in terms of the physical construction of the environment.

Gladstone and McGeehan [74,75] describe a statistical model of an outdoor mobile channel that is defined using the placement of buildings within the environment. The principles of reflection are used to determine the paths of propagation from the transmitter to the receiver. The path lengths are calculated, that information being used to calculate delays and path strengths. It is found that the resulting probability distributions model the measured distributions more closely than more basic statistical models such as the Rayleigh fading model.

It is possible to use a more complete description of the environment over which the propagation is occurring to determine the channel response. Increasing the complexity of the model will have the effect of increasing the modelling time, and ultimately modelling the channel will become infeasible as more detail is incorporated into the model.

For an outdoor mobile channel, Lebherz, Wiesbeck and Krank [76] use a combination of a two dimensional model incorporating the effects of diffraction in the vertical transmitter to receiver plane, and a three dimensional reflection and scattering model that is constructed from an accurate description of the environment. As expected, with a more completely defined model, the resulting simulated channel is closer to the measured channel when compared with simpler models.

McKown and Hamilton [77] introduce a ray tracing model for the indoor environment that calculates the signal power and delay spread over a specified area of a floor plan for 1.8GHz and 18GHz carrier frequencies. Honcharenko *et al.* [78] take a similar approach using a three dimensional model that incorporates scattering to determine the average signal power over an office floor. Their results are compared to measurements conducted at 900MHz and found to model the distance-power relationship well.

This thesis is an extension of the work performed on channel modelling by ray tracing using the electromagnetic properties of structures found in the indoor environment to define the reflection and transmission coefficients experienced by a transmitted radio signal. A full three dimensional model of the environment is required as the floors and ceilings of a building play an important rôle in the propagation of electromagnetic signals. The effects of radio propagation by diffraction on the received signal are evaluated using the model.

2.2.3 Additional considerations

Modelling the real environment, as the channel models described above attempt to do, requires investigation into a number of other areas to make the model as complete as possible. Some of these factors may already be incorporated in the models above, but it is worth providing a review of the work that relates directly to these factors.

Noise

In the indoor radio channel there are a large number of noise sources, some due to naturally occurring thermal noise in the system, and others due to radio transmissions at the same or similar frequencies as well as impulsive noise from a variety of man made sources. Noise due to other radio transmissions at similar frequencies is termed interference, and is normally treated separately from noise. For many channel modelling problems noise is treated as a Gaussian distributed random variable, called additive white Gaussian noise (AWGN) as it is spectrally flat. However measurements [79,80] show that the actual environment is not as simple as this model suggests.

Potential models for noise processes include Poisson process models proposed by Furutsu and Ishida [79]. Their work shows how a Poisson model and a Poisson-Poisson model can describe randomly occurring impulses, often generated by electronic processes, and packets of noise describing processes that are similar to atmospheric noise respectively. The modelling capabilities of these distributions are compared with data obtained from atmospheric noise measurements made by a radio station operating at frequencies between 1.0MHz and 20MHz.

Blackard, Rappaport and Bostian [80] describe a set of measurements performed in an indoor environment to determine the sources of impulsive noise. It was found that photocopiers, printers, elevators and microwave ovens are sources of significant noise with amplitudes of 50dB above thermal noise occurring and pulse lengths of up to 10μs. Certain noise sources were found to affect channels only at certain frequencies. An example of this is seen in the noise generated by a microwave oven only being detected when the receiver was operating at 2.44GHz, and not at 918MHz or 4.0GHz.

Polarization

Channel models, particularly outdoor models, assume that the transmitted and received signals are of the same polarity, and there is little cross-polarization in the channel, that is little of the transmitted signal power is

translated into an electromagnetic signal of orthogonal polarity. In the outdoor scenario this assumption is reasonably accurate [46]. However, measurement experiments in the indoor environment [47] have shown that there is a high degree of cross-polarization in the channel. Such cross-polarization, or depolarization of a transmitted wave, is a result of double reflection on a surface [81]. Celli *et al.* [82] describe the resonant excitation of a rough surface which gives rise to the cross-polarization of the scattered wave. Thus, a receiver which is polarized in the same manner as the transmitter may receive as little as a half of the potentially received power due to the translation of the transmitted signal into the other polarization. This phenomenon can be exploited through the use of polarization diversity reception that is more efficient in space for the receiver than antenna diversity [44] which requires a modest antenna separation.

2.3 Summary

This chapter has described some literature covering the work that has been performed on channel measurement and the modelling of these results. For an indoor communication system a wideband model of the channel is required as such a system will, by necessity, require a large bandwidth over which to operate. Statistical models of the wideband channel, while being useful in evaluation of proposed communication systems, are not generally based on a physical mechanism of channel propagation. The degree to which the channel can be accurately modelled by a statistical based approach is limited, especially with respect to the dependence between the signal powers received at different time delays.

The measurements and models presented in this chapter also exhibit a strong dependence on the type of structures that exist in the environment. Some of the models presented incorporate correction factors for signals that pass through certain structures, such as floors. Such an approach results in a model that is very cumbersome to use with many different parameters to

be accounted for depending upon the type of environment within which the communication system is operating.

Such limitations prompt the investigation of channel models that are based on the physical structure of the environment within which radio communication systems operate. Using the physical properties of the environment as the basis for a channel model leads to a model that describes a set of scenarios without special cases, such as floor attenuation factors. The model has the additional property that it inherently describes the correlation between channel impulse response delay weights, and between various instances of the channel impulse response.

Chapter 3

Ray Tracing Model

3.1 Introduction

To create a model of a communication system, mathematical descriptions of the transmitter, the receiver, and the effect that the environment has on the transmitted signal must be determined. Once the mathematical descriptions of these components are combined, then the model can be used to evaluate the performance of a theoretical system without the necessity of constructing it in hardware before evaluation. The final model may be in the form of equations, but due to the complexity of the environment is more likely to be incorporated into a computer simulation that combines a simplified description of the environment with the equations governing the propagation of the transmitted wave in the presence of simple structures.

This chapter outlines the elements of polarized electromagnetic radiation, and the effects of a dielectric surface or slab within the medium. The resulting sets of equations provide a simplified description of the environment which can be used in a computer simulation to compare results obtained from the model with those obtained in practical measurements. A description of the basic elements of a ray tracing algorithm are presented, as is a more detailed description of the ray tracing process. Further details of the software may be found in Appendix B.

3.2 Electromagnetic Radiation

In order to define a suitable transmitter and receiver for an indoor model it is useful to examine theoretically "ideal" models. The source that is best suited to simulation is one that radiates equally in all directions; whose transmitted power decreases with distance from the receiver; but for a fixed distance has constant power irrespective of transmitter orientation. In this context, the radiated power is given by the Poynting vector [83, p. 389]. This is the ideal omnidirectional antenna, or point source. If we define some power P_1 at a radial distance r_1 from the transmitter, we can write an equation for the power P at distance r as

$$P(dB) = P_1(dB) - 20\log_{10}\left(\frac{r}{r_1}\right). \tag{3.1}$$

Proakis [2, p 508] defines P_1 as

$$P_1(dB) = 20\log_{10}\left(\frac{\lambda}{4\pi r_1}\right). \tag{3.2}$$

This equation is valid for the far field of the transmitter, that is for $r \gg \lambda$, but when the receiver moves into the near field the equation no longer holds. At some distance, r_0, the received power as defined by (3.1) may exceed the transmitted power. Clearly this does not describe the real situation correctly, and it is also clear that the equation has a singularity, called a caustic, at $r = 0$. On reviewing the definition, this is a perfectly understandable result as a finite power has been defined for all spheres concentric on the transmitter. As the radius of the sphere decreases, the power density on the sphere increases giving rise to infinite power at an infinitesimally small radius.

The theoretical point source model is also deficient in another respect; electromagnetic theory shows that such a source of radiation is impossible [84]. For an electric and magnetic field to be generated—and hence radiated—there must be a change in charge, that is a current. With a point source, or point charge, such a change or flow of charge is not possible. However, it is possible to define a dipole of an infinitely small size with some alignment. For a dipole

aligned on the z-axis at the origin (Figure 3–1) with current I_0 defined within the length Δz, an expression for $I(z)$, the current on the z-axis can be defined by

$$\int_{-\frac{\Delta z}{2}}^{\frac{\Delta z}{2}} I(z')\,dz' = I_0\,\Delta z\,, \tag{3.3}$$

where $I_0\,\Delta z$ is the current moment. This results in the magnetic field being defined, in spherical coordinates, as

$$\underline{H} = \underline{\hat{\phi}}\,\frac{I_0\,\Delta z}{4\pi}\left(\frac{\gamma}{r}+\frac{1}{r^2}\right)\exp(-\gamma r)\sin\theta \tag{3.4}$$

where $\gamma^2 = -\omega^2\mu\epsilon$. That is $\underline{H}$ is a vector that rotates around the z-axis. The term ω is the angular frequency of oscillation, ϵ the permittivity of the medium, and μ the permeability of the medium. The electric field is given by

$$\begin{aligned}\underline{E} \;=\; \frac{I_0\,\Delta z}{2\pi}\exp(-\gamma r)\Bigg\{&\underline{\hat{r}}\left(\sqrt{\frac{\mu}{\epsilon}}\frac{1}{r^2}+\frac{1}{j\omega\epsilon r^3}\right)\cos\theta\\ &+\underline{\hat{\theta}}\,\frac{1}{2}\left(\frac{j\omega\mu}{r}+\sqrt{\frac{\mu}{\epsilon}}\frac{1}{r^2}+\frac{1}{j\omega\epsilon r^3}\right)\sin\theta\Bigg\}.\end{aligned} \tag{3.5}$$

$\underline{\hat{r}}$, $\underline{\hat{\theta}}$ and $\underline{\hat{\phi}}$ are unit vectors in the directions of r, θ and ϕ respectively where r, θ and ϕ define a point in spherical coordinates. ϕ is the angle made between the vector from the origin to the point of interest and the plane $y = 0$ with respect to the xy–plane, and θ is the angle between the z-axis and the point of interest (Figure 3–1). Thus, the Poynting vector, which denotes the power that is being radiated, is defined by

$$\begin{aligned}\underline{E}\times\underline{H}^* \;=\; \left(\frac{I_0\,\Delta z\,\beta_0^2}{4\pi}\right)^2\sqrt{\frac{\mu}{\epsilon}}\Bigg\{&\underline{\hat{r}}\sin^2\theta\left[\frac{1}{(\beta_0 r)^2}+\frac{1}{j(\beta_0 r)^5}\right]\\ &+\underline{\hat{\theta}}\,j\sin(2\theta)\left[\frac{1}{(\beta_0 r)^3}+\frac{1}{(\beta_0 r)^5}\right]\Bigg\},\end{aligned} \tag{3.6}$$

where $\beta_0 = \omega\sqrt{\epsilon\mu} = -j\gamma$, $\underline{\hat{r}}$ and $\underline{\hat{\theta}}$ are unit vectors in the radial and polar angular directions, and $\underline{H}^*$ denotes the complex conjugate of $\underline{H}$.

For points distant from the transmitter, the terms $(\frac{1}{r})^2$ and higher powers can be neglected, resulting in a plane wave where

$$\underline{H} = \underline{\hat{\phi}}\,\frac{I_0\,\Delta z\,\gamma}{4\pi}\frac{}{r}\exp(-\gamma r)\sin\theta = \underline{\hat{\phi}}\,\frac{I_0\,\Delta z\,j\beta_0}{4\pi}\frac{}{r}\exp(-j\beta_0 r)\sin\theta\,, \tag{3.7}$$

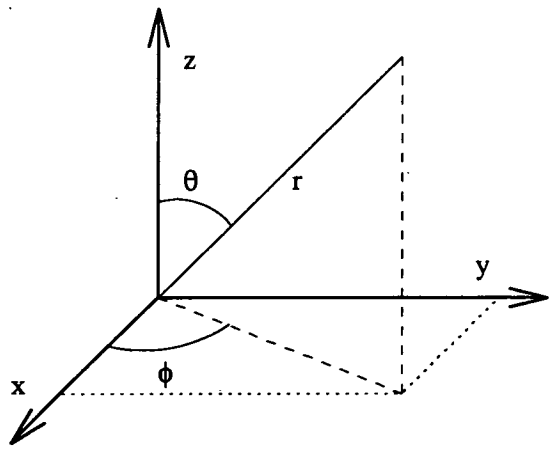

Figure 3–1: System of spherical coordinates used for field equations

and

$$\begin{aligned} \underline{E} &= \frac{I_0 \Delta z}{4\pi} \exp(-\gamma r)\, \underline{\hat{\theta}}\, \frac{j\omega\mu}{r} \sin\theta \\ &= \frac{I_0 \Delta z}{4\pi} \exp(-j\beta_0 r) \sqrt{\frac{\mu}{\epsilon}}\, \frac{j\beta_0}{r} \sin\theta\, \underline{\hat{\theta}} \end{aligned} \tag{3.8}$$

Thus, the power, P, at a given point in space, assuming that it is far from the transmitter, can be expressed as

$$P = |\underline{E}||\underline{H}| = \frac{\underline{E} \cdot \underline{E}^*}{\eta}\,, \tag{3.9}$$

where $\underline{E}^*$ denotes the complex conjugate of $\underline{E}$, and η is the intrinsic impedance of the medium given by

$$\eta = \sqrt{\frac{\mu}{\epsilon - j\frac{\sigma}{\omega}}} \tag{3.10}$$

which simplifies to $\eta = \sqrt{\frac{\mu}{\epsilon}}$ when $\sigma = 0$. Using this, an equation for P can be derived as

$$P = \left(\frac{I_0 \Delta z \beta_0}{4\pi}\right)^2 \sqrt{\frac{\mu}{\epsilon}} \sin^2\theta \frac{1}{r^2} \tag{3.11}$$

Thus the relationship in (3.1) can be expressed as

$$P_1(\mathrm{dB}) = 10\log_{10}\left\{\left(\frac{I_0 \Delta z \beta_0}{4\pi}\right)^2 \sqrt{\frac{\mu}{\epsilon}} \sin^2\theta \frac{1}{r_1^2}\right\} \tag{3.12}$$

The implication for constructing a software model for the channel is that if the reflecting and diffracting surfaces are sufficiently far from the radiating

source, the radiation can be treated as a plane wave, and calculations involving only one field, namely the $\underline{E}$ field, need to be performed. This creates a significant reduction in computational complexity.

3.3 Dielectric Surfaces

Only perfect conductors can reflect electromagnetic (EM) waves perfectly. In reality all surfaces are to some extent dielectrics and have associated μ, ϵ and σ values of permeability, permittivity and conductivity respectively. We can define the loss that is incurred by non-ideal conductors as a reflection coefficient, R, where $\frac{\underline{E}_r}{\underline{E}_i} = R$. $\underline{E}_r$ and $\underline{E}_i$ are the reflected and incident electric fields respectively. The reflectivity coefficient varies according to the angle of incidence, the polarization of the incoming wave, its frequency and the characteristics of the surface. For horizontal polarizations the coefficient may be generalised to a constant value, although in reality it does vary. Dempsey [85] shows graphs of reflection coefficients with values of R, the reflection coefficient, between 0.6 and 1.0. For vertical polarizations however, the coefficient varies between 0 and 1.

3.3.1 Electromagnetic polarization

Horizontal polarization is defined as the electric field, $\underline{E}$, of the incident wave being parallel to the surface off which it is reflecting. Thus the magnetic field, $\underline{H}$, is perpendicular to the surface, and lies in a plane known as the plane of incidence (Figure 3–2). Vertical polarization is defined as the electric field being perpendicular to the surface, and the magnetic field being parallel (Figure 3–3).

3.3.2 Reflection

If we assume that a surface can be approximated by an infinite plane separating two media that have different conductivity and permittivity parameters, then equations relating a reflected EM wave to its incident EM wave and the

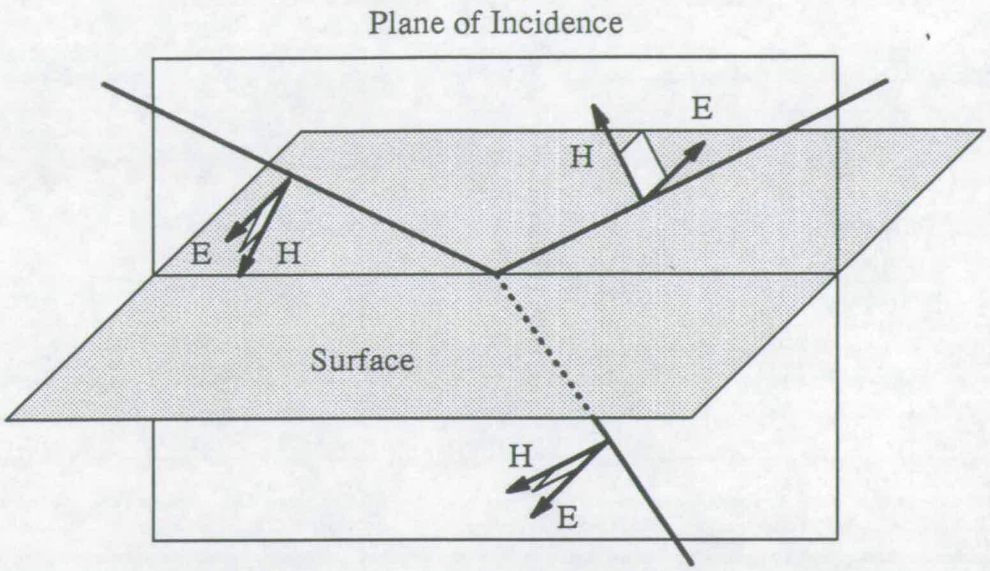

Figure 3–2: Horizontal polarization of an electric field

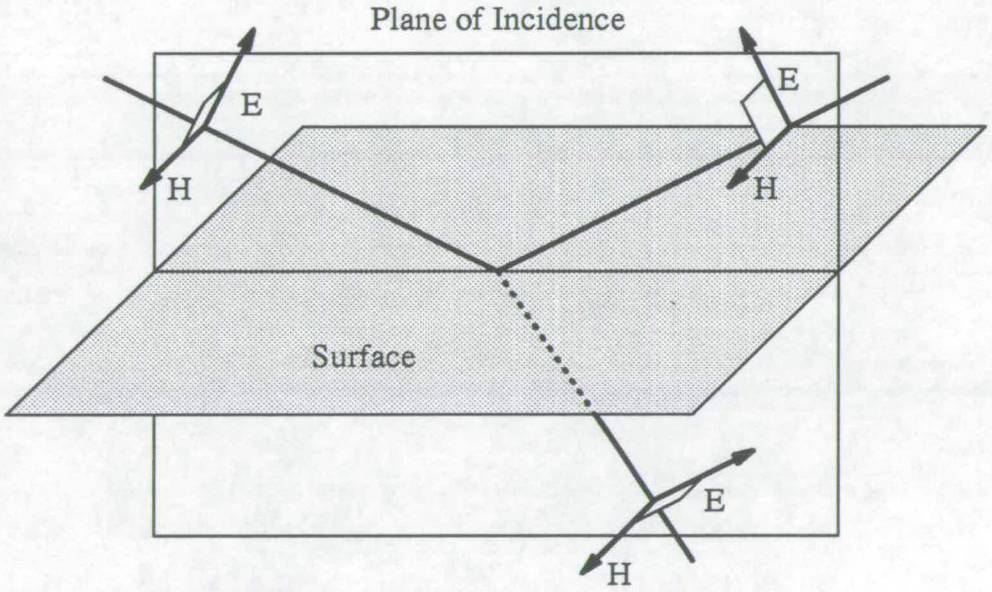

Figure 3–3: Vertical polarization of an electric field

dielectric properties of the two media can be obtained. Initially we will assume that the media are infinitely wide so that the surface is the only discontinuity in the environment. Both media are also assumed to be homogeneous, and the surface between them perfectly smooth.

The polarization of a wave reflected off a surface has an effect on the reflection coefficient associated with the reflected wave. The effects of polarization are quantified as follows [86]:

We can define the intrinsic impedance, $\eta = \frac{E}{H}$, of a medium by (3.10). The relative permeability, μ_r, can be taken as unity for non-magnetic materials, thus $\mu = \mu_0 = 4\pi \times 10^{-7}$. Assuming this to be the case, we can define n' as a function of the two media as

$$n'^2 = \left(\frac{\eta_1}{\eta_2}\right)^2 = \frac{\epsilon_2 - j\frac{\sigma_2}{\omega}}{\epsilon_1 - j\frac{\sigma_1}{\omega}}, \tag{3.13}$$

where the incident and reflected fields exist within medium I, and the refracted component within medium II. The reflected field $\underline{E}_r$ can then be defined in terms of the incident field $\underline{E}_i$ for both vertical and horizontal polarizations. In the case of horizontal polarization, with grazing angle of incidence, ψ, as

$$\frac{\underline{E}_r}{\underline{E}_i} = \frac{\sin\psi - \sqrt{n'^2 - \cos^2\psi}}{\sin\psi + \sqrt{n'^2 - \cos^2\psi}} = R_h e^{j\phi_h}, \tag{3.14}$$

and for the vertical polarization case,

$$\frac{\underline{E}_r}{\underline{E}_i} = \frac{n'^2\sin\psi - \sqrt{n'^2 - \cos^2\psi}}{n'^2\sin\psi + \sqrt{n'^2 - \cos^2\psi}} = R_v e^{j\phi_v}, \tag{3.15}$$

where R_h and R_v are reflection coefficients with phase angles ϕ_h and ϕ_v.

Derivations for these, and selected subsequent equations are presented in Appendix A.

3.3.3 Transmission

In the same way that reflection at the boundary of an infinitely large surface between two media can be defined, the transmission of the electromagnetic

wave through the second medium may also be defined. For horizontal polarization

$$\frac{\underline{E}_t}{\underline{E}_i} = \frac{2\sin\psi}{\sin\psi + \sqrt{n'^2 - \cos^2\psi}}, \tag{3.16}$$

and for vertical polarization

$$\frac{\underline{E}_t}{\underline{E}_i} = \frac{2n'\sin\psi}{n'^2\sin\psi + \sqrt{n'^2 - \cos^2\psi}}, \tag{3.17}$$

where $\underline{E}_t$ is the electric field of the transmitted wave.

If the second medium is bounded by a second infinite surface parallel to the first, with the third medium having the same electromagnetic properties as the first, then we can approximate the effect of a wall in a particular environment. Initially neglecting the internal reflection caused by the second boundary, we can calculate the field of an electromagnetic wave that passes through the surface (Figure 3–4). Defining $\underline{E}_{t_2}$ as the electric field transmitted through the second skin, then for a horizontally polarized incident wave we can calculate that

$$\frac{\underline{E}_{t_2}}{\underline{E}_i} = \frac{4\sin\psi\sqrt{n'^2 - \cos^2\psi}}{\left(\sin\psi + \sqrt{n'^2 - \cos^2\psi}\right)^2}, \tag{3.18}$$

and similarly for a vertically polarized incident wave

$$\frac{\underline{E}_{t_2}}{\underline{E}_i} = \frac{4n'^2\sin\psi\sqrt{n'^2 - \cos^2\psi}}{\left(n'^2\sin\psi + \sqrt{n'^2 - \cos^2\psi}\right)^2}, \tag{3.19}$$

where the attenuation due to propagation through medium II is accounted for by a constant factor.

3.3.4 Reflection and transmission coefficients for a non-infinitely thick slab

The definitions for the reflected and transmitted electromagnetic waves from a wall given above neglect the effects of internal reflection of the electromagnetic wave within the wall. These reflections give rise to additional components of the propagating wave as illustrated in Figure 3–4.

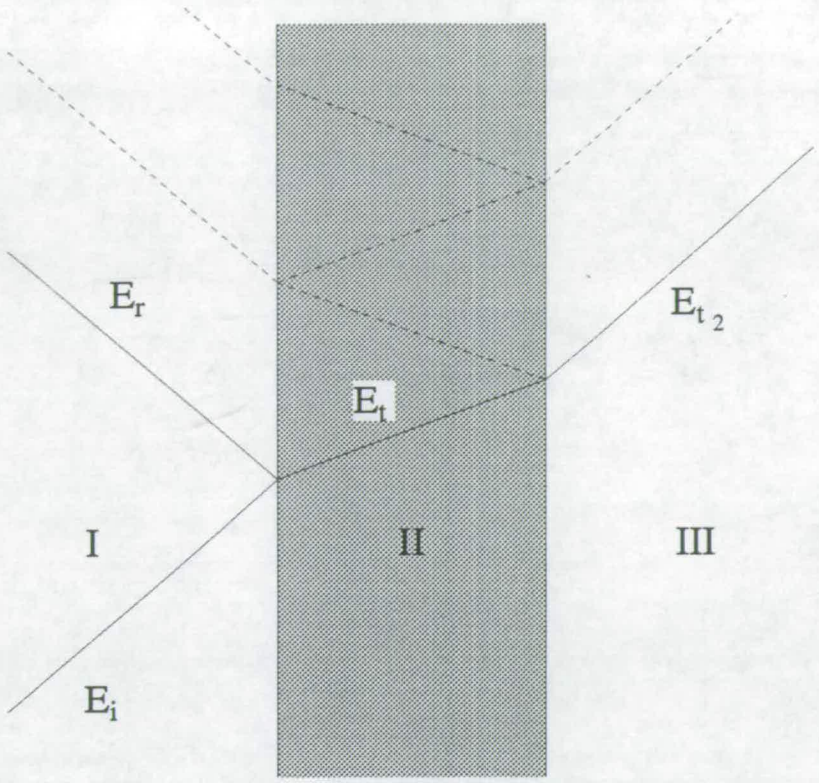

Figure 3–4: Transmission through an infinite wall

Now let us define the remainder of the reflected waves, and transmitted waves in sequence, such that $\underline{E}_{t_k}$ is the k^{th} transmitted wave across a boundary and $\underline{E}_{r_k}$ is the corresponding internal reflection where $k \geq 2$. Thus for k being odd, the transmitted wave will be in region I, and for k being even in region III of Figure 3–4. For horizontal polarization we can derive

$$\frac{\underline{E}_{r_{k+1}}}{\underline{E}_{r_k}} = (-1)\frac{\sin\psi - \sqrt{n'^2 - \cos^2\psi}}{\sin\psi + \sqrt{n'^2 - \cos^2\psi}} \tag{3.20}$$

and for vertical polarization

$$\frac{\underline{E}_{r_{k+1}}}{\underline{E}_{r_k}} = (-1)\frac{n'^2\sin\psi - \sqrt{n'^2 - \cos^2\psi}}{n'^2\sin\psi + \sqrt{n'^2 - \cos^2\psi}} \tag{3.21}$$

We can therefore derive expressions for $\underline{E}_{t_k}$ as

$$\frac{\underline{E}_{t_k}}{\underline{E}_i} = (-1)^k \frac{4\sin\psi\sqrt{n'^2 - \cos^2\psi}\left(\sin\psi - \sqrt{n'^2 - \cos^2\psi}\right)^{k-2}}{\left(\sin\psi + \sqrt{n'^2 - \cos^2\psi}\right)^k} \tag{3.22}$$

for a horizontally polarized incident wave, and

$$\frac{E_{t_k}}{E_i} = (-1)^k \frac{4n'^2 \sin\psi \sqrt{n'^2 - \cos^2\psi} \left(n'^2 \sin\psi - \sqrt{n'^2 - \cos^2\psi}\right)^{k-2}}{\left(n'^2 \sin\psi + \sqrt{n'^2 - \cos^2\psi}\right)^k} \tag{3.23}$$

for a vertically polarized one.

Combining these electric fields along with the phase difference between two adjacent rays being emitted from the surface of the dielectric, Burnside and Burgener [87] derive a reflection coefficient and a transmission coefficient for the total reflected and transmitted fields as

$$R = \frac{R_1(1 - P_d^2 P_a)}{1 - R_1^2 P_d^2 P_a} \tag{3.24}$$

and

$$T = \frac{(1 - R_1^2) P_d P_t}{1 - R_1^2 P_d^2 P_a}, \tag{3.25}$$

where R_1 is the reflection coefficient defined in (3.14). P_d is the phase delay incurred by propagation through the dielectric slab, P_a the delay in the reflection propagation direction between successive reflections, and P_t the phase difference for the primary transmitted field from the incident field. As the width of the dielectric slab shrinks to zero, the phase differences terms disappear from the equations, and thus $R = 0$ and $T = 1$ as expected for an infinitely thin dielectric slab. However, as indicated in Appendix A, the reflection and transmission coefficients are for horizontally polarized fields only with R_1 being chosen appropriately for the electric or magnetic field. Since we are dealing with the electric field, and may have vertically polarized fields we can modify these expressions to give

$$R = R_1 \left[\frac{\cos^2\theta_t - R_1^2 P_d^2 P_a \cos^2\theta_t - P_d^2 P_a \sin^2\psi + R_1^2 P_d^2 P_a \sin^2\psi}{\cos^2\theta_t \left(1 - R_1^2 P_d^2 P_a\right)} \right] \tag{3.26}$$

and

$$T = \frac{(1 - R_1^2) P_d P_t}{1 - R_1^2 P_d^2 P_a} \frac{n'^2 \sin^2\psi}{n'^2 - \cos^2\psi} \tag{3.27}$$

where

$$\cos\theta_t = \frac{1}{n'} \sqrt{n'^2 - \cos^2\psi}. \tag{3.28}$$

However, the derivation of (3.24) and (3.25) assumes that the incident wave is a plane wave, and hence there is no attenuation due to expansion as the distance from the transmitter increases. As can be seen from (3.1) this is not the case for a spherical wave front. When the equations (3.22) and (3.23) are modified to reflect this factor, the infinite series used to formulate (3.24) to (3.27) is no longer a geometric series as the attenuation factor is not constant over each internally reflected segment.

3.4 Diffraction

Diffraction is a phenomenon that is caused by discontinuities in a surface where an electromagnetic wave impinges on that surface. The mechanism results in the discontinuity acting as a radiating point or edge for a fraction of the electromagnetic wave. Thus an electromagnetic wave appears to propagate around a corner. For application to a ray tracing model it is useful to consider diffraction in terms of ray propagation.

Keller [88] considers the diffraction caused by an infinite edge of a perfectly conducting plane. A wave incident on an edge produces a cone of scattered components as shown in Figure 3–5. For the angles α, θ and β as defined in Figure 3–6, the diffraction coefficient D is given by

$$D = -\frac{e^{j\frac{\pi}{4}}}{2(2\pi k)^{\frac{1}{2}}\sin\beta}\left[\sec\left(\frac{1}{2}(\theta-\alpha)\right) \pm \operatorname{cosec}\left(\frac{1}{2}(\theta+\alpha)\right)\right]. \tag{3.29}$$

The upper sign is used for the boundary condition that on the half plane the field u is zero, and the lower for $\frac{\partial u}{\partial n} = 0$ where n is in the direction of the surface normal. The first case corresponds to the $\underline{E}$, or electric, field for horizontal polarization, and the second to the $\underline{H}$, or magnetic, field for vertical polarization.

The diffracted field u_e is then given by

$$u_e = D u_i r^{\frac{1}{2}} e^{ikr} \tag{3.30}$$

where r is the distance of the observation point from the point of diffraction on the edge.

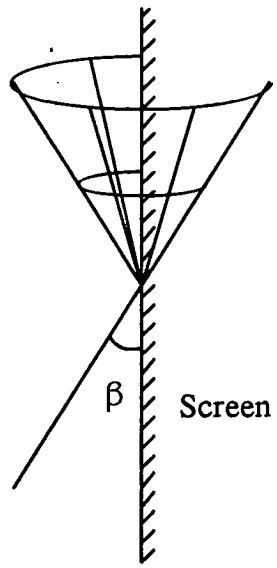

Figure 3–5: Elevation view of diffraction

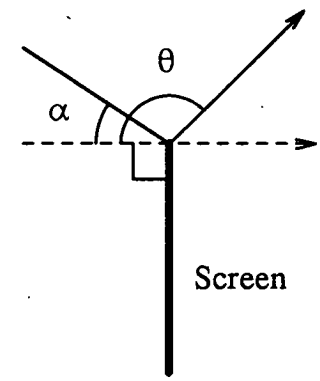

Figure 3–6: Plan view of diffraction

The coefficient can be modified to incorporate the case of a diffracting wedge to

$$D = -\frac{e^{j\frac{\pi}{4}} \sin\frac{\pi}{m}}{m(2\pi k)^{\frac{1}{2}} \sin\beta} \left[\left(\cos\frac{\pi}{m} - \cos\frac{\theta-\alpha}{m} \right)^{-1} \mp \left(\cos\frac{\pi}{m} - \cos\frac{\theta+\alpha+\pi}{m} \right)^{-1} \right] \tag{3.31}$$

where $(2-m)\pi$ is the interior angle of the wedge. Thus for right angled corners, as frequently found in buildings, the diffraction coefficient can be defined by

$$D = -\frac{e^{j\frac{\pi}{4}}}{\sqrt{3}(2\pi k)^{\frac{1}{2}} \sin\beta} \left[\left(\frac{1}{2} + \cos\frac{2(\theta-\alpha)}{3} \right)^{-1} \mp \left(\frac{1}{2} + \cos\frac{2(\theta+\alpha+\pi)}{3} \right)^{-1} \right], \tag{3.32}$$

where α, β, and θ are defined by Figures 3–5 and 3–7. The diffracted field of an incident ray is a cone of rays emanating from the point of incidence. If α or θ are in the range $-\frac{\pi}{2}$ to $-\pi$ then the diffraction coefficient is defined as being zero.

Kouyoumjian and Pathak [89] extend the geometrical theory of diffraction (GTD) to remove the discontinuities at the boundaries of reflection and shadowing for the perfectly conducting wedge problem. This extension is called

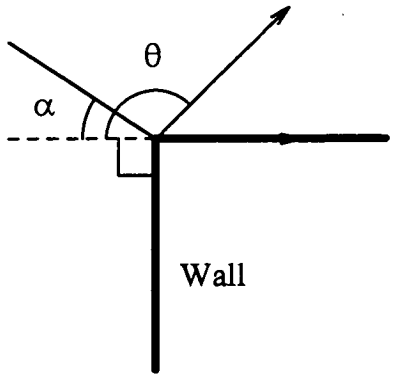

Figure 3–7: Diffraction around a right angled corner

the unified theory of diffraction (UTD) and is described by the following sets of equations.

$$\begin{aligned} D = & \left(\frac{-\exp(-j(\pi/4))}{2m\sqrt{2\pi k}\sin\beta}\right) \\ & \times\left[\left\{\cot\left(\frac{\pi+(\theta-\alpha)}{2m}\right)F[kLa^{+}(\theta-\alpha)]\right.\right. \\ & \left.+\cot\left(\frac{\pi-(\theta-\alpha)}{2m}\right)F[kLa^{-}(\theta-\alpha)]\right\} \\ & \mp\left\{\cot\left(\frac{\pi+(\theta+\alpha)}{2m}\right)F[kLa^{+}(\theta+\alpha)]\right. \\ & \left.\left.+\cot\left(\frac{\pi-(\theta+\alpha)}{2m}\right)F[kLa^{-}(\theta+\alpha)]\right\}\right] \end{aligned} \tag{3.33}$$

$$F(X) = 2j\sqrt{X}\exp(jX)\int_{\sqrt{X}}^{\infty}\exp(-j\tau^2)\,d\tau \tag{3.34}$$

$$a^{\pm}(\gamma) = 2\cos^2\left(\frac{2m\pi N^{\pm}-\gamma}{2}\right) \tag{3.35}$$

where $N^{\pm}$ is an integer which most closely satisfies

$$2\pi mN^{\pm}-\gamma = \pm\pi \tag{3.36}$$

and L is a distance parameter with values dependent on the type of illumination. F, which involves the Fresnel integral, can be expressed as an infinite series. This can be reduced to

$$F(X)\simeq\left[\sqrt{\pi X}-2X\exp\left(\frac{j\pi}{4}\right)-\frac{2}{3}X^2\exp\left(-\frac{j\pi}{4}\right)\right]\exp\left[j\left(\frac{\pi}{4}+X\right)\right] \tag{3.37}$$

when X is small, or as

$$F(X) \simeq 1 + j\frac{1}{2X} - \frac{3}{4}\frac{1}{X^2} - j\frac{15}{8}\frac{1}{X^3} + \frac{75}{16}\frac{1}{X^4} \tag{3.38}$$

when X is large.

Lawton and McGeehan [90] refine the UTD equations to incorporate the additional effects of dielectric surfaces forming the edge as opposed to perfectly conducting ones. The diffraction coefficient, D, is then defined by

$$\begin{aligned} D = & \left(\frac{-\exp(-j(\pi/4))}{2n\sqrt{2\pi k}\sin\beta}\right) \\ & \times \left[\cot\left(\frac{\pi+(\theta-\alpha)}{2n}\right) F[kLa^+(\theta-\alpha)]\right. \\ & \quad + \cot\left(\frac{\pi-(\theta-\alpha)}{2n}\right) F[kLa^-(\theta-\alpha)] \\ & + R_0^{\parallel}{}_{\perp} \cot\left(\frac{\pi+(\theta+\alpha)}{2n}\right) F[kLa^+(\theta+\alpha)] \\ & \left. \quad + R_n^{\parallel}{}_{\perp} \cot\left(\frac{\pi-(\theta+\alpha)}{2n}\right) F[kLa^-(\theta+\alpha)]\right] , \end{aligned} \tag{3.39}$$

where $R_0^{\parallel}{}_{\perp}$ and $R_n^{\parallel}{}_{\perp}$ are the reflection coefficients for the two surfaces which are dependent on angle of incidence and reflection respectively. They assume different values for parallel and perpendicular polarizations as previously shown in Section 3.3.

3.5 Electromagnetic Scattering

Surfaces in an environment are always, to some degree, rough surfaces which affects the reflection of electromagnetic waves. If the heights of the surface irregularities are less than $\lambda/(16\sin\psi)$ where ψ is the grazing angle of incidence, then the scattering effects of the surface can be ignored [86].

Landron, Feuerstein and Rappaport [91] modify the Fresnel reflection coefficients (3.14) and (3.15) by a scattering loss factor, ρ_s, to account for the lower energy caused by rough surface scattering. ρ_s is defined by

$$\rho_s = \exp\left[-8\left(\frac{\pi\sigma_h\cos\theta_i}{\lambda}\right)^2\right] I_0\left[8\left(\frac{\pi\sigma_h\cos\theta_i}{\lambda}\right)^2\right] , \tag{3.40}$$

where σ_h is the standard deviation of the surface height about its mean value, and I_0 is the modified Bessel function of order zero. Thus,

$$(R_h)_{rough} = \rho_s R_h \tag{3.41}$$

and

$$(R_v)_{rough} = \rho_s R_v \, . \tag{3.42}$$

However, it is clear from (3.41) and (3.42) that no depolarization is accounted for in this calculation. Such depolarization is caused by resonant excitation of surface irregularities [82] which cannot be accounted for through low order perturbation theory normally associated with rough surface scattering models. Instead, high order resonant scattering processes have to be considered in order to model this effect. Valenzuela [81] uses a set of second order equations to model an electric field incident on a slightly rough slab, assumed to be infinitely thick, using a theory developed by Rice [92] as opposed to a perturbation based model.

Detailed examination of the scattering properties of surfaces for various types of surface irregularities, [93], may be carried out, however the relevance of such results to modelling a comparatively large scale system, such as radio microcell, where information on the average signal amplitude and distributions are required must be questioned. Scattering models will alter the magnitude of a reflected signal, and alter its phase. As the phase distributions of the multipath signals are effectively uniform, this factor may be neglected. Where the surface is relatively smooth, the attenuation of the signal will also be minimal.

3.6 Ray Geometry Effects

In addition to the electromagnetic considerations highlighted above, the representation of a ray tracing environment is an important part of the model. The environment within which a practical transmitter operates consists of a number of surfaces which are of a finite size. This implies that a transmitted wave may or may not be reflected by an object before being received by an antenna at some other location. Similarly, a transmitted wave may or may not be reflected by two objects before being received by an antenna. Each of these propagation mechanisms from a fixed transmitter to a receiver will be classified as a propagation path. The absence of a singly reflected path does not necessarily exclude the presence of a doubly reflected path that incorporates the same object in its propagation. Hence, each possible propagation path, with multiply reflected waves, must be considered.

One possible representation of the environment that reduces the complexity of dealing with multiply reflected signals involves the notion of a reflected wave being considered as a directly transmitted wave from a fixed image source, with a modified signal power and possibly polarity, that exists on the opposite side of the reflecting surface. Using this fixed image source, it is possible to quickly exclude propagation paths that do not exist due to the finite size of the reflecting surface. In Figure 3–8 a path exists from the transmitter to receiver 1 via the reflecting object in the environment. This can be determined either from calculating the intersection point of the transmitted signal on the reflecting plane by using a rule based on the angle of incidence being equal to the angle of reflection, or directly by the intersection point of the line connecting the image to receiver 1 and the reflecting plane. Once the point of reflection has been determined, its existence on the object surface may be checked.

The effects of a finite sized reflecting surface is illustrated by considering receiver 2. Although the line connecting the image to receiver 2 crosses the reflecting plane, the intersection point of the line connecting the image to receiver 2 and the plane does not lie on the reflecting surface, therefore no

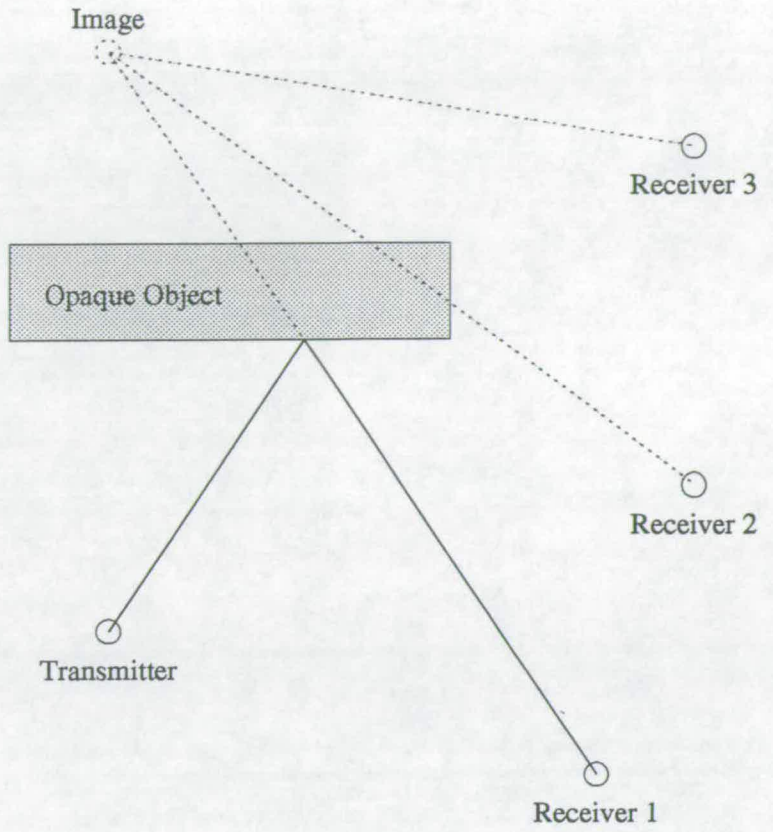

Figure 3–8: Ray tracing propagation

reflection path exists between the transmitter and the receiver. Receiver 3 is an example of a receiver position that, because it is on the opposite side of the reflecting plane to the transmitter, will not receive a multipath component directly from this reflection. However, for both receiver 2 and receiver 3, the lack of a direct reflected path does not preclude a multiply reflected signal arriving at the receiver via a reflection off this example reflecting object.

As well as electromagnetic propagation occurring in free-space, propagation paths may exist through transmissive components in the environment. Such paths will attenuate the propagated wave by an amount dependent on the construction material, the angle of incidence, and the thickness of the panel as shown above.

Thus the ray traced model must consider each possible propagation path from the transmitter to the receiver by reflecting the source in all the objects in

the environment, then each resulting image in all the other objects, and so on. Clearly some mechanism must exist for limiting the number of propagation paths that are examined as the algorithm just described is non-terminating. A number of possibilities exist: among them are limiting the number of reflections that are considered and comparing the power of each reflected wave with a reference limit below which no signals are considered.

So far, the discussion has described the mechanisms for considering reflection off objects in the environment. Diffractions from corners can be treated analogously, save that the image that is generated is no longer a point source, but a set of possible sources that describe an arc with the centre on the diffracting edge. The location of an image for a particular receiver position is determined by the angle between the receiver position and the reference surface of the edge. Due to the more complex representation of this, and the further expansion of the incident wave, multiply diffracted signals may be ignored for most practical applications. If required, a special case may be included for propagation through a slit where diffraction is an important propagation mechanism.

3.7 Ray tracing algorithm

A representation of the environment is built up from the building description data represented as a list of surface data consisting of two vectors forming two of the edges of a parallelogram. The normal to this surface is defined to be in the direction of the cross-product of the first vector with the second (Figure 3–9). The electromagnetic characteristics of the surface are given along with the set of edges so that the reflection and transmission coefficients can be determined for a given angle of incidence on the surface.

The ray tracing is performed for each receiver position independently as the propagation paths from the transmitter to the receiver can be highly dependent on the position of both communicating entities. The direct path from the transmitter to the receiver is examined initially to see if such a path exists. After this, the transmitter is reflected in each panel of the building, and the effect of

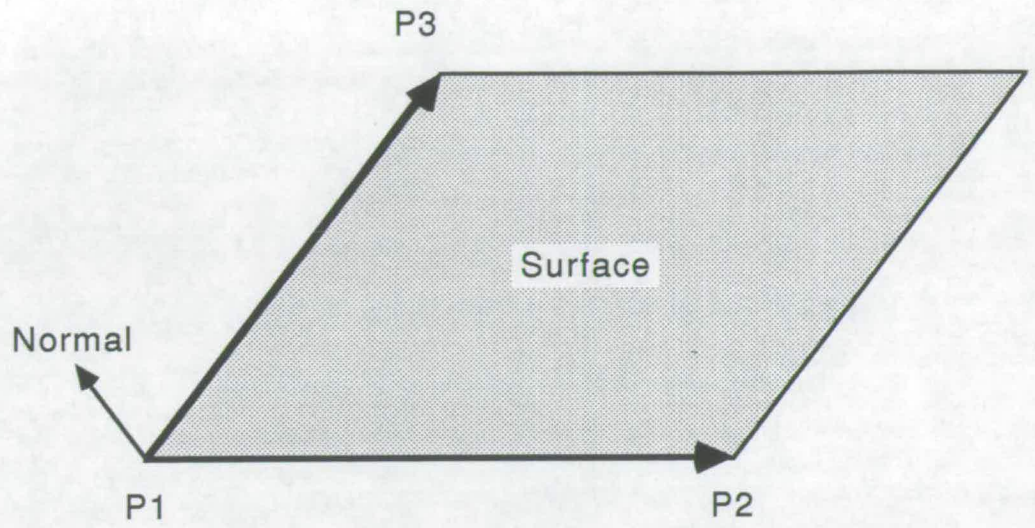

Figure 3–9: Representation of a surface

these reflections on the received signal is computed. After this, the effects of diffraction by the edges of the panels are computed. As the contributions of each of these reflections are computed, they are further reflected in each of the other panels and diffracted by the edges in the building, and so on until the signal power falls below the low signal power level defined in the input file. The diffracted signals are similarly reflected in the panels of the building, but secondary diffractions are ignored as the signal power of these falls off rapidly. In order to reduce excessive computation load, as the reflection coefficients and transmission coefficients can only be calculated once the angles of incidence on each panel are calculated, an upper limit on the number of reflections and diffractions is used to prune the execution tree further.

The details of the results recorded from this process depend on the type of experiment being performed using the simulation. For those experiments requiring only the received signal as a result, vector summation is used to combine all the contributions from the reflections and diffractions, together with the contribution from the transmitter to receiver path and a noise vector that defines the noise floor of the receiver. Other experiments require the

details of each of the contributions separately, these being stored in an array for processing later.

The process of ray tracing is conducted in the following manner:

All sources of radiation are treated in the same manner, save that sources that have already been diffracted are not diffracted by edges. Each of these sources, including the transmitter, are referred to as images. For each image, the distance from the image to the receiver is computed. In the case of an image being a source that has already been diffracted where the image is a circle of a non-zero radius, the effective point source of the diffraction is used: the effective point source is the point on the circle for which the image to receiver path passes through the axis of the image. If this distance is large enough to cause the signal power to fall below the threshold value, then further processing of this image is terminated.

Once the loss incurred by the image to receiver distance has been calculated and found not to be too large, the receiver to the transmitter path, via all of the reflections and diffractions that occur, is traced after first calculating the electric field that is produced by the transmitter for the appropriate direction of emission. During the ray tracing operation, each of the points of reflection and diffraction that occur in the path are checked to ensure that the appropriate panel exists at that point. As panels and edges are of a finite size, an image only exists for a subset of possible receiver positions where the image to receiver path passes through the reflecting panel or diffracting edge respectively.

In order to determine whether a reflected image is visible from a receiver position it is necessary to check whether the vector from the image to the receiver passes through the surface. The first stage of this calculation involves calculating the intersection point between the vector connecting the image and the receiver positions, $\underline{v}$, and the plane. This point is given by

$$\underline{P}_i = \underline{P}_t + k\underline{n}$$

where

$$k = \frac{\underline{P}_t \cdot \underline{n} - \underline{P}_s \cdot \underline{n}}{\underline{v} \cdot \underline{n}} = \frac{\underline{P}_t \cdot \underline{n} - \gamma}{\underline{v} \cdot \underline{n}} .$$

The resulting intersection point, $\underline{P}_i$, can then be compared with the edges of the surface to check whether the point falls within the surface or not. The comparison is shown graphically in Figure 3–10. Vectors parallel to the edges of the surface are projected from the intersection point, $\underline{P}_i$. If each of the vectors strike the other edge in less than their length, where the length of the vector is equivalent to the length of the edge, then the point is in the plane. A similar procedure is used for checking that a diffracted image is visible where the intersection point is the intersection of two vectors, and checking that it is within the finite edge size is a one-dimensional problem.

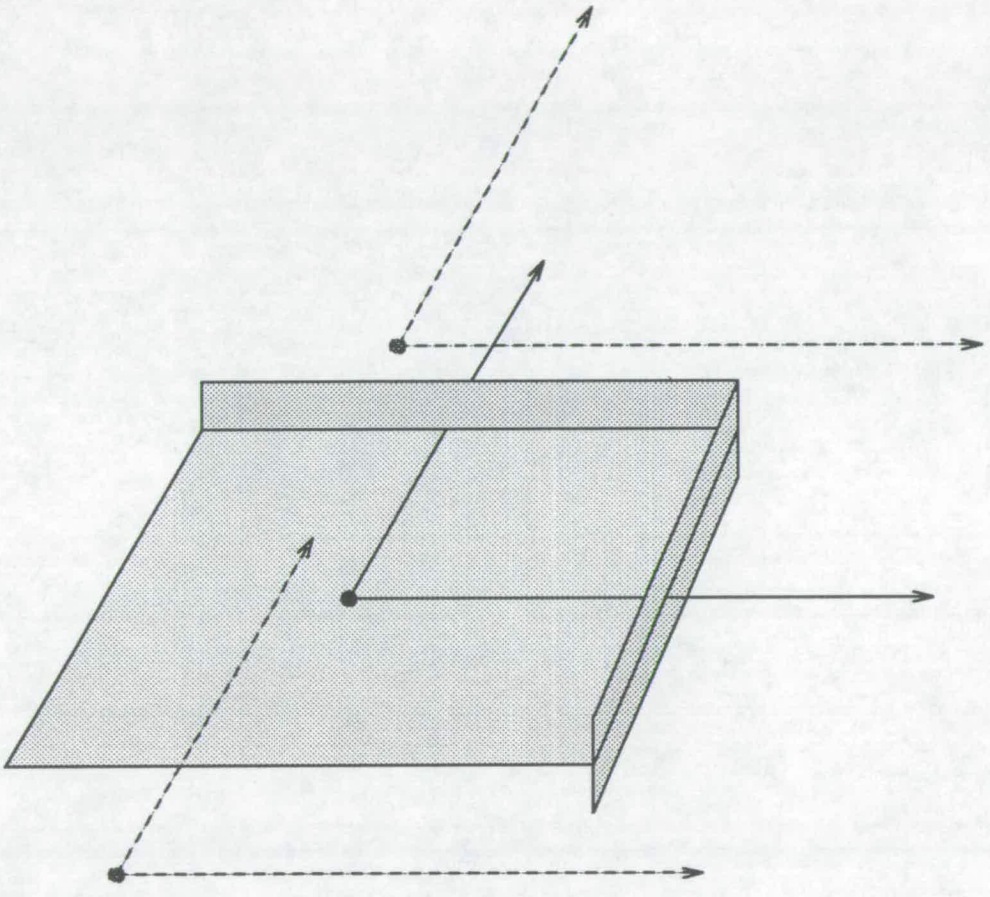

Figure 3–10: Calculation to determine if a point is in a plane

Once it has been ascertained that the image to the receiver path strikes all the reflecting surfaces and diffracting edges that define the image, the path is checked segment by segment to determine if any of the other panels in the

building are struck by this path. If any are, then the signal is to be attenuated by the transmission loss incurred by that panel. The segments of the image to receiver path are defined as the paths from each point of reflection or diffraction to the next such point in sequence, and the two segments from the transmitter to the first reflection or diffraction point, and the receiver to the final reflection or diffraction point.

Finally, the received signal is calculated from the incident electric field by calculating the polarization of the receiver for the direction of incidence. This field is combined with the electric field arriving at the receiver resulting in a complex scalar whose magnitude represents the signal amplitude, and phase represents the phase with respect to the transmitter phase.

At this stage the effect on the received signal of the currently examined image has been ascertained, and now the image is reflected in all of the other panels of the building, the process being recursively carried out for each of these new images. The same process is carried out for the diffracting edges, excluding any edges that lie on the panel that has created the image that we are examining, for all images that have not been diffracted previously.

3.7.1 Calculation of the reflection and transmission coefficients

The reflection and transmission coefficients for walls and surfaces in the environment can be determined once the angle of incidence, and the polarization of the incident field with respect to the surface are known. In order to calculate the horizontally and vertically polarized fields, it is assumed that the point of reflection is far enough from the source of the field for the field to be treated as a plane wave, and thus the electric and magnetic fields are perpendicular to the direction of propagation.

Using the surface normal, $\underline{n}$, the angle of grazing incidence, ψ, is given as

$$\psi = \sin^{-1}\left(\frac{\underline{u}_i \cdot \underline{n}}{|\underline{u}_i|}\right), \tag{3.43}$$

where $|\underline{n}| = 1$, $\underline{u}_i$ is a vector in the direction of propagation, and $\cdot$ denotes a vector dot product. The direction of the horizontally polarized component of

the incident field is given by

$$\underline{h} = \frac{\underline{u}_i \times \underline{n}}{|\underline{u}_i|} , \tag{3.44}$$

where $\times$ denotes the vector cross product. Likewise, the direction of the vertically polarized component of the incident field is given by

$$\underline{v}_i = \frac{\underline{h} \times \underline{u}_i}{|\underline{u}_i|} . \tag{3.45}$$

From these, the components of the incident electric field are computed as

$$E_h = \underline{h} \cdot \underline{E} \quad E_v = \underline{v}_i \cdot \underline{E} , \tag{3.46}$$

where E_h is the component of the electric field, $\underline{E}$, that is horizontally polarized with respect to the surface, and E_v is the vertically polarized component. The reflected field can then be expressed as

$$\underline{E}' = E_h R_h \underline{h} + E_v R_v \underline{v}_r , \tag{3.47}$$

where v_r is in the direction of the vertically polarized component of the reflected field, given by

$$\underline{v}_r = \left(\underline{n} \cdot \underline{v}_i\right) \underline{n} - \left((\underline{n} \times \underline{h}) \cdot \underline{v}_i\right) (\underline{n} \times \underline{h}) . \tag{3.48}$$

Once the reflected field has been determined, it is used as the field for incident waves on further reflecting surfaces, diffracting edges, or on the receiver. The process of determining the electric field that is diffracted by an edge is similar in form where the vertically and horizontally polarized components of the incident electric field are determined, modified by the diffraction process, and recombined to form the diffracted field. The effects of wave expansion from the point source (free-space loss) are incorporated into the received field at the end of the calculation as only the amplitude of the field components are affected by this process. A correction factor is introduced when diffraction is incorporated in the propagation mechanism due to the additional expansion process that is introduced by a diffracting edge.

3.8 Conclusions

This chapter has outlined the mathematical basis for the modelling of an electromagnetic wave generated at a transmitter and subsequently reflected and diffracted by ideal planes and edges. The complexity of the equations, for even a simple scenario, indicate that a computer simulation of this model must restrict the accuracy with which the model can be represented.

The degree to which a computer simulation must simplify the model is dependent on the complexity of the environment, and the available computing resource. As this is a necessary situation, regardless of the computing resource available, examination of the degree to which particular propagation mechanisms and modifications affect the received signal must be performed.

In the subsequent chapters selected elements of the electromagnetic model presented here will be used in varying degrees of complexity to ascertain the modelling performance improvement, or degradation, obtained from applying more accurate descriptions of the propagation mechanisms to a simulation system.

Chapter 4

Narrowband Experimental Work

4.1 Introduction

This chapter outlines the experimental procedure involved in two sets of narrowband channel measurements performed in Canada. The data from these measurements is used to evaluate the performance of the simulation system for these environments. A basic form of the ray tracing model is applied to an artificial simulation model in order to determine the characteristics of the simulation process, and to highlight some of the limitations of such a model. This model is then applied to a description of the environment within which one set of measurement experiments was performed. The significance of diffraction to the propagation of electromagnetic waves within buildings is evaluated using a more refined model applied to the second set of measurement experiments.

4.2 Channel Measurements

Narrowband measurements were performed at two locations in Canada by two different experimental teams [30,38]. The first of these measurement experiments was conducted in a building owned by the Mitel Corporation, hereafter referred to as Site A. The second set of data is obtained from experiments performed in the Engineering faculty of Carleton University, referred to as Site B. A brief description of the experimental procedures used and some initial results are presented below.

4.2.1 Site A measurements

Measurements performed at Site A were conducted by an honours year undergraduate student from Carleton University [38]. The measurement system consisted of a narrowband transmitter, emitting a continuous wave (CW), and receiver pair operating at 945MHz. The receiver was a vertically aligned dipole antenna located near the centre of the building close to the ceiling. The measurements were collected at a sample rate of 60Hz for a period of 60 seconds on each measurement run. The mobile transmitter was carried by hand around square areas of 8m $\times$ 8m at various locations over the floor space of the building. Measurements were performed on two floors of the Mitel building: one of the floors was fully furnished with office partitions to section off areas, and the other was empty bar one storage area containing metallic lockers and electrical equipment. The measurements used for evaluating the performance of the simulation system are those performed in the second of these floors in order to reduce the complexity of the simulation model required. A simplified floor plan of the building is given in Figure 4–1.

Due to obstructions in the shaded area of Figure 4–1 marked "A", caused by elevator shafts and locked offices, measurement results over the area were unobtainable. No measurements could be collected in a second area, "B", as this area was full of metallic equipment, making it physically impossible to move the transmitter around an 8m $\times$ 8m area as done in the remainder of the experiment runs.

To produce a plot of the signal power as it varies over the building, the floor was divided into 64 squares of equal size, defined by pillars that support the building. Within each of these squares, save for the areas already noted, a measurement run was performed from which the average signal power can be determined. From these measurement results, the average signal powers for the 10 squares for which no measurement results could be obtained are interpolated from the data points on the perimeter. The result of this procedure is a three dimensional graph of position and average power where the average signal power from each measurement run of 60s within the 8m$\times$8m blocks is

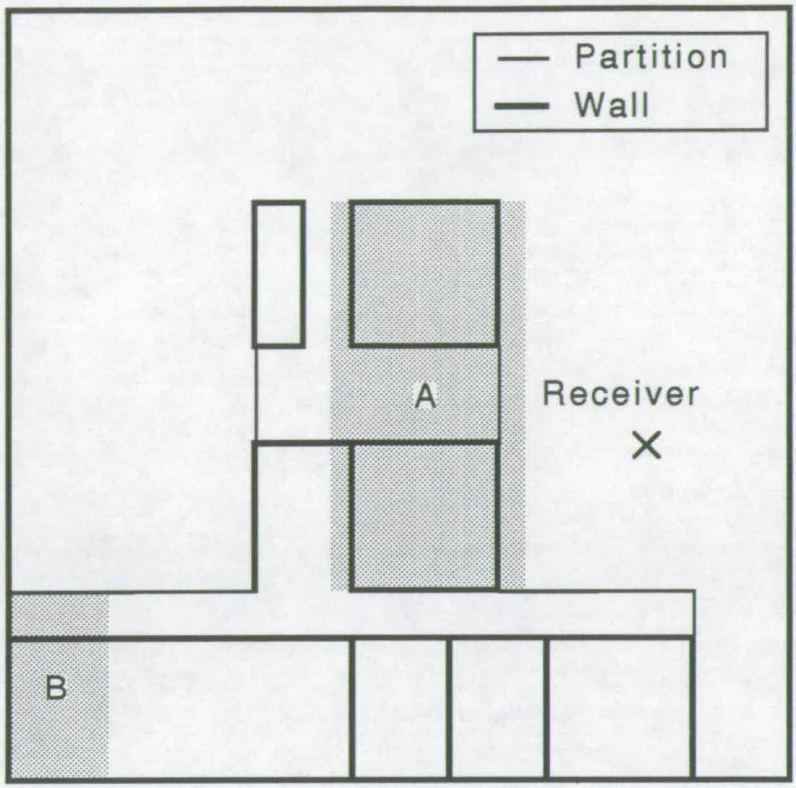

Figure 4–1: Schematic of floor at Site A

plotted at the centre of the associated square on the plot. Once the average signal power has been determined for each of the 64 squares, contour lines of equal signal power can be added to the figure to illustrate more clearly how signal power varies across the building floor. The plot resulting from this process is shown in Figure 4–2 which details the transmission loss as the source is moved about Site A. As indicated previously, measurement results were not obtained for two areas of Site A. Figure 4–2 delimits this area by two rectangular boxes within which the contour lines are a function of the interpolation process. The perimeters of the two boxes shown on the figure pass through the centre points of 8m×8m squares surrounding those for which measurement results are unobtainable. Features, such as the corridor between the lift shafts, and the partitioned area along one length of the building, can be identified from shape of the contours on the plot.

One section from a typical set of data obtained during a measurement

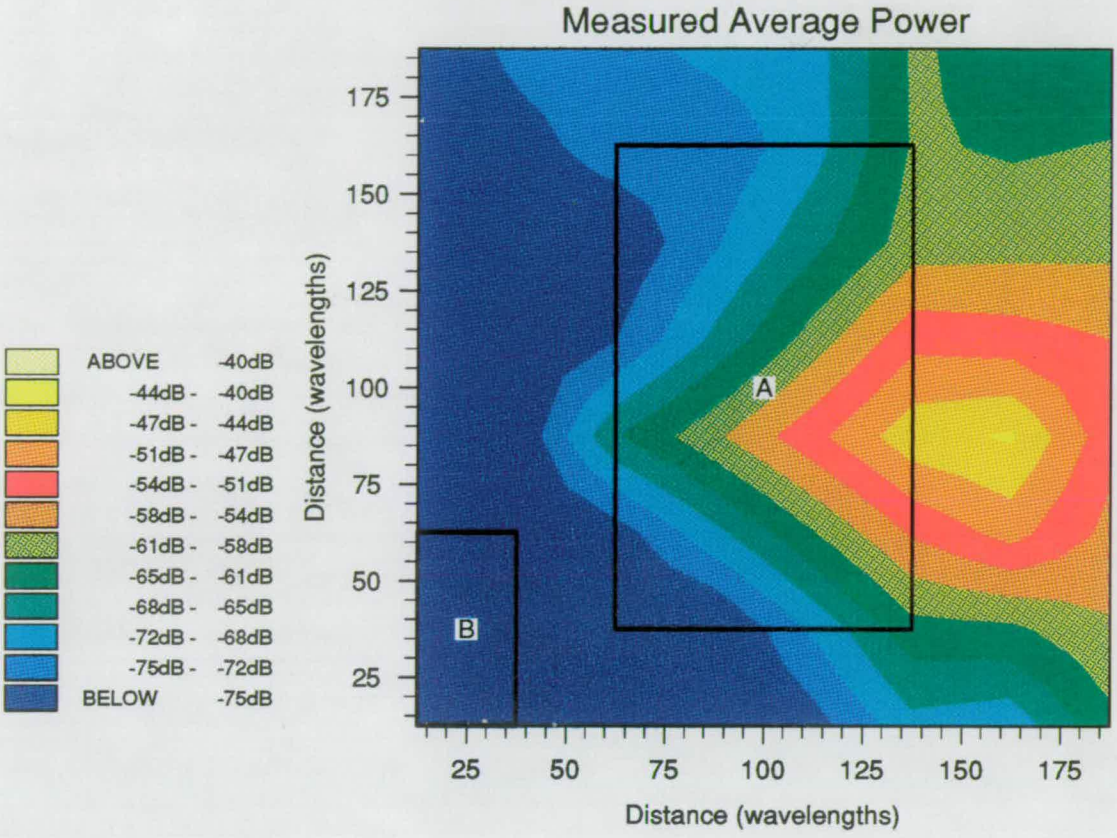

Figure 4–2: Plot of signal power over an empty floor of Site A

run—one of the 60s measurement experiments conducted within an 8m×8m square—is shown in Figure 4–3. The rapidly varying nature of the signal in the indoor environment is apparent in the figure, as is the slowly changing mean component over the measurement run. As can be seen from the figure, the speed of movement of the antenna and the pattern of movement are not regular. This can be deduced from the irregular spacing of the fades, and was observed while the measurements were being conducted. In addition to this, the height of the transmitting antenna was not kept fixed, nor was the orientation maintained in a vertical position. This implies that the data obtained cannot be used for temporal based measurements, and therefore must be restricted to analysis by statistical processing of moments only.

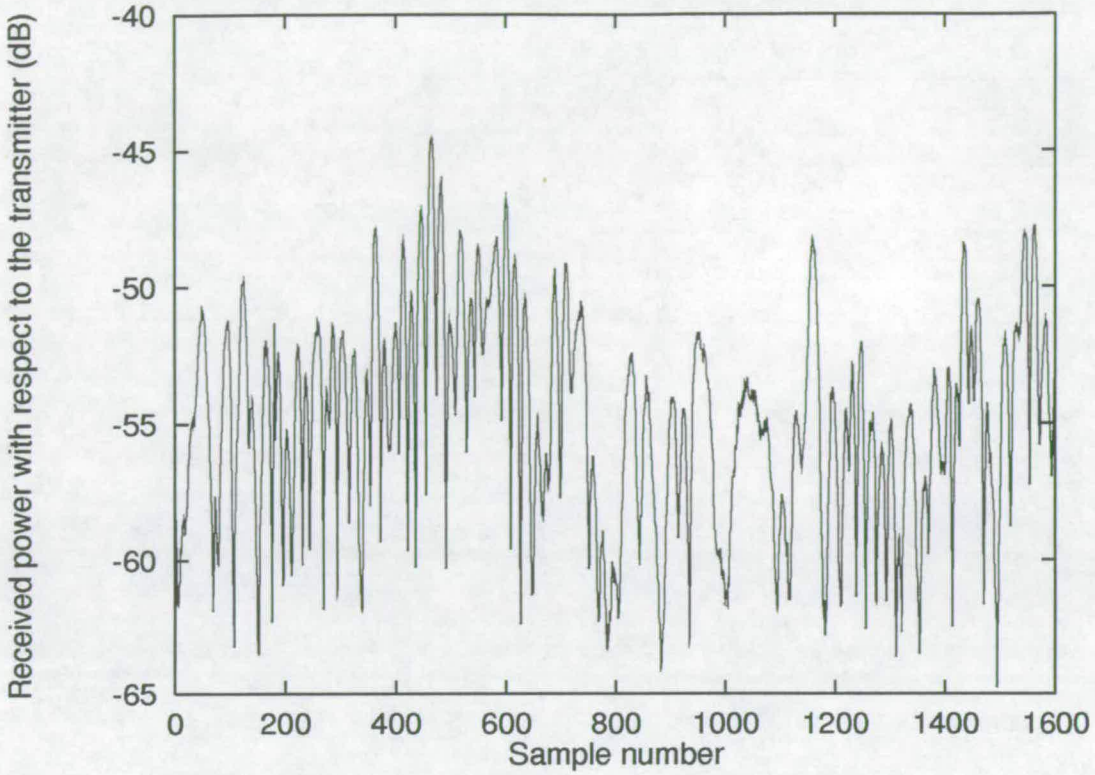

Figure 4–3: Sample of a measurement run at Site A

4.2.2 Site B measurements

The measurements performed at Site B were conducted by Todd *et al.* [30] in a populated floor of the Department of Systems and Computer Engineering at Carleton University. The building is a fully furnished one, with personnel moving around during the experiments. The building construction consisted of cement floors with linoleum tiles over the floor, plasterboard walls with metal frames, and a false ceiling below a corrugated steel roof. The doors within the building were constructed from steel, and windows were reinforced with wire mesh. The simplified floor plan of this building is shown in Figure 4–4 illustrating the 30m $\times$ 45m building. The shaded area of the figure represents a set of metallic lockers that partition the room into two offices.

The receiver is located centrally in the building with test sites distributed over the floor area. Measurements of received signal strength were collected while moving the mobile transmitting antenna in a circular pattern of 1m cir-

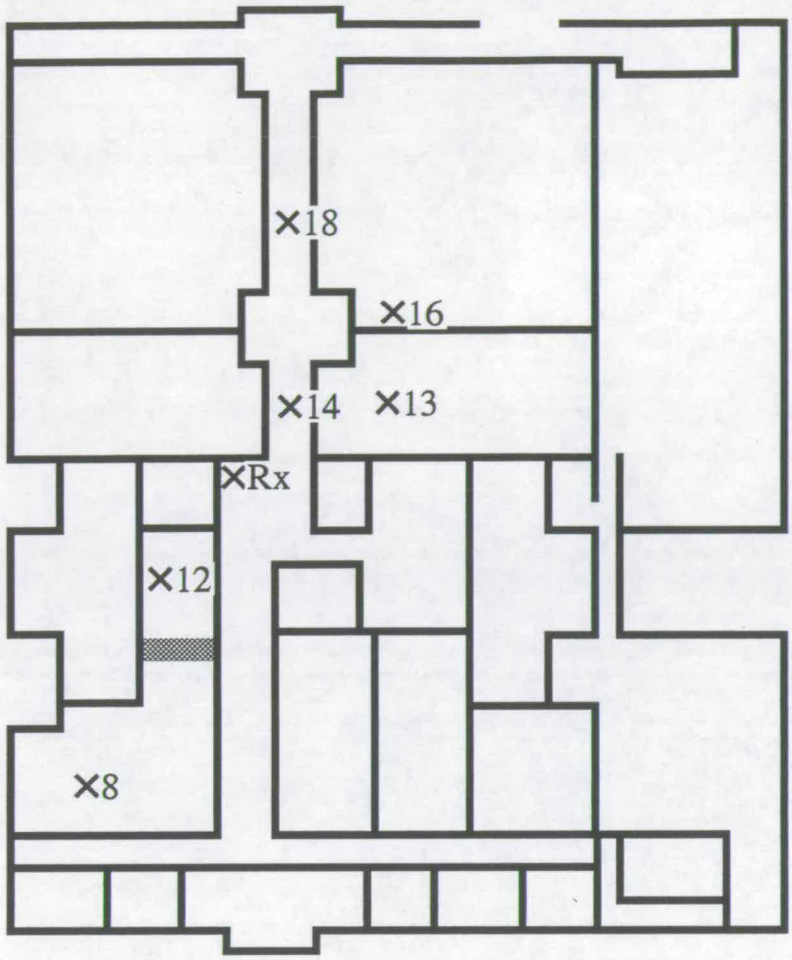

Figure 4–4: Schematic of floor at Site B

cumference, defined by a wooden assembly. The experiments were conducted with two antennae, and two transmitter frequencies centred at 1.75GHz. Once again a continuous wave (CW) was transmitted. The primary aim of the experiment was to determine the advantages of using frequency and spatial diversity, and to analyse various combining strategies.

Data obtained from experiments conducted around locations 8, 12, 13, 14, 16 and 18, indicated on Figure 4–4, were kindly made available for use in this work by the authors of [30].

A section of the power profile for one antenna at one frequency of an experimental run is shown in Figure 4–5. From this figure, the regular speed of the transmitting antenna movement can be observed as the fades are separated

by regularly spaced distances. Once again the slowly fading component of the signal can be seen as an overall trend of variation over the plot. The section of data shown relates to the signals received from a transmitter moved around location 8 of Figure 4–4.

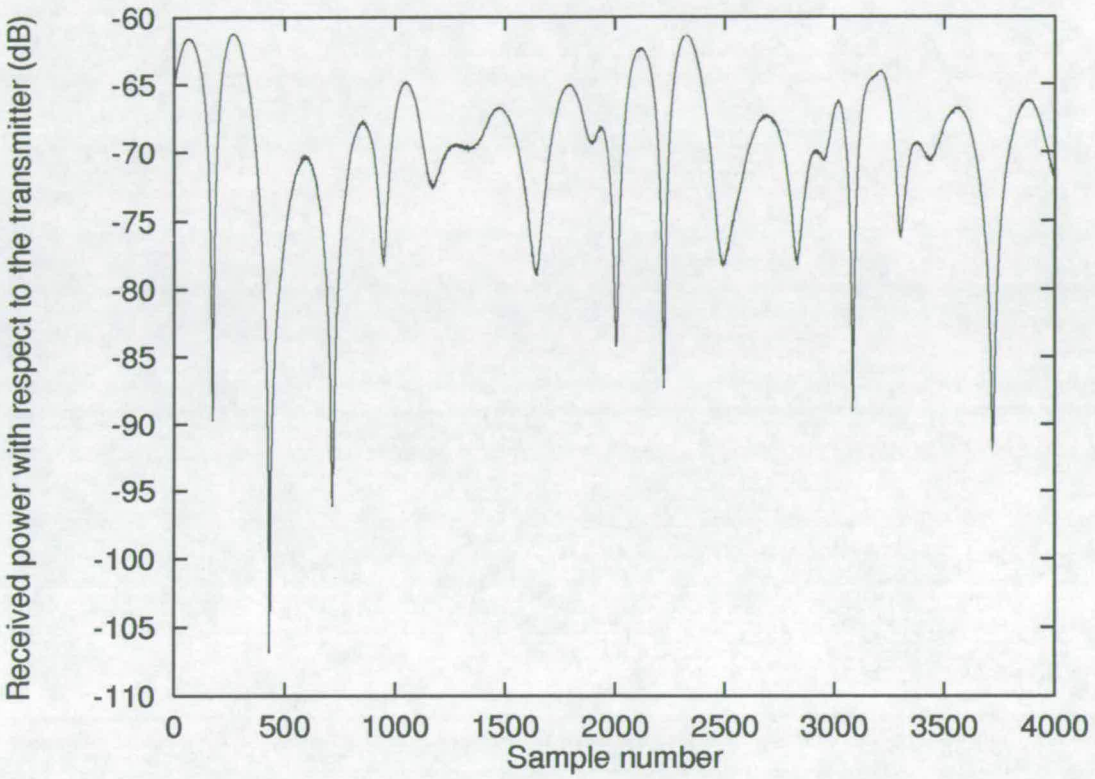

Figure 4–5: Sample of experimental run at Site B

It is worth noting that the two sites have similar dimensions in terms of wavelength distances. Site A is 64m wide, that is approximately 200 wavelengths, and Site B is 30m wide, also approximately 200 wavelengths for the higher frequency of operation. In Figures 4–1 and 4–4 the two buildings are shown to the same scale relative to a wavelength distance.

4.3 Basic narrowband ray tracing model

In this section we will deal with a basic ray tracing model based solely on geometrical optics, with no regard to the electromagnetic properties of construction materials nor any account taken of propagation by diffraction. Such a model, although it is basic, may be used for the modelling of complex structures due to its simplicity and speed of execution when implemented in a simulation system.

4.3.1 Model design

The model that we will consider consists of a description of the environment, within which the communication system is operating, in the form of a list of panels, or walls, and fixed reflection and transmission coefficients associated with each panel. The fixed coefficients obviate the calculation of the angle of arrival at a panel which would otherwise be necessary for the determination of the reflection or transmission coefficients as outlined in Section 3.3.

To evaluate the characteristics of such a model, a simple office environment was constructed which was 83 wavelengths long and 55 wavelengths wide with the schematic shown in Figure 4–6. Table 4–1 outlines the constants and parameters chosen for this experimental environment. Using this construction, a sample phase and power plot were produced from the simulation system described above. The results of this are shown in Figures 4–7 and 4–8 for the section of the receiver track highlighted in the diagram.

From the figures the general characteristic of fades occurring every half wavelength of distance travelled can be observed. In addition to this, a discontinuity at just over 9 wavelengths along the section of track can be observed in the power profile, and an associated phase reversal can be seen in the phase profile. This discontinuity can be attributed directly to the effects of the corner close to the receiver track obstructing one of the propagation paths, indicated in Figure 4–6 by a shaded line reflected off one of the walls. This shows that

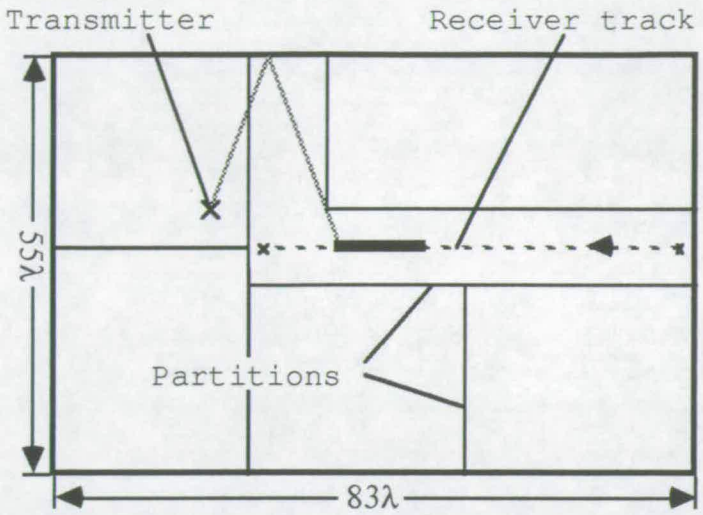

Figure 4–6: Schematic of a simple office environment

Building Height	16 wavelengths
Transmitter height	11 wavelengths
Receiver height	9 wavelengths
Wall reflection coefficient	0.5, 50%
Floor reflection coefficient	0.3, 30%
Ceiling reflection coefficient	0.1, 10%
Wall transmission coefficient	0.45, 45%

Table 4–1: Data for the basic office environment

geometric optics predict that the fields produced from such a scenario are discontinuous, which is not the case in reality. Including the effects of diffraction around this corner, using a model such as the UTD model, would produce a continuous result which would be observed in the power plot as a smooth change between the two sections of the curve.

The remaining phase reversals in the figures are associated with the periods of deepest fading in the power plot. This can be associated with an increasing path length in the main contributor(s) to the overall received signal, which in the case of this experiment must be a reflected wave. Analysis of the contributing signals in the simulated system reveals that, in some cases, the reversal of phase is associated with the electromagnetic waves travelling in the opposite

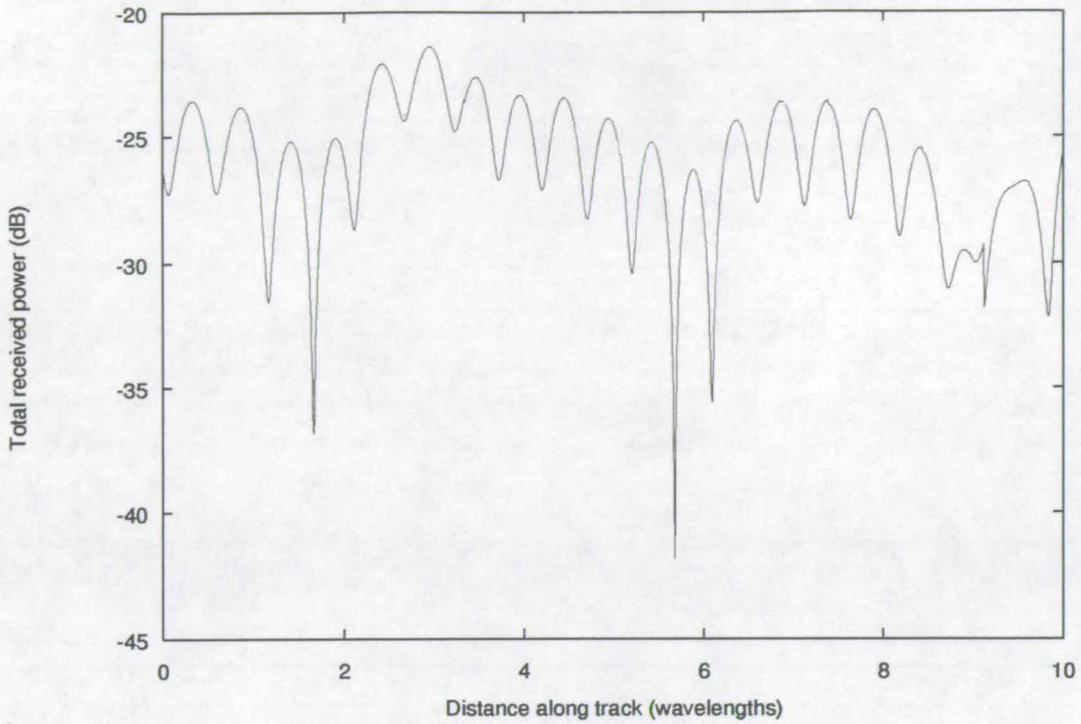

Figure 4–7: Power profile for simple office

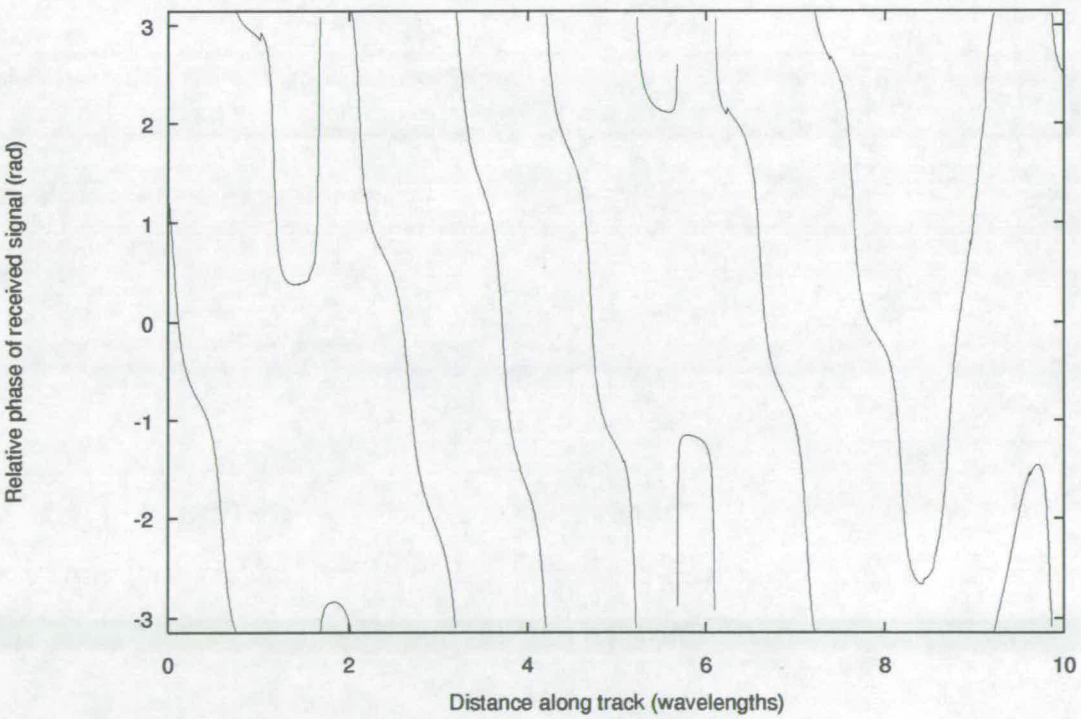

Figure 4–8: Phase profile for simple office

direction to the receiver adding destructively, resulting in the major contributor being the reflected wave from the wall at the far end of the receiver track.

The above example is an artificially constructed one and shows little about the types of signals to be expected in the real environment, its purpose being to illustrate some of the features of the ray tracing model in its most basic form. In order to compare the model with a realistic environment, and compare the results with measured data from that environment, the floor plan of the empty floor in Site A (Figure 4–1) was converted into a set of panels with reflection and transmission coefficients. The values of principal variables selected for the simulation run are shown in Table 4–2. The values of reflection and transmission coefficients, in the absence of other data, contrary or otherwise, were arrived at through a process of empirical determination of likely values, and refinement of those values with reference to the results of the measurement experiments.

Using the model as described above, with the data given in Table 4–2, the experimental procedure described in Section 4.2.1 was simulated in the following manner. The building area was divided into 64 8m×8m squares corresponding to the 64 squares used in the measurement procedure. Within each of these areas, one experimental run was executed. An experimental run, for this particular simulation, consists of selecting 1000 random transmitter positions within the 8m×8m grid prescribing this experimental run. The ray tracing code is executed for each of the transmitter positions to calculate the received signal power. The mean value of all of the received powers is determined, that value being assigned to the centre point of the square under consideration. Once all of the 64 experimental runs are completed, a plot of average signal power as the transmitter moves around the building may be constructed. This whole process involves consideration of over 30000 images for each transmitter position, most of which will not form a contribution to the received signal due to either falling below the low signal threshold, or being excluded due to the finite size of the reflecting surfaces. The programme takes 40 hours to run to completion on a Sun 4 ELC workstation.

Noise floor	-80dB
Low signal power cut off[a]	-80dB
Ceiling height	2.3m
Receiver height	2.05m
Transmitter height	0.9m–1.8m
Area of experimental runs	8m × 8m
Building size	64m × 64m
Floor reflection coefficient	0.2, 20%
Ceiling reflection coefficient	0.0, 0%
External wall reflection coefficient	0.025, 2.5%
Internal wall reflection coefficient	0.15, 15%
Internal wall transmission coefficient	0.4, 40%
Soft partition reflection coefficient	0.25, 25%
Soft partition transmission coefficient	0.3, 30%
Elevator wall reflection coefficient	0.35, 35%
Elevator wall transmission coefficient	0.05, 5%
Number of samples per experimental run	1000

[a]See Section 3.7 of Appendix B for an explanation of the significance of the low power value

Table 4–2: Principal values for simulation of Site A

The resulting two dimensional plot of average signal power over the building, to be compared with Figure 4–2, is shown in Figure 4–9. Common features can be seen in both plots, with areas of similar average signal amplitude at the corners of the building, and close to the receiver location. The simulation modelling of the area at the centre of the building varies from the measured results, however the measured results for this area are interpolated values from the measurements made around the perimeter of the area "A" of Figure 4–2. A distinct rise can be observed in the measured results for the areas at the left of the plot opposite the end of the central corridor, and at the top left of the building. These features are evident in the simulated results as well, albeit in magnified form.

In order to investigate further the similarities and differences between the channel of the simulated environment, and the channel experienced during the

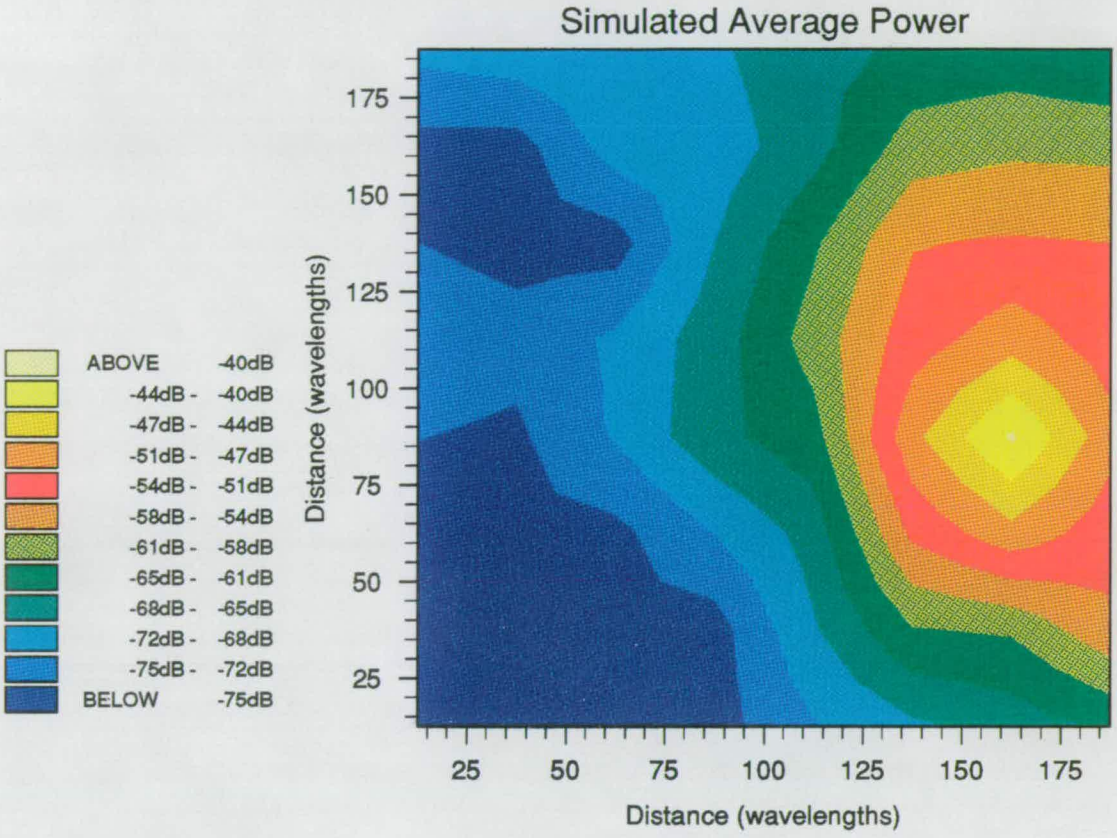

Figure 4–9: Plot of simulated signal power over the empty floor of Site A

measurement procedure in the real environment, a probability density graph (Appendix B) of signal amplitude as the transmitter moves around within one of the 8m×8m squares that were used to plot the variation of received signal power as the transmitter moved around the building is plotted in Figure 4–10. The probability density graph of the measured signal amplitude is formed from the data obtained on one 60s experiment consisting of moving the transmitter within an 8m×8m square. Data consisting of 1000 simulated signal amplitudes taken for random transmitter locations within the corresponding 8m×8m square in the simulated environment were combined to form the probability density graph of the simulated signal amplitude.

From this plot it is clear that the simulated channel is characterised by a probability function with different parameters from the measured channel. It

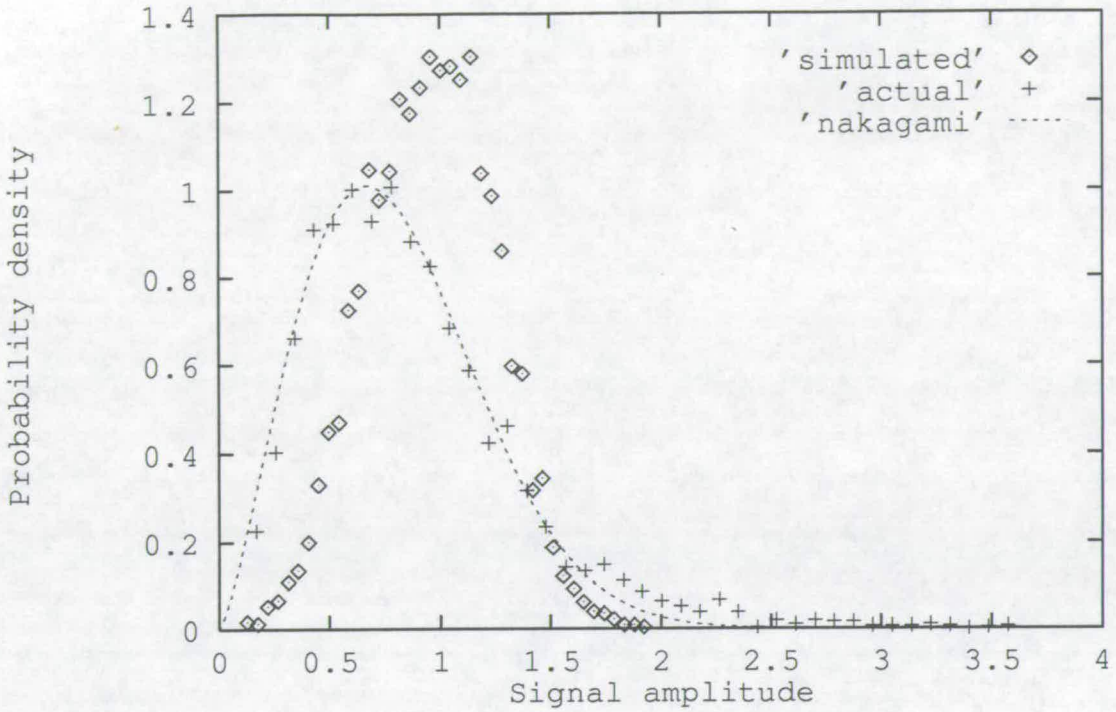

Figure 4–10: Simulated and actual probability density functions with closest fitting Nakagami curve to the measured data

is worth noting, though, that both sets of results are closely modelled by a Nakagami distribution (Appendix C).

The Nakagami distribution, like the Rayleigh and Ricean distributions, is based on the Normal, or Gaussian, distribution. The Nakagami probability density function is described by

$$p(R) = \frac{2m^m}{\Gamma(m)\Omega^m} R^{2m-1} \exp\left(-\frac{m}{\Omega}R^2\right) \quad R \geq 0 \tag{4.1}$$

where m is a shape parameter, and Ω controls the spread of the distribution. For integer values of m, the distribution describes the summation of m orthogonal independent Rayleigh distributed random variables. That is, for N Rayleigh distributed random variables X_i, the probability density function of the random variable Y, defined as

$$Y = \sqrt{\sum_{i=1}^{N} X_i^2}\,, \tag{4.2}$$

is given by a Nakagami distribution with $m = N$. For $m = 1$, the Nakagami distribution reduces to the Rayleigh distribution. The Nakagami distribution has the additional property that it can closely approximate a Ricean distribution. On fitting the Nakagami distribution to the probability distributions of the fading measured on radio channels, it is found, in many cases, to describe the data with greater accuracy than a Ricean distribution, and, by definition, can be no worse than a Rayleigh distribution.

The Rayleigh distribution arises frequently in channel modelling as it describes the signal amplitude resulting from a large number of multipath components, each with approximately the same amplitude, adding together. It is described by the following probability density function:

$$p(R) = \frac{R}{\sigma^2} \exp\left(-\frac{R^2}{2\sigma^2}\right) \quad R \geq 0\,, \tag{4.3}$$

where σ controls the variance of the distribution. The Ricean distribution describes a signal amplitude distribution where the multipath components form an underlying Rayleigh process, with one dominant component arising from a line of sight path between the transmitter and the receiver. It is described by the two parameter probability density function

$$p(R) = \frac{R}{\sigma^2} \exp\left(-\frac{R^2 + s^2}{2\sigma^2}\right) I_0\left(\frac{Rs}{\sigma^2}\right) \quad R \geq 0\,, \tag{4.4}$$

where s controls the mean of the distribution, σ its variance, and $I_0(\cdot)$ the modified Bessel function of the first kind, order zero.

On further examination, it is found that the Nakagami distribution models the majority of measured and simulated results more closely than a Ricean distribution, and more closely than the Rayleigh distribution. This implies that the assumptions used to derive a Rayleigh or Ricean distributed channel are not valid for indoor communications. As will be seen in Section 6.3, the assumption that all of the multipath signals arriving at the receiver are of equal magnitude does not hold.

From Figures 4–2, 4–9 and 4–10, it can be observed that the simulated system does not model the measured data exactly, however there is a degree

of similarity between the plots of the simulated and measured results. The differences between the simulated results and the measured results can be accounted for by considering three factors:

- Model simplifications
- Assumptions used to construct the model
- Experimental procedure.

In the three sections that follow, each of these factors will be considered in turn.

4.3.2 Model simplifications

In the simulation model a number of simplifications are made, both in the propagation mechanisms that are available, and in the construction of the set of panels describing the building. The model assumes that reflection occurs only on smooth surfaces, and consequently the reflected signal is well defined in amplitude and phase. To a receiver, the reflected signal from a smooth surface is observed as if it were emanating from a perfect transmitter, with attenuated amplitude, located on the other side of the reflecting plane. In contrast, the reflected signal from a rough surface is observed as a less well defined transmitter whose amplitude and phase fluctuates as the receiver changes position. In addition to the smooth surface simplification, a further simplification is made by ignoring the effects of finite size of the planes. The simulation system assumes that a reflecting object can be treated as an infinite reflector when a reflected path exists, and can be ignored when one does not. No account is taken of the Fresnel zone associated with electromagnetic propagation. In order to correct this, the UTD [89] would have to be incorporated into the model.

Propagation resulting from diffracting corners and edges is also not included in this basic model. As there are a number of diffracting components in the building, the pillars located at the vertices of each measurement square constituting a sizable number of diffracting components neglected in the simulation, this may be a significant factor in the differences of results between the simulated system and the measurements.

The transmitter and the receiver are assumed to be lossless components in the system, and both are assumed to incorporate omnidirectional antennae of unity gain. In addition to this, the effects of polarization, and more importantly depolarization, are ignored.

4.3.3 Assumptions used to construct the model

A number of parameters were not available for constructing the simulation system, among them the reflection and transmission coefficients for the walls, ceiling, floor and partitions. Values for these parameters were estimated with reference to [77] and on consultation with members of Carleton University engaged in channel measurements. However, as indicated in Section 3.3, assuming that these parameters can be represented by constants regardless of the angle of incidence of a plane wave is an oversimplification of the propagation mechanisms involved.

4.3.4 Experimental procedure

Unfortunately, the experimental procedure used to conduct the measurements at Site A was not well controlled. A number of factors contribute to the dubiety of the application of these results to anything more than a general verification of the simulation results. The lack of control over the height of the transmitting antenna, and its orientation with respect to the receiving antenna, form one major source of experimental uncertainty. In addition to this, the degree to which an area for a given measurement run is covered is uncertain, but must be assumed to be uniform over the area in the absence of any other information.

A further factor accounting for some difference between the measured and the simulated results is the presence of a human body in proximity of the transmitter. At times, the person conducting the measurements would stand in the line of sight path between the transmitter and the receiver, acting as an absorber, and therefore affecting the results. Even if the line of sight had been preserved at all times, the effect of a body close to the transmitter can not fully

be ignored as a number of reflected paths may be obstructed even when the line of sight path is not. Unfortunately, this source of uncertainty exists in the majority of channel measurement procedures.

4.4 Ray Tracing Model including the effects of Diffraction

The model as described previously neglects the effects of diffracting edges in the simulation, and may be a contributing factor in the difference between the simulated results and the measured results. To improve the accuracy of the simulation system, the effects of diffracting corners can be incorporated into the simulation. On examination it becomes clear that in the indoor environment, except perhaps for partitions, the only diffracting features of the building structure are corners, and then only on their external side, that is one which juts out towards the source of the electromagnetic wave, and not those at the edges of an enclosed space which are directed away from the source of the electromagnetic wave. This can be observed by setting n of (3.31) to $\frac{1}{2}$ representing a wedge of interior angle $\frac{3\pi}{2}$. In this case, (3.31) simplifies to $D = 0$. Thus we need only deal with a limited set of corners.

As Site A contains a large number of potential diffractors in the form of the supporting pillars that are ignored in the basic simulation above, it was deemed prudent to use the measured data for Site B to assist in the comparison of the two models. In addition, the tighter control over the experimental procedure used in the measurements for Site B increase confidence in their validity. In conjunction with the floor plan shown in Figure 4–4, the information shown in Table 4–3 was used in creating the simulation of the environment. Values of reflection coefficients for the ceiling, floor and walls of this simulation were taken from the simulation previously conducted for Site A, as was the value of the transmission coefficient for internal walls.

For each of the locations marked on the diagram, the set of measured results that relate to that particular experimental run are compared with the data

Noise floor	-80dB
Low signal power cut off	-80dB
Ceiling height	2.4m
Lower ceiling in one area	2.2m
Receiver height	1.6m
Transmitter height	1.6m
Radius of circular track	0.16m
Wall reflection coefficient	0.15, 15%
Floor reflection coefficient	0.2, 20%
Ceiling reflection coefficient	0, 0%
Wall transmission coefficient	0.4, 40%

Table 4–3: Principal values for basic model simulation of Site B

obtained from the corresponding simulation experiment. Both of the results are then compared with the closest fitting Nakagami distribution defined by the MoMSE criterion (Appendix B). Table 4–4 gives a list of the results of this analysis in terms of the Nakagami distributions that best fit the data around the six locations identified previously in Figure 4–4. Figure 4–11 shows the comparison of the two data sets for location 8 with the Nakagami distribution that most closely models the measured results.

(m,Ω)	Measured	Simulated
Location 8	$(0.997, 1.92 \times 10^{-7})$	$(1.509, 1.25 \times 10^{-7})$
Location 12	$(1.044, 5.50 \times 10^{-6})$	$(2.450, 1.73 \times 10^{-6})$
Location 13	$(0.953, 1.05 \times 10^{-6})$	$(2.285, 5.90 \times 10^{-7})$
Location 14	$(1.096, 1.67 \times 10^{-5})$	$(1.242, 1.89 \times 10^{-6})$
Location 16	$(1.007, 5.12 \times 10^{-7})$	$(1.043, 6.16 \times 10^{-8})$
Location 18	$(0.982, 5.81 \times 10^{-7})$	$(1.844, 3.00 \times 10^{-7})$

Table 4–4: Results from measurement and simulation of Site B

The table shows that the simulated results obtained for locations 13 and 18 in particular have shape and mean values that vary considerably from the measured results. Neither location is in a position such that diffraction plays an important rôle as a primary source of received signal. This would indicate that the coefficients for transmission and in particular for reflection that have

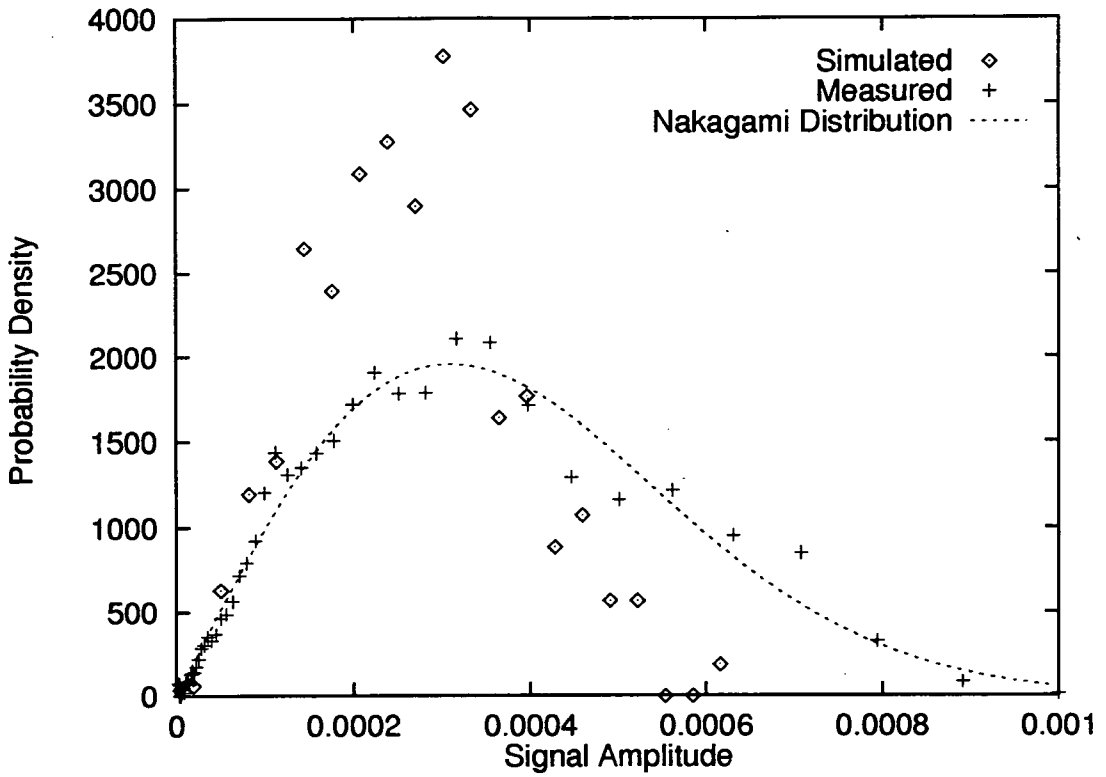

Figure 4–11: Measured and simulated probability density function for experiments conducted at location 8

been chosen are too low. The fact that the reflection coefficient is too low can be deduced from the data given for location 14 as the reflection coefficient that is involved in the propagation of a diffracted ray to location 14 is critical in calculation of the received power. The simulation results for locations 8 and 16 where power is mainly from transmitted rays and diffracted rays the results are closer to the measured results. The simulation results for location 12 are significantly different from the measured results. In addition to the lack of information on transmissivity and reflectivity of the building structure, one possible source of error that particularly relates to the experiment conducted at locations 8 and 12 is the effect of a metallic locker structure that partitions the room into two. The reflection and transmission characteristics of this locker are unknown. Some of the additional sources of the differences in the simulation can be identified as

- fixed transmission and reflection coefficients

- neglecting the effects of scattering
- neglecting the effects of the human experimenter conducting the measurements
- neglecting the movement of other personnel in the building
- no furniture is modelled
- inexact transcription from the building plan to the actual environment and to the simulation.

Some of the sources of the differences, such as the last two items, are limitations of any modelling system as simplifications must be made, and assumptions that the information provided on the environment is an exact representation of that environment without any margin of error. Similarly, modelling the effects of human movement in a building proves to be a highly complex task, and is generally impossible to quantify in enough detail to model the environment with a reasonable degree of accuracy.

From the list given above, the sources of difference between the simulation results and the measured results over which some degree of control can be exerted are the simplifications of surfaces to having fixed reflection and transmission coefficients, and the assumption that the surfaces are perfectly smooth, and therefore do not scatter reflected signals. In order to correct the first of these simplifications, the electromagnetic properties of the walls must be determined, and the polarization dependent reflection and transmission coefficients derived from these results.

Scattering from rough surfaces involves the ray tracing algorithm increasing the complexity of its calculations to such an extent that running such a simulation on a building such as Site B becomes impossible as the time taken to perform the simulation is too great. The simulation of the ray tracing model is developed in order to understand the major propagation characteristics of the indoor environment. Refining this model to include scattering in order to generate a more accurate simulation of the real environment, while providing a better simulation, does not necessarily result in much more useful information on the propagation mechanisms. Addition of scattering into the simulation

package will result in the multipath components arriving at the receiver being spread out in time and having variations in amplitude. Providing that the surfaces from which the scattering is occurring are not too rough, the other model inaccuracies will far outweigh the benefits of incorporating scattering into the simulator.

4.4.1 Ray Tracing Model incorporating the Geometrical Theory of Diffraction

The initial basic model outlined at the beginning of the chapter neglects the effects of diffraction in the environment, which may have a significant rôle in the propagation of electromagnetic waves in the indoor environment. In order to investigate this process more thoroughly, it is necessary to construct a model that models diffraction, as the one described in the previous section does, and compare it with one that ignores this propagation mechanism.

In an environment with few reflecting objects, or where the transmitter to receiver path is shadowed, diffraction may play a crucial rôle in the propagation of the signal from the transmitter to the receiver. This is most often seen in the outdoor environment where one of the communicating entities is frequently shadowed by buildings. Models such as those developed by Lebherz *et al.* [76] and Saunders and Bonar [94] incorporate diffraction as one of the significant contributors to the combined electromagnetic field at the receiver. However, for the indoor environment where a larger number of reflecting objects exist, more paths resulting from reflections alone will exist, and the degree to which diffracting paths affect the resulting received signal needs to be determined.

For two of the locations in Site B, locations 8 and 13, the simulation described above was repeated after removing the effects of diffraction. The results of this simulation are shown in Table 4–5 in the form of the best fitting Nakagami distributions, and for location 8 in Figure 4–12.

From the table and the figure, clearly the effects of diffraction do not significantly alter the distribution of the small scale fading statistics, nor the large scale mean of the system. From analysis of the propagation mechanism, it can

Location 8			
	m	Ω	MoMSE
Measured data	0.997	1.915×10^{-7}	0.0127
Simulated with diffraction	1.509	8.959×10^{-8}	0.0457
Simulated without diffraction	1.492	7.721×10^{-8}	0.0273
Location 13			
	m	Ω	MoMSE
Measured data	0.953	1.046×10^{-6}	0.0215
Simulated with diffraction	2.285	5.902×10^{-7}	0.0277
Simulated without diffraction	3.006	6.083×10^{-7}	0.0333

Table 4–5: Comparison of diffracting and non-diffracting models

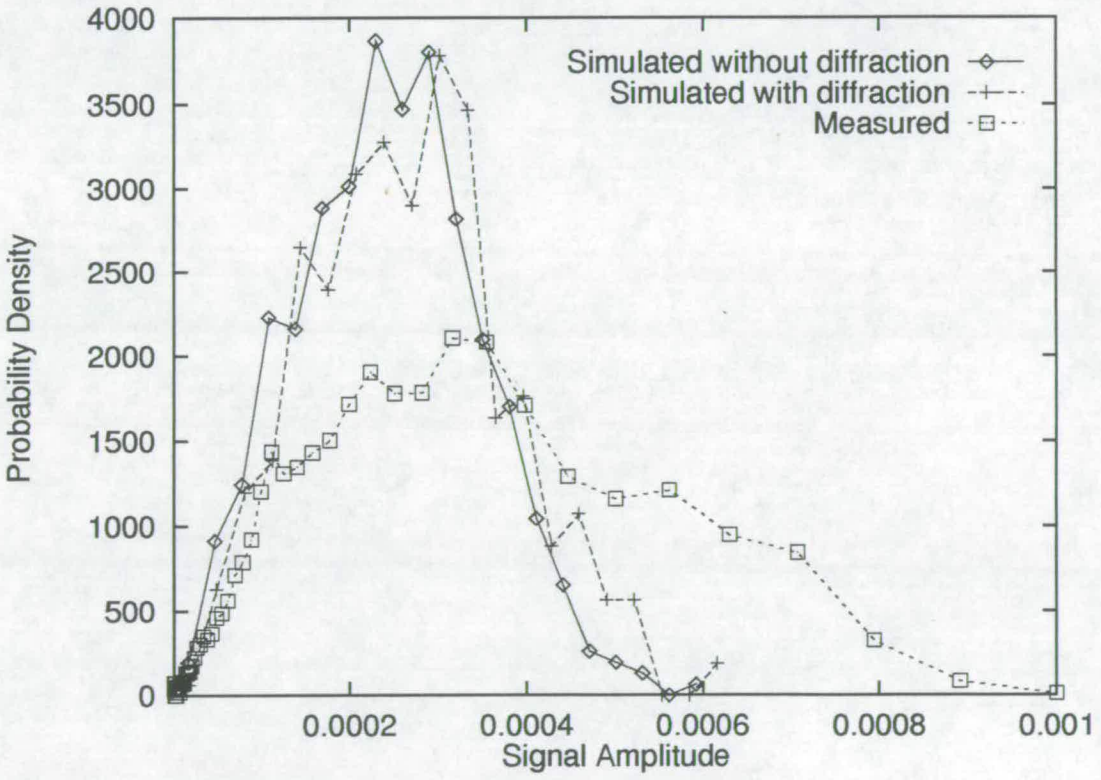

Figure 4–12: Comparison of models that incorporate and ignore diffraction

be seen that diffraction, being an expanding form of propagation, makes only a small contribution to the overall received signal for receivers not located close to the diffracting edge. The diffraction coefficient defined in (3.31) relates the diffracted field to the incident field, which in the case of the indoor situation, is expanding with respect to $1/s$ where s is the distance from the transmitter. Equation (3.30) indicates that the incident field, which has already been attenuated because of expansion, is then further attenuated with respect to $1/\sqrt{r}$ where r is the distance of the receiver from the edge. The two stage expansion process results in the field being received via diffraction having a much lower amplitude than a reflected field of the same path length. This accounts for the observed insensitivity to diffraction.

Thus it is proposed that diffraction, while playing a crucial rôle in propagation of electromagnetic transmission in a number of environments and scenarios, contributes only a small portion of the total received signal in the indoor environment for most transmitter and receiver positions. Clearly the details of the particular environment within which the transmitter and receiver operate will dictate how important diffraction will be, however in general for the indoor environment with a large number of reflecting objects, there will be few transmitter and receiver positions where reflections will not form the major part of the received signal. By ignoring the effects of diffraction in a simulation system, the execution time for a large system, such as Site B, can be dramatically reduced at the expense of some accuracy.

The ray tracing algorithm has a complexity of $O(n^k(n + d))$, that is execution time $\propto n^k(n + d)$, where n is the number of surfaces in the environment, d the number of diffracting edges and k the maximum number of reflection and diffractions in any one path from the transmitter to the receiver. By neglecting the effects of diffraction, the complexity of the system reduces to $O(n^{k+1})$, and the programme execution time is reduced by a factor of $\frac{n+d}{n}$.

With the effects of diffraction incorporated in the model, the simulation system takes 500 processor hours of computation time on a parallel computer to calculate the received signal from 500 transmitter positions. This time may

be reduced to 340 hours by neglecting the effects of diffraction. As the simulation system is not attempting to predict the received signal for a particular environment, but is to be used as a tool to determine the major factors affecting radio propagation, such loss in accuracy is acceptable as the execution time is reduced.

4.5 Conclusions

This chapter has described the measurement of the radio channel in two environments, and simulations that attempt to recreate the results obtained. The ray tracing simulation approach, while not producing results that exactly match the measured results, does produce a reasonable approximation to the measured results with respect to the average signal power. Probability distribution functions of signal amplitude during each experimental run do differ from those of the measured channel, however both measured and simulated distributions are closely modelled by Nakagami distributions.

From analysis of differing degrees of complexity in modelling it was ascertained that diffraction plays a limited rôle in propagation for the indoor environment, and therefore can in general be neglected if exact models are not required. In order to increase the accuracy of the simulation model investigation into the effect that scattering and the electromagnetic nature of structures has on the propagation of electromagnetic signals needs to be incorporated into the model. As the electromagnetic modelling of the structures within an environment needs to be conducted before the effects of scattering determined, the following chapter will describe the results from an electromagnetic based simulation model. It will be found that due to the limitations of computing resources, it becomes infeasible to incorporate the effects of scattering in addition to this. However, for surfaces with small feature sizes compared to the transmission wavelength such a simplification is not invalid.

Chapter 5

Electromagnetic Simulation

5.1 Introduction

In the previous chapter, a set of simulation results were presented for various degrees of modelling complexity. In this chapter, the results of a simulation model that is at the limit of complexity for the computing resources available are presented. This model uses the electromagnetic properties of the structures in the building to determine the reflection and transmission coefficients for polarized fields that are incident on the structures. Figures for the conductivity and permittivity of typical building structures are, for want of more accurate information, derived from results of measurements made on the electromagnetic properties of concrete. Due to the inordinate length of time taken to conduct the simulation experiments, 1500 processor hours of computation time for 300 transmitter positions when the effects of diffraction are incorporated in the simulation, the results of modelling the channel with and without diffraction as a propagation mechanism are presented for one experimental location, the remainder of the experiments being conducted without incorporating the effects of diffraction. An analysis of each experiment is presented with reference to the physical structure of the environment.

5.2 Ray Tracing Model incorporating Electromagnetic Polarization

One of the assumptions inherent in the models described in the previous chapter is that of a constant value for the reflection and transmission coefficients, regardless of the angle of incidence and the polarization of the incoming electromagnetic wave. In order to correctly define the reflection and transmission coefficients it is necessary to know the electromagnetic properties of the surface off which the reflection is occurring, and the thickness of that surface as indicated in Section 3.3; consequently, the reflection and transmission coefficients for a given incident electromagnetic wave are dependent on the grazing angle of incidence, and also on the polarization of that wave.

Unfortunately, relatively little published literature is available describing the electromagnetic properties of construction material, the literature that does exist tends to be applied to non-destructive testing (NDT). Wilson and Whittington [95,96] give a detailed description of the determination of electromagnetic properties of concrete during the initial phase of drying out. In [96] a model for the electromagnetic properties of concrete, valid for frequencies between 1MHz and 100MHz, was presented as

$$\sigma = \sigma_B \frac{\omega^2 \tau_1^2}{1 + \omega^2 (\tau_1 + \tau_2)^2} \tag{5.1}$$

for the conductivity, and

$$\varepsilon_r = \frac{\varepsilon_s + \omega^2 \varepsilon_B (\tau_1 + \tau_2)^2}{1 + \omega^2 (\tau_1 + \tau_2)^2} \tag{5.2}$$

for the permittivity, where

$$\sigma_B = \frac{1}{\sigma_3}\left[\sigma_4 + \frac{\sigma_3 - \sigma_4}{1 + \omega^2\tau_4^2}\right]\left[\sigma_2 + \frac{(\sigma_3 - \sigma_2)\,\omega^2\tau_3^2}{1 + \omega^2\tau_3^2}\right], \tag{5.3}$$

$$\varepsilon_B = \frac{1}{\varepsilon_3}\left[\varepsilon_4 + \frac{\varepsilon_3 - \varepsilon_4}{1 + \omega^2\tau_4^2}\right]\left[\varepsilon_3 + \frac{\varepsilon_2 - \varepsilon_3}{1 + \omega^2\tau_3^2}\right]. \tag{5.4}$$

The constants σ_2, σ_3 and σ_4 are conductivity parameters; ε_2, ε_3 and ε_4 are dielectric constants; and τ_1, τ_2, τ_3 and τ_4 are time constants associated with

the physical properties of the material being considered. The values of these constants given for concrete are

$$\sigma_2 = 3.78 \times 10^{-2} \qquad \sigma_3 = 1.0 \qquad \sigma_4 = 6.25 \times 10^{-6}$$

$$\varepsilon_s = 9 \times 10^9 \qquad \varepsilon_2 = 60 \qquad \varepsilon_3 = -300 \qquad \varepsilon_4 = 8.19$$

$$\tau_1 = 1.5 \times 10^{-3} \qquad \tau_2 = 6.883 \times 10^{-9} \qquad \tau_3 = 2 \times 10^{-9} \qquad \tau_4 = 3.2 \times 10^{-9}$$

Using these values, and setting ω appropriately for 1.75GHz frequency operation, a value for n'^2 can be derived as $n'^2 = 7.92 + j8.35 \times 10^{-3}$ for use in (3.14) to (3.27). This value can then be used in determining the reflection and transmission coefficients for a simulation of Site B, assuming that the above model is extensible to the 1GHz range of frequencies.

However, it is not possible to use (3.24) to (3.27) for the simulation of Site B as neither the wall thickness is known, nor the degree of homogeneity within the wall. It is expected that the wall construction consists of plasterboard attached to some framework, causing medium II of the model described in Section 3.3 to be non-homogeneous, that is the medium cannot be described by an expedient choice of η, the intrinsic impedance of the medium. To simplify the simulation, the medium is assumed to be homogeneous, but only the primary reflection, and primary transmission are considered in the simulation, and in addition to this, the wall is assumed to be infinitely thin so that no further attenuation of the transmitted wave takes place. To this end, (3.14) and (3.15) are used for reflecting a horizontally and vertically polarized ray respectively, and (3.18) and (3.19) are used to describe the transmission of the ray through the wall.

Once again, Site B was selected as a suitable candidate for the simulation experiments in order to be able to compare the simulation results with measured data. The parameters for the simulation are set to those shown in Table 5–1.

Initially, the simulation was conducted on a complete description of Site B, including the diffracting corners within the building, for the experimental location 13 of Figure 4–4. Due to the nature of the simulation process, and the complexity involved in calculating the effects of the electromagnetic surfaces in the environment, the time required to perform this calculation was prohibitive, even when conducted on a 51 processor parallel machine. As a comparison, the

n'^2	$7.92 + j8.35 \times 10^{-3}$
Noise floor	-100dB
Low signal power cut off	-120dB
Maximum number of reflections	4
Ceiling height	2.4m
Lower ceiling in one area	2.2m
Receiver height	1.6m
Transmitter height	1.6m
Radius of circular track	0.16m

Table 5–1: Principal values for electromagnetic simulation of Site B

same simulation was performed using a description of the environment that does not incorporate any diffracting edges. This was to determine whether the effect observed in the previous chapter also holds true when the simulation model is using an electromagnetic description of the environment as opposed to one with fixed reflection and transmission coefficients. The result of this comparison is seen in Figure 5–1, and it is observed that the resulting two probability distributions, whilst they are not identical, are sufficiently close to be treated as the same when the approximations made in the calculations are taken into account. For the reason of the excessive computation time required to perform the simulation incorporating the effects of diffraction, and the small gain in accuracy that is obtained by doing so, comparisons between the simulated results and those obtained from measurements will be restricted to the simplified simulation that ignores the effects of diffraction.

The simulation was run for the six experiments conducted in Site B at the locations marked on Figure 4–4. The results for each of the simulation experiment, and its corresponding measurement experiment, are presented in the form of two graphs; one plotted on a linear scale for the signal amplitude, the second on a logarithmic scale. The two plots highlight various differences between the two sets of results. An analysis of the results of each experiment is presented below.

Location 8 Results for the experiments conducted at location 8 are presented

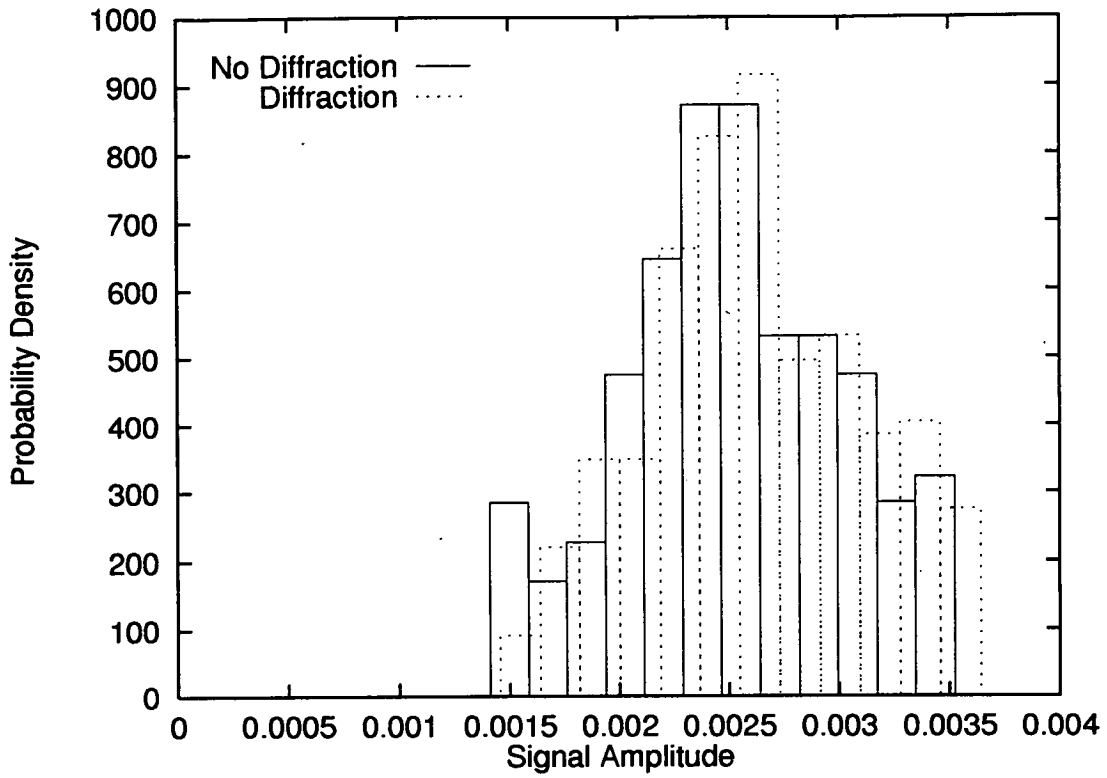

Figure 5–1: Comparison of probability distributions resulting from a simulation of location 13 that ignores the effects of diffraction, and one that incorporates the effects of diffraction in the model

in Figures 5–2 and 5–3. From Figure 5–2 the basic result that the simulation is producing signal amplitudes that exceed the measured results substantially can be observed. One possible reason for this difference is that the reflection and transmission coefficients that result from the electromagnetic properties chosen for the walls are more optimistic than the real environment. Such an error will result in the mean value for the distribution being higher in the simulation than experienced by the physical channel as we see here.

Figure 5–3, showing the two sets of results plotted on a logarithmic amplitude scale, indicates a second fundamental difference between the simulated results and the measured results. Not only are the simulated results higher in mean value, but the tails of the two distributions differ significantly. The measured results show a long tail at low signal levels

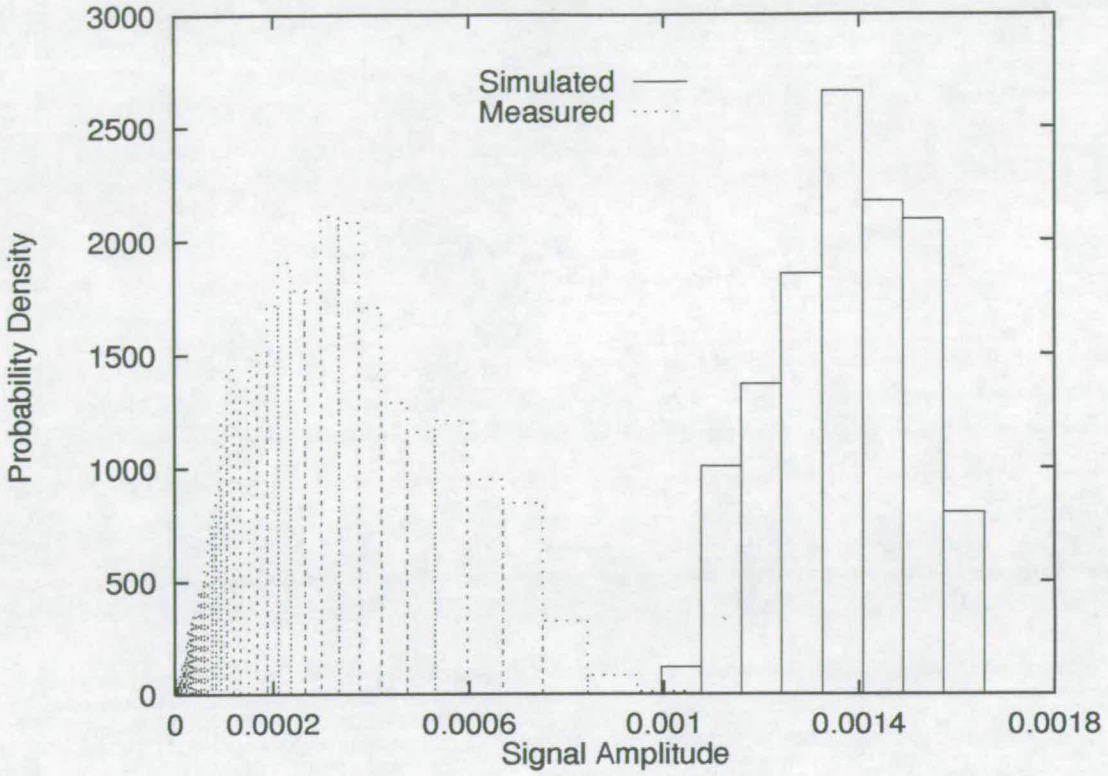

Figure 5–2: Simulated and measured results for location 8

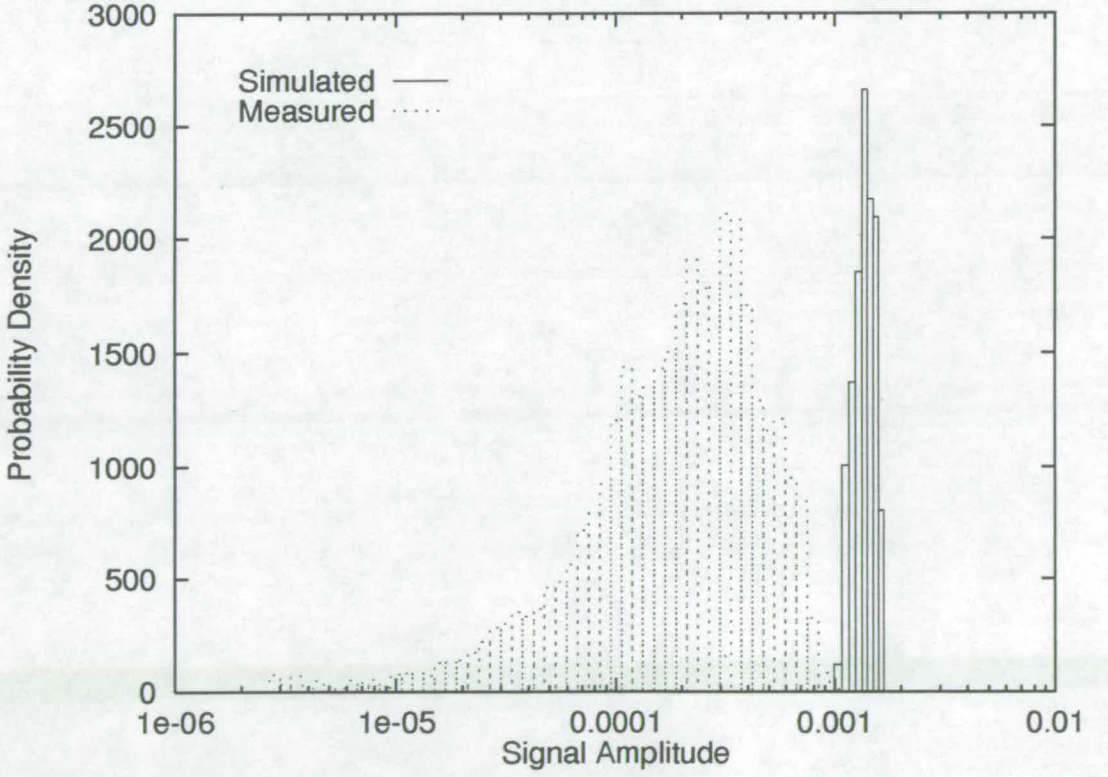

Figure 5–3: Simulated and measured results for location 8

and at high signal levels. The simulated results, on the other hand, indicate that the majority of the signal power is concentrated in the main peak of the distribution with little spreading around the mean.

The lowest signal powers experienced in a mobile radio system result from destructive interference of the dominant signal by a second dominant signal that is in anti-phase to the first. If the two signals are close in power, then the fade is a deep one, and correspondingly if the two signals are not close in power levels, then the fade is shallow. As the simulated results exhibit a very short tail at the low power region of the distribution, it can be deduced that the received signal is dominated by one strong signal arriving at the receiver—other signals arriving at the receiver being substantially smaller in magnitude. A similar argument can be proposed for the truncated tail at the high signal amplitude end of the distribution for the simulated results.

Location 8 is the experimental location furthest from the receiver, the two locations being separated by a number of walls, and a set of metallic lockers shown as a shaded area on Figure 4–4. The room within which the experiments were conducted contains other office furniture such as desks and chairs with metallic supports, and computers. The simulation takes no account of structures that do not form an integral part of the building, so the effect of these pieces of furnishings on the channel impulse response is neglected. As a result of neglecting to take account of the effects of the metallic lockers, the signal power leaving the room from the side closest to the receiver will be substantially higher than the practical situation. This gives rise to a substantially greater LOS component, and stronger reflections from the back wall of the room, resulting in the mean signal amplitude of the simulation results being significantly higher than that for the measured results.

Location 12 Figures 5–4 and 5–5 show the results of the comparison between simulated and measured results for the experiments conducted at location 12 of Site B. As found in the results of location 8 the mean value of

the simulated results exceeds those for the measured results, although the relative difference between the modal values of the two distributions is not as great.

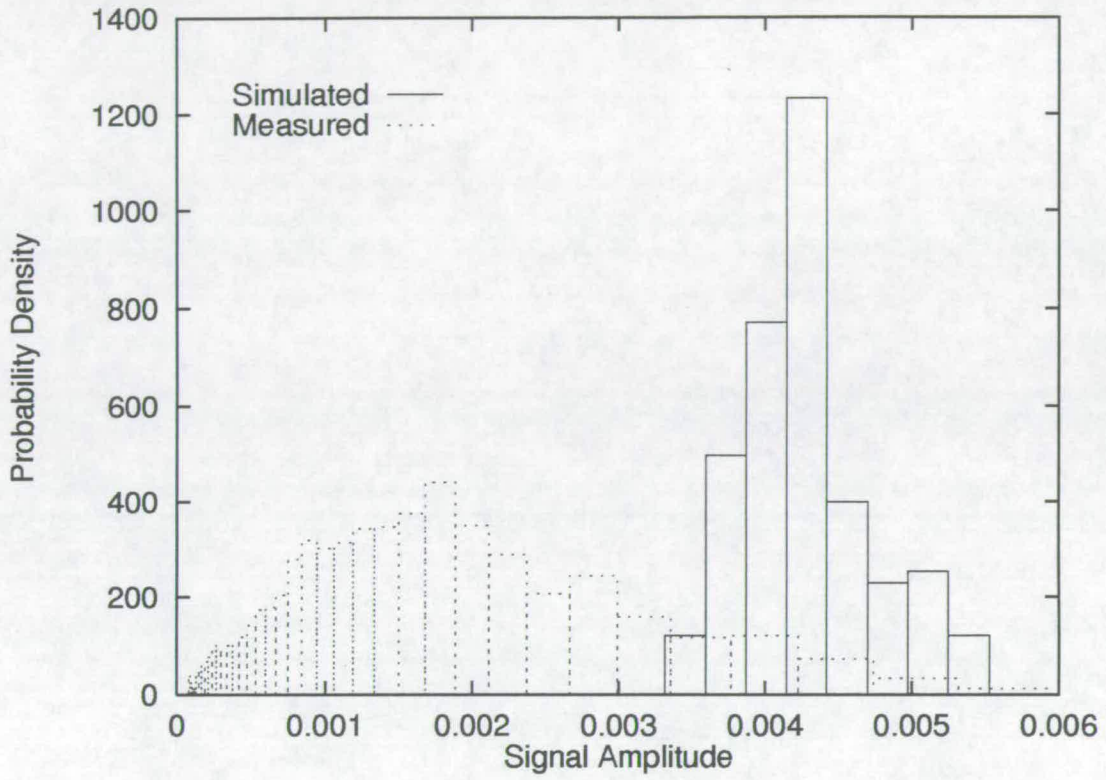

Figure 5–4: Simulated and measured results for location 12

Two possible causes can be proposed for this greater degree of conformance. Firstly, that as the LOS components, and its principal reflections, are passing through a wall, and not around a metallic locker as for location 8, the strength of these components is better defined. Assuming that this is the case, then examination of the results for location 8 in the light of the results shown here and for the other locations, will show that neglecting to model the locker structure has caused the received signal to be much stronger than found in the measured results. It should also be noted that although the measured results for location 12 include multipath signals reflected from the metallic locker, the signal strength of the simulated results are closer to those found on measurement than for location 8.

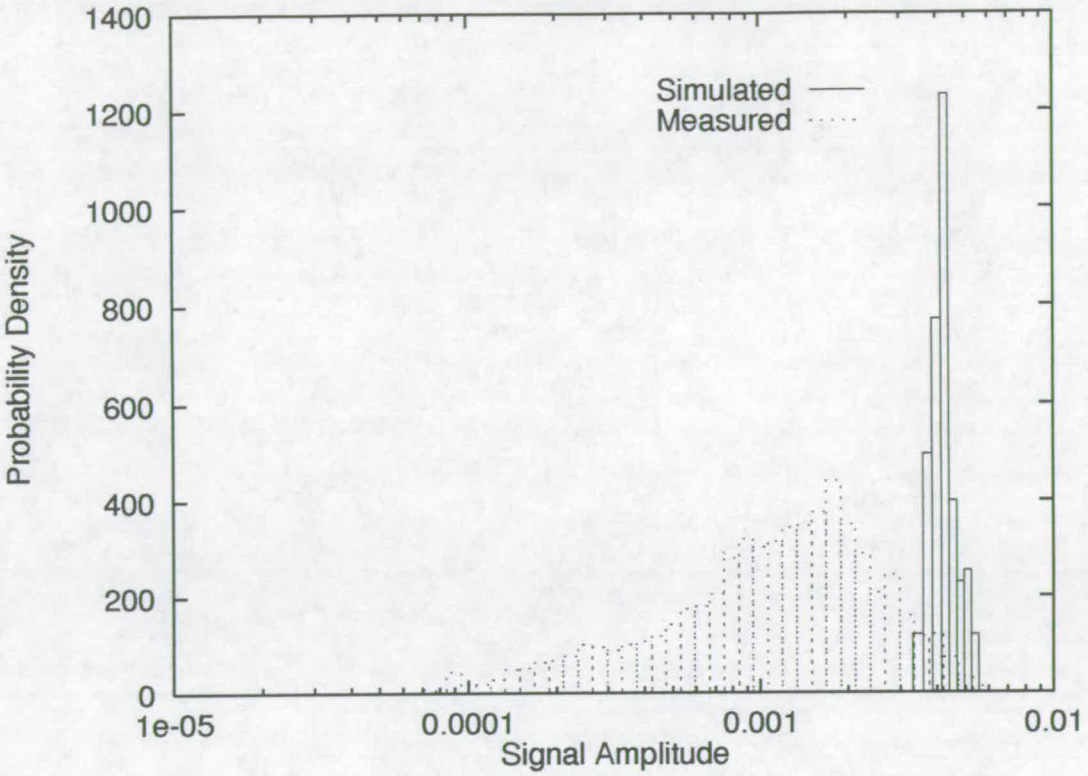

Figure 5–5: Simulated and measured results for location 12

A second cause of the greater degree of conformance results from the reflection and transmission coefficients generated by the electromagnetic description of the walls. If we propose that the reflection coefficient is too low, and the corresponding transmission coefficient is too high, then for all the experiments performed, the median result will be greater than the measured result as the principal component is the LOS one. Too low a reflection coefficient will result in fewer signals that approach the power of the LOS signal, resulting in the narrow spread of signal amplitudes observed in the plots considered. For the experiment conducted at this location, this is observed in the low deviation of amplitudes around the mean value due to the low reflection coefficient, and the lack of a metallic reflector in the room. Analysis of the remaining results for the experiments conducted around the other four locations will provide further justification for both of the theories presented.

On comparing Figure 5–5 with Figure 5–3 a difference in the structure of

the distribution of the simulated results can be observed. Of particular note is the shape of the distribution tail above the modal value. For location 12, a much sharper initial drop, and a longer tail is observed than for location 8. This trend is also seen to some extent in the measured data. When Ricean distributions are fitted to the results of the simulations for locations 8 and 12 it is found that those for location 8 conform more closely to a Ricean distribution. The results of this comparison are shown in Table 5–2. This leads to the conclusion that the multipath signals arriving at location 8, save for the initial LOS signal, consist of a number of approximately equal strength signals. These combine to form an approximately Rayleigh distributed signal, which when added to the LOS component gives rise to the distribution observed. While location 8 is far from the receiver site, and small changes in distance do not affect the received signal amplitude greatly, location 12 is close to the receiver. Thus reflected components from location 12, although they do not travel considerably further than other reflected signal from the same transmitter location, do have significantly different strengths. This results in the non-Ricean distribution observed.

Ricean Distribution	s	σ	MoMSE
Location 8	0.00138	2.64×10^{-8}	0.058
Location 12	0.00417	1.35×10^{-7}	0.262

Table 5–2: Results of fitting a Ricean distribution to the simulation data

Location 13 Results for the experiments conducted at location 13 of Figure 4–4 are shown in Figures 5–6 and 5–7. Once again, the different mean values between the simulated and the measured results can be observed, as can the different tail shapes.

In these results it is found that the rise in the lower tail of the measured results distribution is also present in the lower tail of the simulation results, albeit at a position much closer to the modal value of the distribution. It is probable that this is a result of the transmitter moving into a shadowed

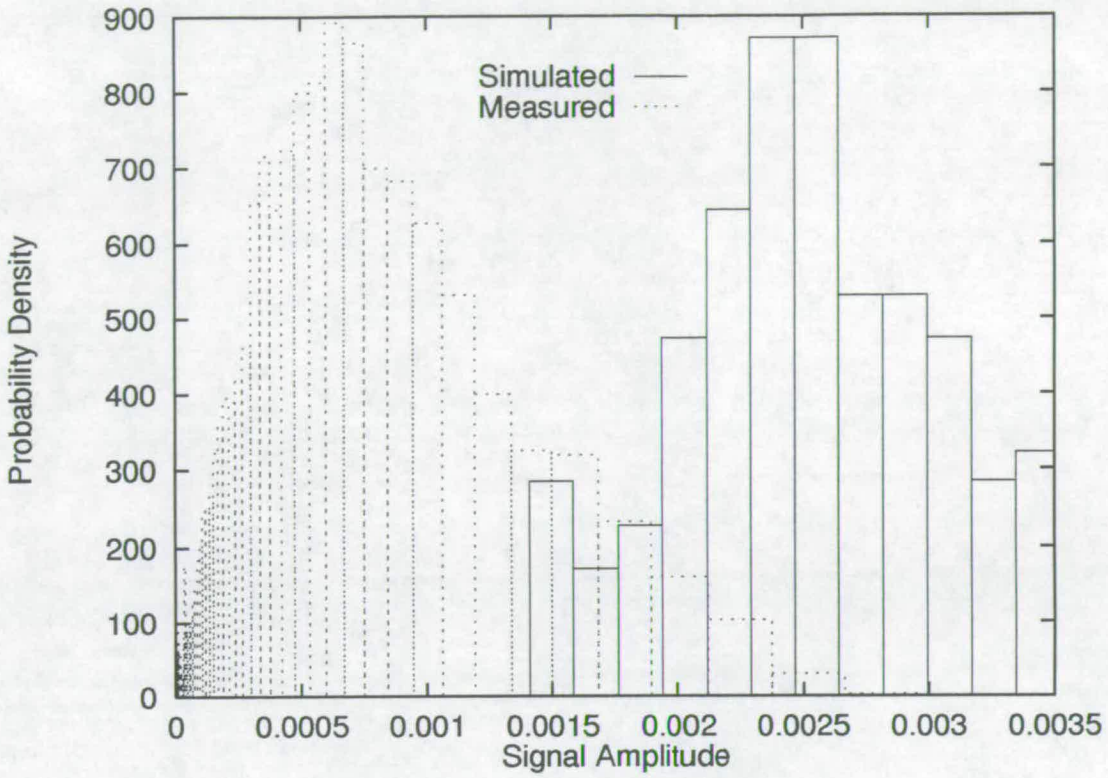

Figure 5–6: Simulated and measured results for location 13

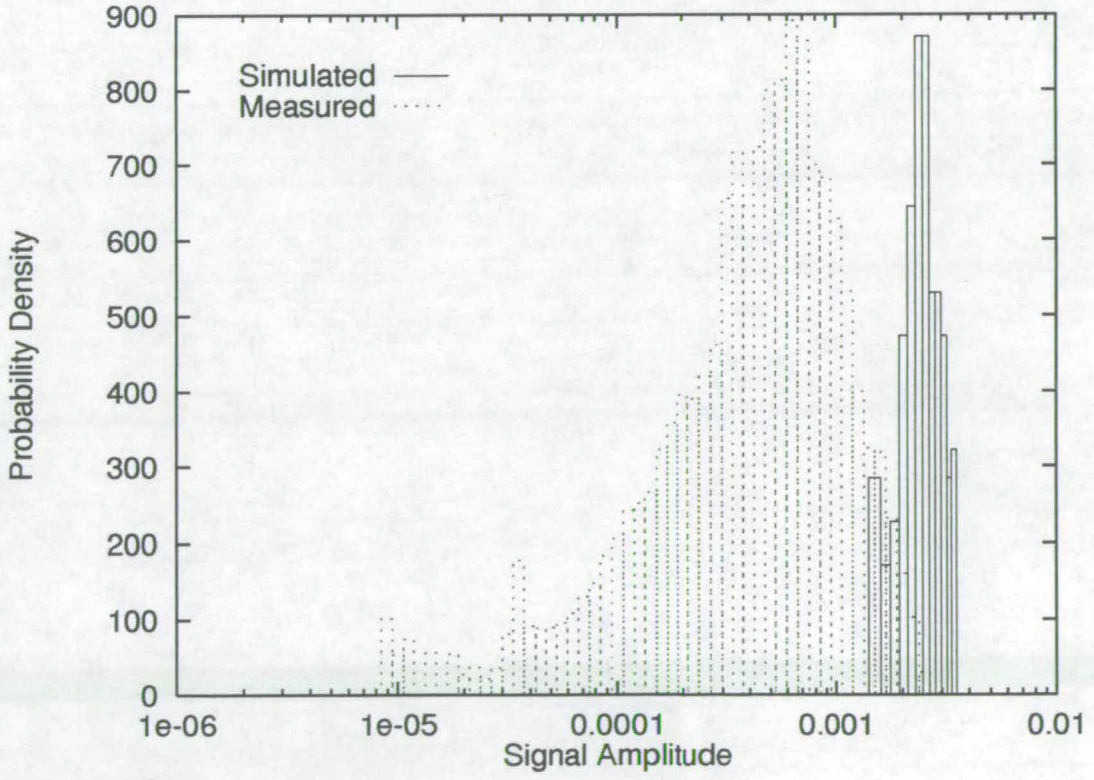

Figure 5–7: Simulated and measured results for location 13

area of reception from a non-shadowed one. With reference to Figure 5–1 it is observed that the rise in the probability graph is not present when the GTD is incorporated into the model. This would suggest that the measured results have such a rise due to a shadowing process. This is not observed on the complete electromagnetic simulation of location 13 that incorporates the GTD as a propagation mechanism, however this may be due to errors introduced in transcription of the building layout, as well as the transmitter and receiver locations.

Location 14 Results for the simulation and measurement experiments conducted at location 14 are shown in Figures 5–8 and 5–9. Unlike the previous three sets of results, the modal values of the two distributions are very similar. However, as before, the tails of the simulation results decay significantly faster than the measured counterparts.

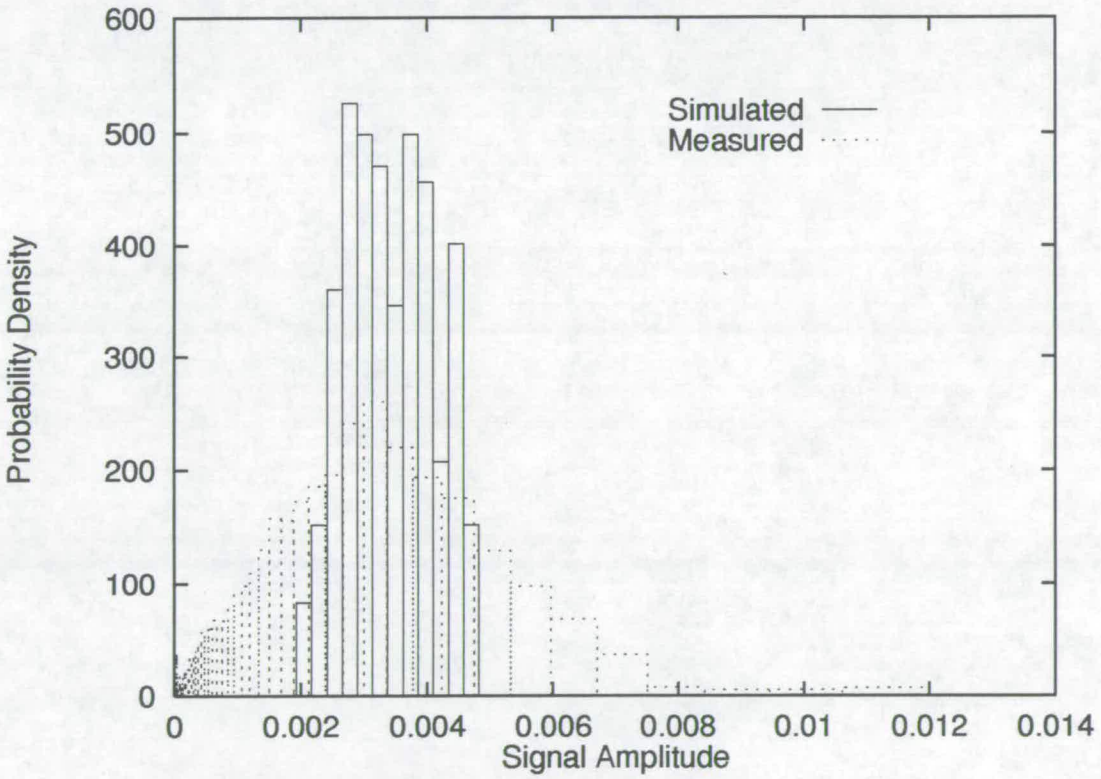

Figure 5–8: Simulated and measured results for location 14

For the modal values of the simulated and measured results to be close, either the simulation system is correctly calculating the propagation of

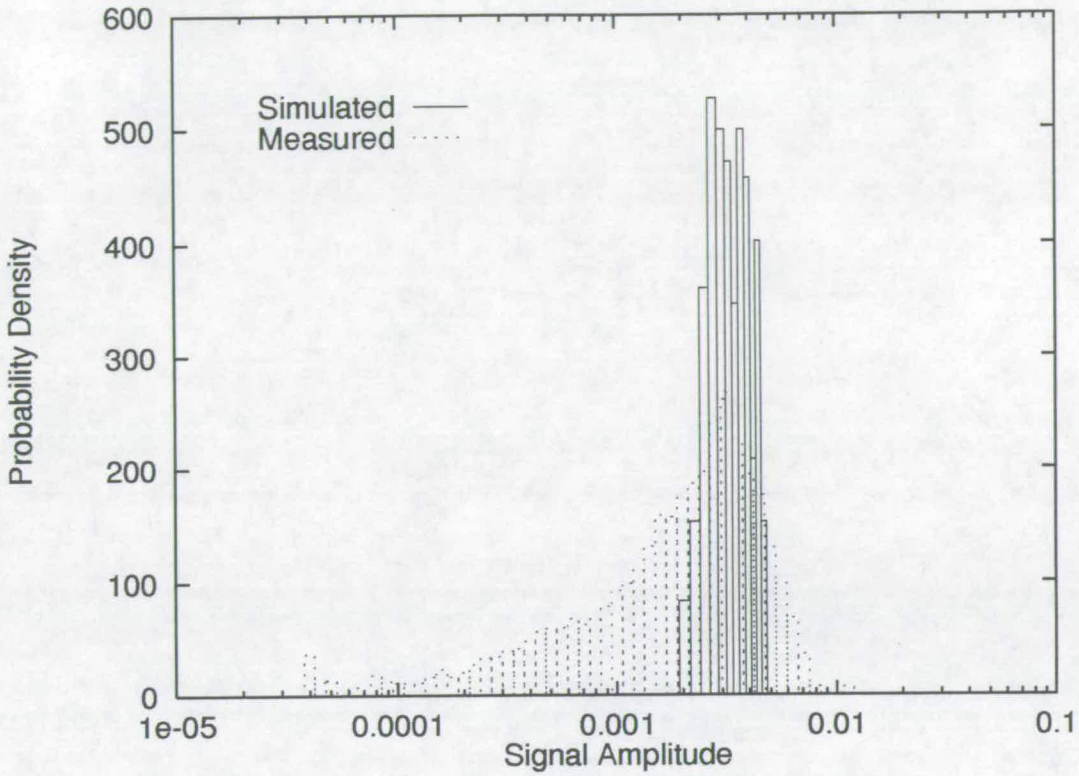

Figure 5–9: Simulated and measured results for location 14

the transmitted signal from location 14 to the receiver, or the degree of conformance is an artifact of some other difference between the simulation results and the measured results that has not been observed in the other results.

Location 14 is singular in its placement close to a diffracting corner that is close to the receiver location. Observing that in Figure 5–1 the effect of adding in diffraction as a propagation mechanism, besides removing one of the features in the lower tail of the distribution, the overall mean value of the distribution increased. For location 13 the increase was not significant, however for location 14 it is expected that such an increase would be significant due to the proximity of the diffracting edge to the transmitter position. The multipath signals that contribute to the received signal in the simulation system as it stands, without incorporating the effects of diffraction, consist of a direct signal that is attenuated by two walls, and reflected signals that may or may not have been already attenuated

by passing through walls. Thus, it is still possible that the transmission coefficient that results from the choice of variables to describe the electromagnetic properties of the walls is too high. The drop in signal amplitude that would result from reducing the transmission coefficient would be compensated by the inclusion of the effects of diffraction.

Location 16 Figures 5–10 and 5–11 show the results of the simulation and measurement experiments for location 16. As in the majority of the plots, a clear difference in the modal values between the two sets of results can be observed, however the relative difference is not as great as most. Like location 14, location 16 is sited close to diffracting corners, thus the arguments that hold for location 14 also hold true for this experiment. As the receiver for location 16 is further from the diffracting corners than location 14, the effects of the diffraction will be diminished, and so the signal amplifying influence of the diffraction mechanism on the measured results is not observed to such a great degree as for location 14.

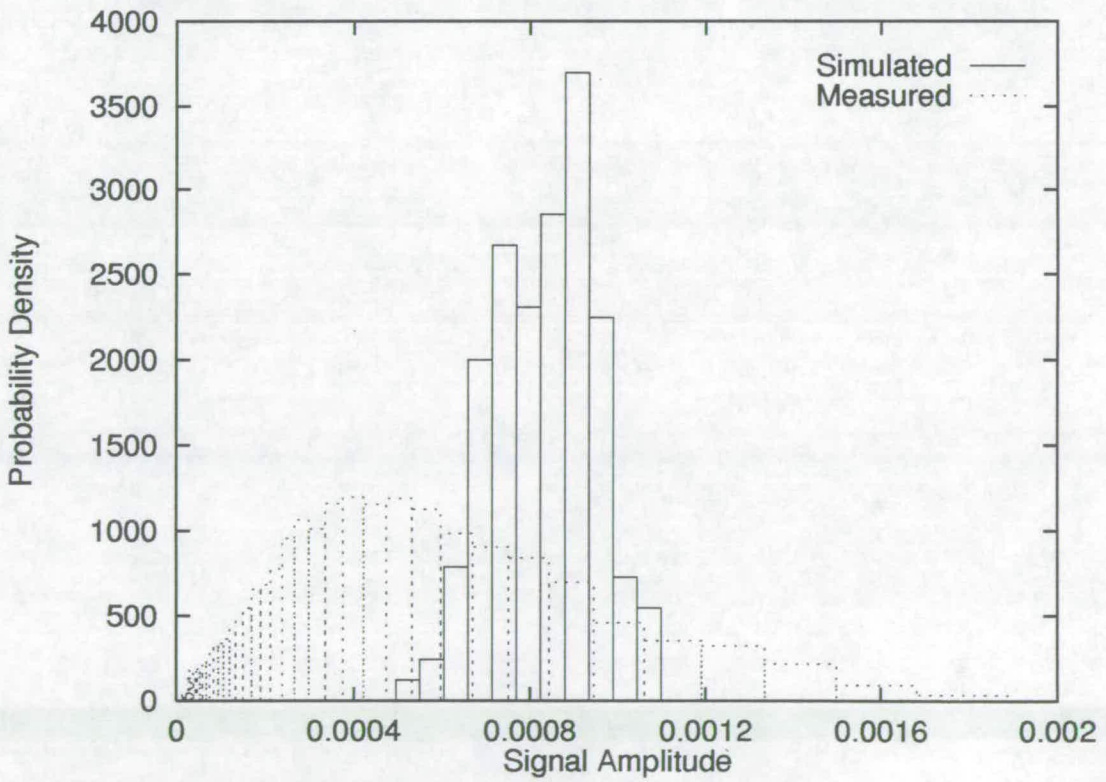

Figure 5–10: Simulated and measured results for location 16

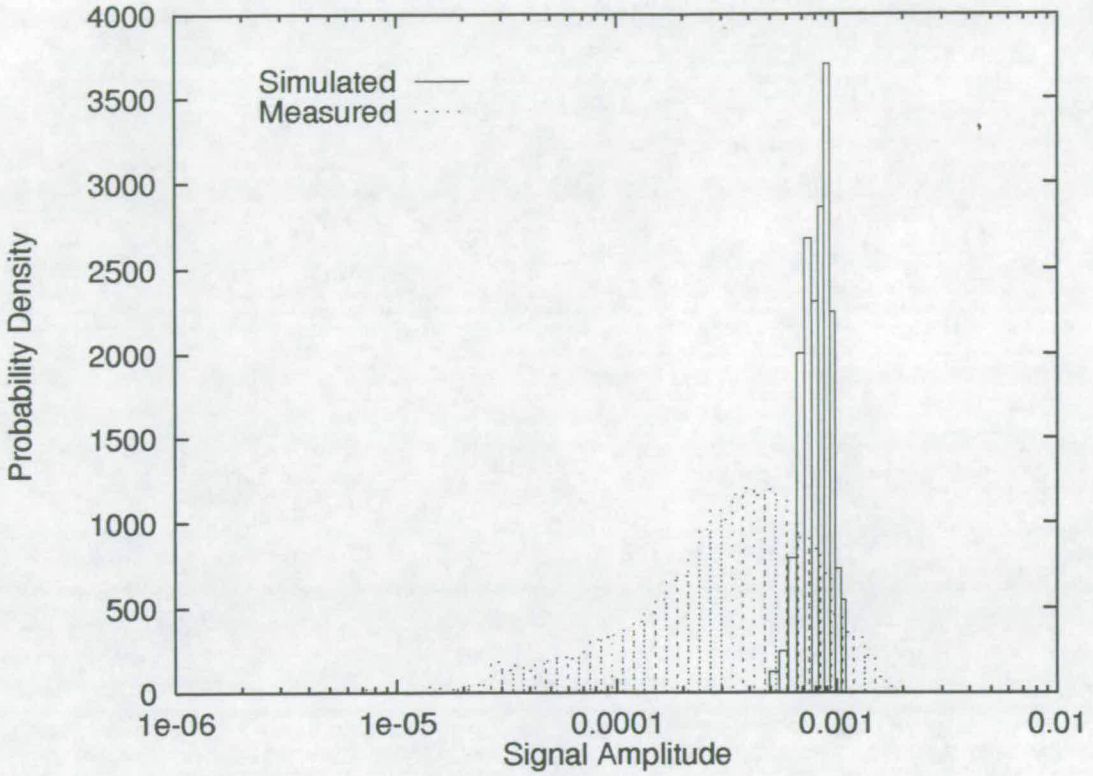

Figure 5–11: Simulated and measured results for location 16

Location 18 Results for the experiments conducted at location 18 are shown in Figures 5–12 and 5–13. This location is far from any diffracting edges that may alter the received signal strength, and as for locations 8 and 13, the modal value of the simulated results is much larger than the modal value of the measured results. In addition to this, a sizable spread of values around the modal value can be observed in the figures indicating that there are multipath signals arriving at the receiver with magnitudes approaching that of the dominant signal. This is a result of the close proximity of the corridor walls to the experimental location resulting in reflected signals that have path lengths approaching that of the direct receiver to transmitter distance, and are therefore not subject to a significantly different free-space propagation loss.

In summary of the above results we can identify a number of features of the simulation system, with particular reference to the experiments performed at Site B, and indoor radio propagation in general.

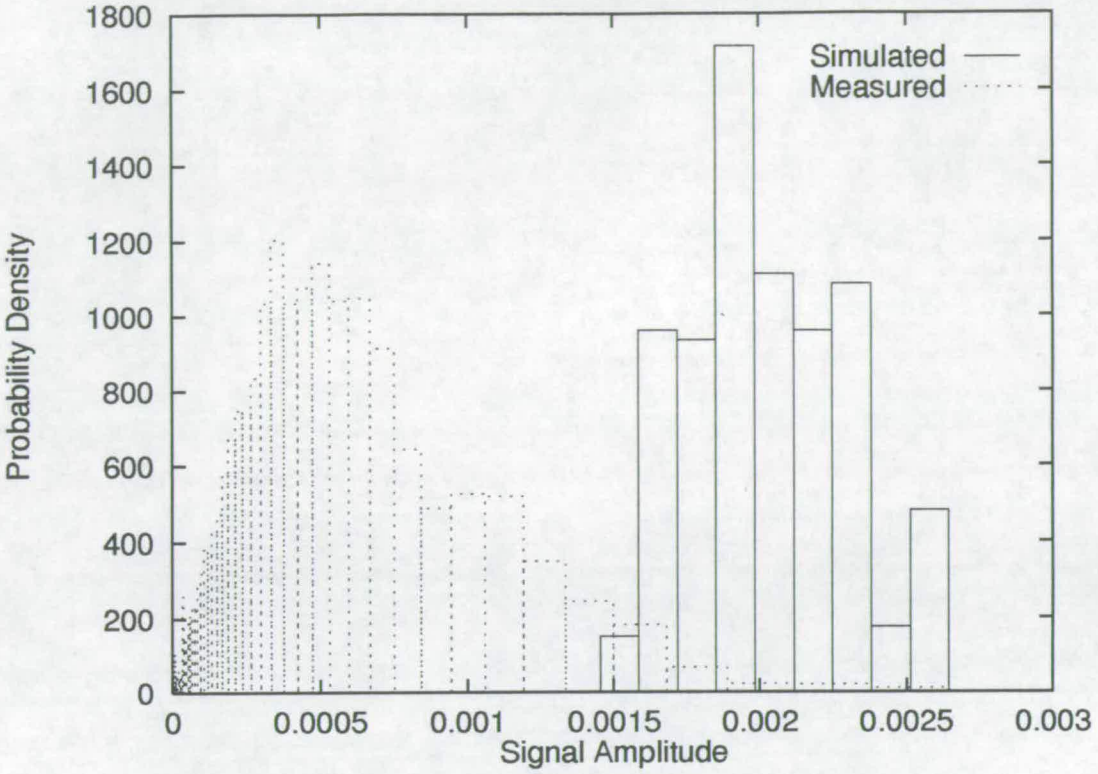

Figure 5–12: Simulated and measured results for location 18

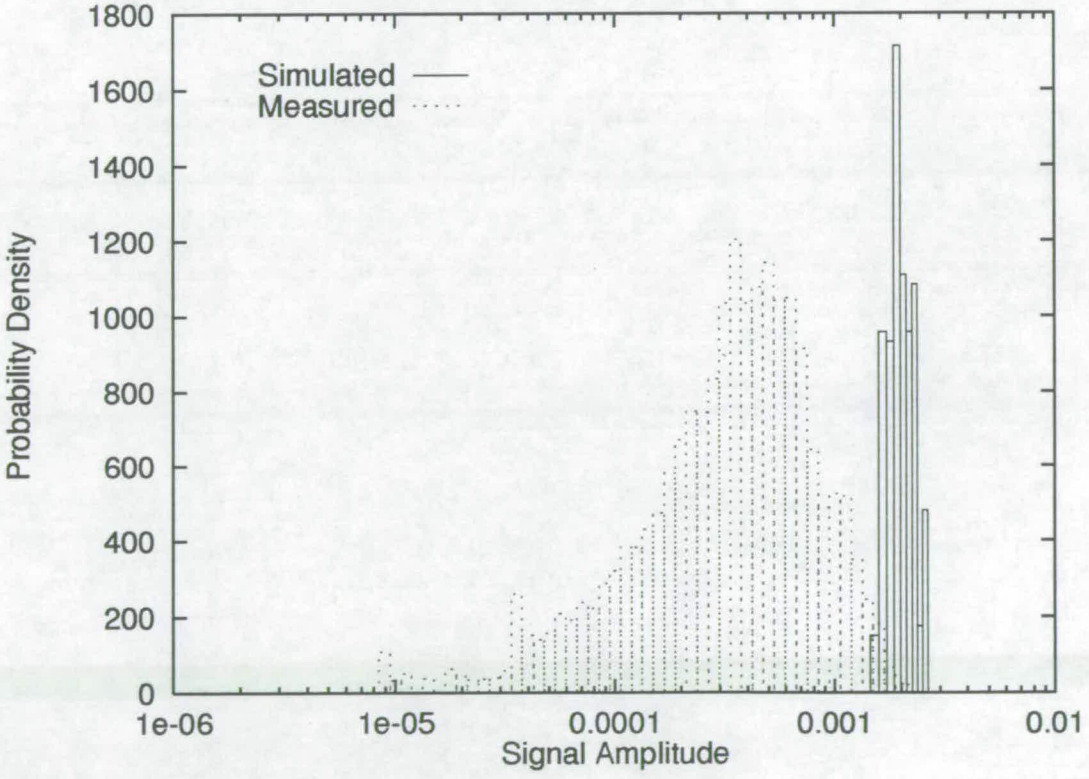

Figure 5–13: Simulated and measured results for location 18

Firstly, for experiments where reflection and transmission are the major propagation mechanisms, the effect of the low simulated reflection and high transmission coefficients can clearly be observed in comparison of the simulated and measured signal amplitudes. The result of this departure of the simulated system from reality is typically observed in the received signal consisting of one strong direct component, and substantially attenuated reflected multipath components. This results not only a higher modal value, but a reduced deviation around this value.

Secondly, it can be observed that for experimental locations close to reflecting surfaces, the resulting probability distribution of signal amplitude can be well described by a Ricean distribution. This is due to a number of multipath components in the received signal with approximately equal signal amplitudes. However, when the transmitter is also close to the receiver, the small changes in multipath lengths result in differences in the amplitudes of the multipath components, thus the probability distribution of received signal amplitude is no longer well described by a Ricean distribution.

Thirdly, the effects of shadowing of the transmitter to receiver path are evident in both the simulation and measurement results. It is found that shadowing of the major signal contribution for subset of the transmitter positions results in a concentration of signal amplitudes at an amplitude lower than the main peak. Observing the effect of incorporating diffraction into the simulation process, the smoother transition between the shadowed and non-shadowed cases is evident in a reduction of the peak at the lower signal amplitude.

Fourthly, the increase in the modal value of the probability distributions when diffraction is incorporated into the simulation is evident. For certain receiver and transmitter positions diffraction is an important propagation mechanism, whereas for others it serves only to increase the received signal amplitude by a small amount.

5.3 Conclusion

This chapter has presented the results of an electromagnetic simulation of Site B using values of permittivity and conductivity derived from measurements made on concrete blocks for describing the internal walls and structures in the building. As in the previous chapter, diffraction has been found to be a significant propagation mechanism for only a limited number of receiver and transmitter locations. The results show that the electromagnetic characteristics of concrete, when applied to the internal structures of the environment, result in a transmission coefficient that is too high, and a reflection coefficient that is too low. In order to obtain models that more closely describe the real environment, more data is required on the electromagnetic properties of construction materials. As the structures in the typical building are a composite of various materials, and are in general non-homogeneous, the reflection and transmission coefficients that are defined by a simple formula, as done in this work, are not sufficient to describe the practical situation. Instead, some accurate measurements of the reflection and transmission coefficients based on angle of incidence for various construction materials are required to increase the accuracy of the model.

Despite the simplifications made in constructing the electromagnetic model, particularly with respect to the determination of reflection and transmission coefficients, the model has been usefully applied to a practical situation. From analysis of the building layout, and the results obtained from the simulation system, the important characteristics for radio propagation from the various experimental locations has been shown. By examining the details of how the propagation from transmitter to receiver takes place, a more detailed picture of indoor propagation can be constructed. The following chapter will address this issue in terms of analysing the wideband response of the simulation system.

Chapter 6

Wideband Simulation Results

6.1 Introduction

This chapter describes some wideband simulations performed with the ray tracing simulator using the structure information of Site A and Site B described in the previous chapters. Unfortunately, no wideband measurements were performed at either of the sites, therefore comparisons of the results obtained from the ray tracing model can be related only to other published results for different locations. Results of analysing the interarrival times of the multipath signals that constitute the received signal for a particular experimental location will be given. These results describe the degree of clustering in the set of multipath signals. A second method of analysing the wideband results, using a joint probability graph, is presented. This provides a detailed overview of the channel impulse response in terms of the multipath signal amplitudes and delays. The two methods of analysis are related, however while the first relates to the clustering of signals, the second relates more to the signal amplitudes than the temporal characteristics of the channel impulse response.

6.2 Interarrival Times of Multipath Components

One of the methods of characterising a multipath channel is in terms of the times of arrival of the multiple signals. An analysis of some measured data has been performed by Yegani and McGillem [70] and the results of this analysis presented as probability functions describing the delays between successive multipath components arriving at the receiver. In the results that they present it is shown that the probability of two signals arriving within a very short time delay tends to zero as the delay approaches zero.

Unfortunately, with the limitations of physical measurement systems, very small time delays cannot be measured, and such delays are not registered, instead the signals separated by very small time delays are treated as one single signal that has a fading amplitude. However, a simulated system has no such resolution problem, so small time delays can be recorded.

As no wideband measurements were performed at either Site A or Site B, Site A was selected for calculation of the interarrival time information since the building can be partitioned easily into line of sight and non-line of sight areas. Then the results of the simulation process can be readily compared with those of [70]. To calculate the interarrival times of the multipath components impinging upon the receiver in the simulation the ray tracing process described previously was applied to each transmitter and receiver position as before, save that the path lengths of each of the multipath components were stored in an array. After sorting the array according to time of arrival, the delays between each path arrival are calculated, this information being ultimately stored in a histogram form, later to be converted to a probability density graph as done for the signal amplitudes in the previous chapter.

The building simulation is divided into two large areas, the bottom left section being classed as an OBS group of transmitter positions, and the upper right as a LOS group. The transmitter is allowed to roam within the defined areas during the experimental procedure. The wide area of points selected in the simulation results in a probability graph, being the combination of a

number of areas with differing propagation paths between the transmitter and receiver, that can be compared with the combined results of [70, figure 3].

Figures 6–1 and 6–2 show the resulting probability graphs for the line of sight transmitter positions and the obstructed line of sight positions respectively. The probability graphs have a large number of entries in the first bin, corresponding to a large number of multipath signals separated by small delays. The peaks are of a size that makes plotting them on a graph while retain the resolution required to see other details impossible. In Figures 6–1 and 6–2 the first entries have ranges that exceed the range of the plot, but the values of the probability graphs for these entries are noted in numerical form in the figures.

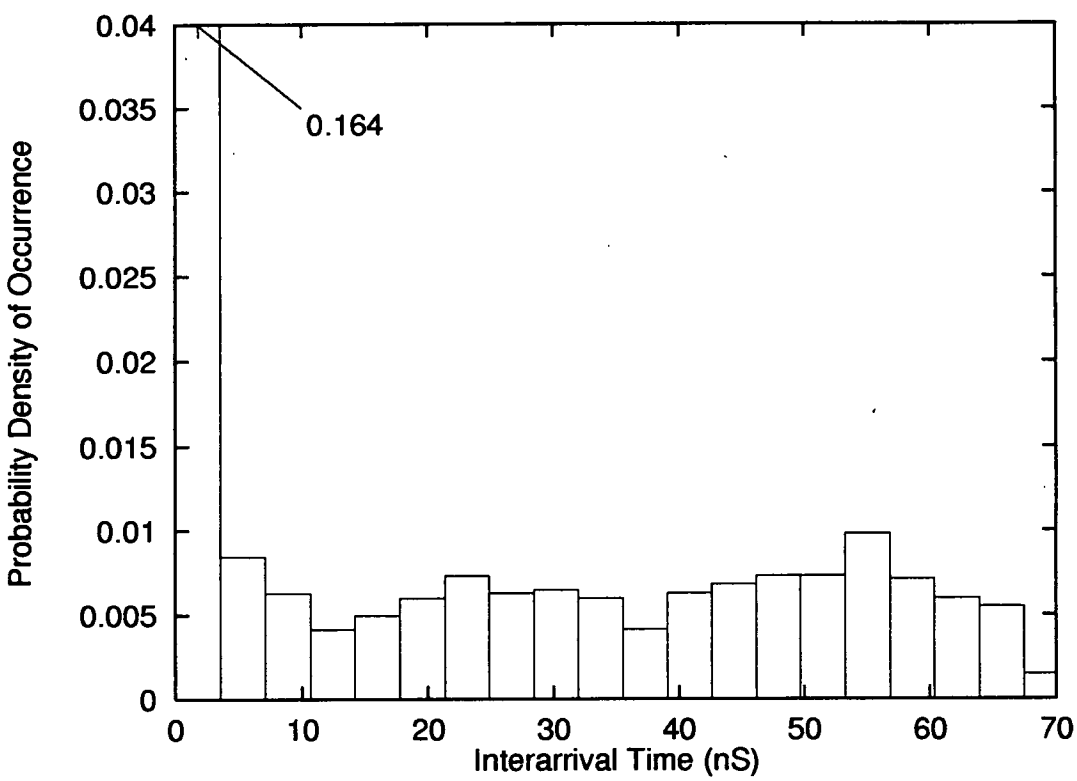

Figure 6–1: Simulated interarrival times for line of sight positions

The initial peak of the distribution is caused by the arrival of multiple signals with similar time delays. Such a situation commonly occurs when a reflection from the floor of the office building exists that is identical to another

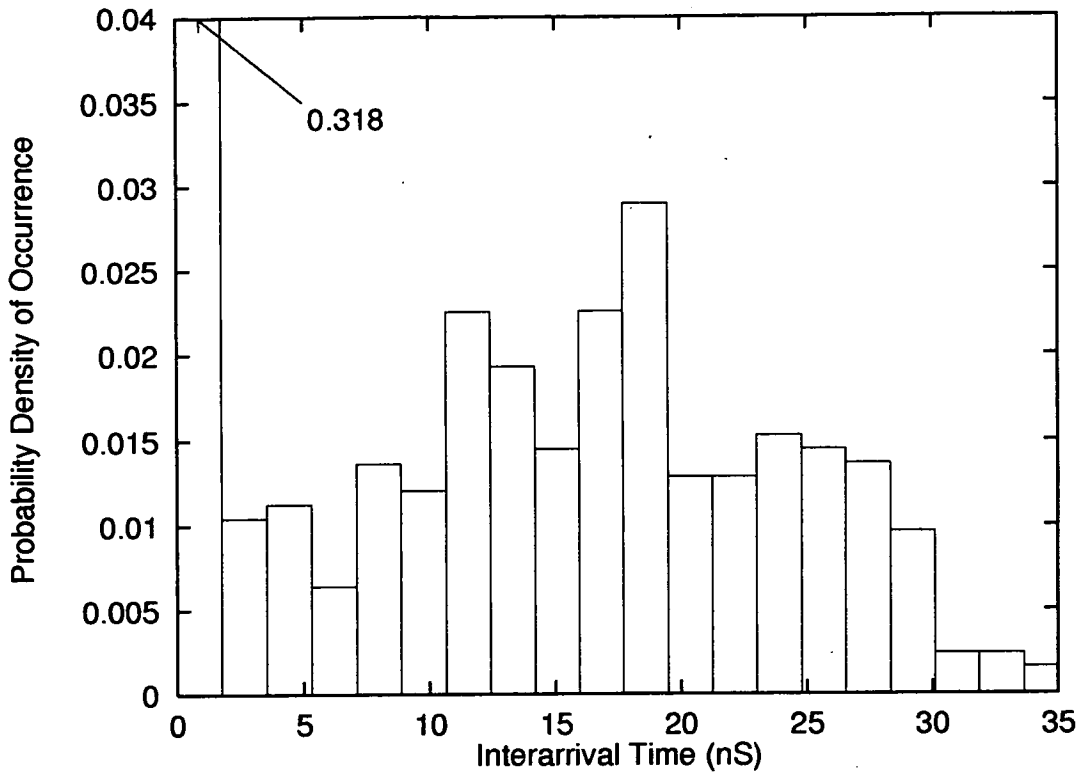

Figure 6–2: Simulated interarrival times for obstructed line of sight positions

propagation path, save for the reflection from the floor. This accounts for the large probability of such short delays between consecutively arriving signals. In the case of the LOS set of receiver positions, a significant number of time delays are longer than 1ns, whereas the majority of the energy in the first peak of the OBS case is contained in the range of 0ns–1ns. Such a result is not surprising, as shorter path lengths from the transmitter to the receiver result in longer delays between the paths involving reflections from the floor and those that do not, hence a direct LOS path will have the longest interarrival delay between the two paths. In addition, the set of transmitter positions chosen for the LOS simulations are closer to the receiver than those used in the OBS simulation. If we define t_1 to be the time for the direct path between the transmitter and the receiver, and t_2 to be the time via a reflection off the floor, then the interarrival time between these two signals is defined as $t_2 - t_1$ (Figure 6–3). Letting h_t be the transmitter height off the floor, h_r the receiver

height and d the transmitter to receiver distance, then the interarrival time of the two signals can be expressed by

$$t_2 - t_1 = \frac{\sqrt{d^2 + (h_t + h_r)^2} - \sqrt{d^2 + (h_t - h_r)^2}}{c}, \tag{6.1}$$

where c is the propagation velocity.

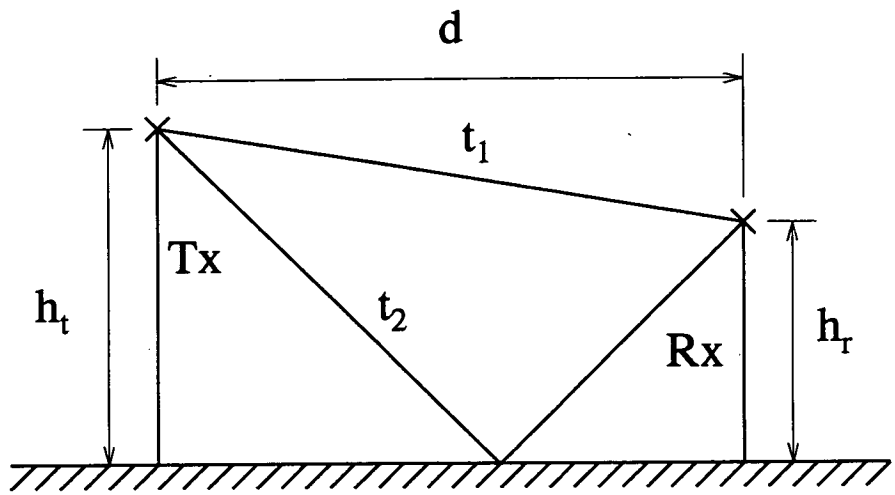

Figure 6–3: Transmitter to receiver path delays

The OBS interarrival time graph has a domain with a maximum value of just over 35ns for the simulation, and the LOS graph a time of just over 70ns. This result for the OBS channel is comparable to the domain of the collected OBS channels given in [70], however the result for the LOS channel requires further explanation as it does not correspond to the values found by Yegani and McGillem. In the channel that we have simulated, the area corresponding to the LOS channel is an open area with very few reflecting objects within the environment. This results in a long delay between the initial direct line of sight signal with its attendant reflections from the floor and ceiling, and the reflected signals from the walls. A 70ns delay corresponds to a distance of 21m or 66 wavelengths at 945MHz indicating that the return path from a wall reflection to the receiver is involved in the long delay for reflected paths. Such a delay may be experienced by a transmitter site located adjacent to the receiver where after the initial set of received signals, the next group of multipath components are

reflections from the far wall. The scenarios that Yegani and McGillem describe are factory environments with light and heavy clutter, but they do not describe one with very little clutter at all as experienced in an empty building, therefore shorter interarrival delays are to be expected from their measurements.

The probability graph for the LOS (Figure 6–1) exhibits a flat region between the initial peak caused by the clustered nature of the arriving signals, and the final tail of the graph. This is a result of the lack of reflecting objects in the environment such that when the receiver roams over the prescribed area for the LOS measurements the long delays vary around some average value. There are two dips present in the graph at delays of around 12ns and 38ns suggesting that the signals arriving at the receiver form three distinct clusters with short interarrival times within the clusters, but longer, clearly defined, times between the clusters, giving the graph the flat nature with two slight concentrations of time delays around 23ns and 55ns. The first cluster would be the result of the direct line of sight path, the second and third clusters being the result of reflection off the walls in the environment. Conversely, the OBS probability graph (Figure 6–2) does not exhibit such a characteristic. This is a result of a higher number of reflecting objects in the OBS environment, and the lack of a clearly defined LOS path. However, the bell shaped section of the OBS probability graph between 6ns and 35ns suggests a connection between these results and the first concentration of delays in the LOS probability graph between similar time delay values, indicating some similarity in the types of environment.

As the resolution of the simulated system at very short time delays is much greater than that for the measured system, it is appropriate to compare the results with those obtained from measurements after first removing the energy contained in the probability graphs for time delays below some threshold, 1.5ns say. After renormalising the probability graphs, comparisons can then be made between the simulated and measured results. Such a comparison is made with reference to the graphs for all LOS and OBS locations in [70, figure 3], the results being shown in Figures 6–4 and 6–5. In addition to the data

extracted from [70], the figures also show the best fitting Weibull probability density function to the simulated data.

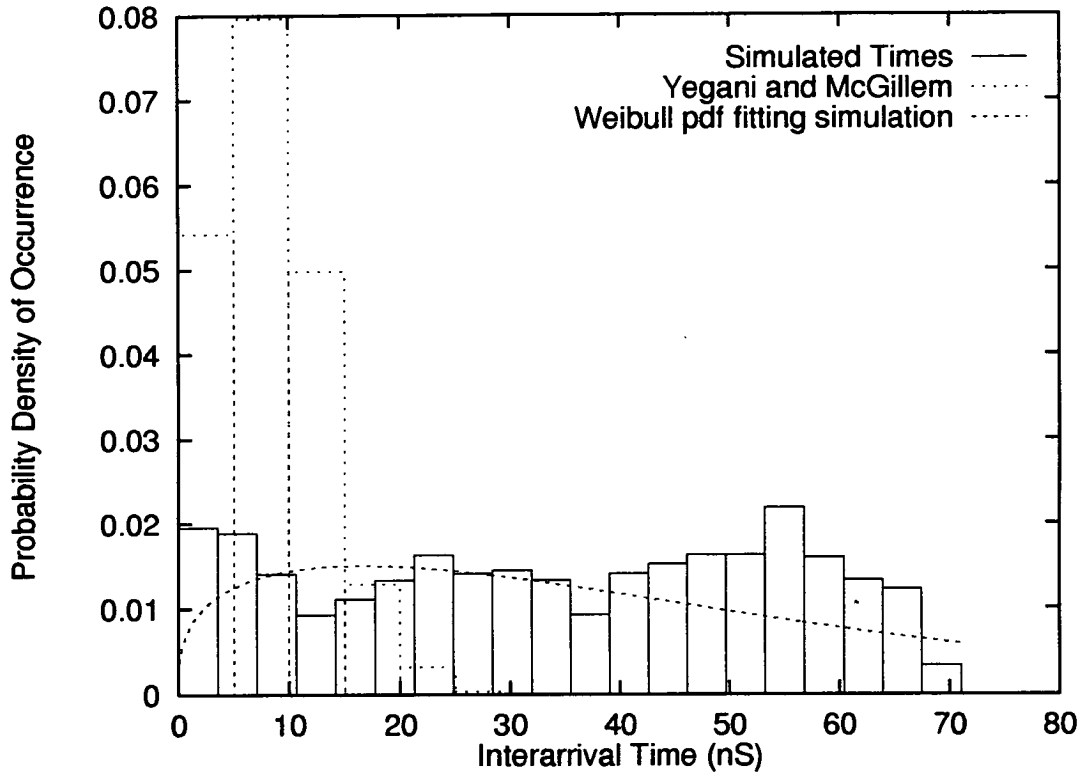

Figure 6–4: Adjusted simulated interarrival times for line of sight positions with results from [70]

The Weibull distribution is a three parameter distribution, the location parameter, ν, being zero for positive random variables as encountered in radio channels. The reduced distribution is then defined by

$$p(R) = \frac{\beta}{\alpha}\left(\frac{R}{\alpha}\right)^{\beta-1} \exp\left[-\left(\frac{R}{\alpha}\right)^{\beta}\right] \quad R \geq 0 \tag{6.2}$$

where β is a shape parameter, and α controls the spread of the distribution. More details on the distribution are provided in Appendix C.

Figure 6–4 shows that even with the adjustment made to the probability graph for the LOS case, the resulting probability graph does not conform to the Weibull pdf, nor to the measured results obtained by Yegani and McGillem. The difference between the two sets of results is due to the number of reflecting

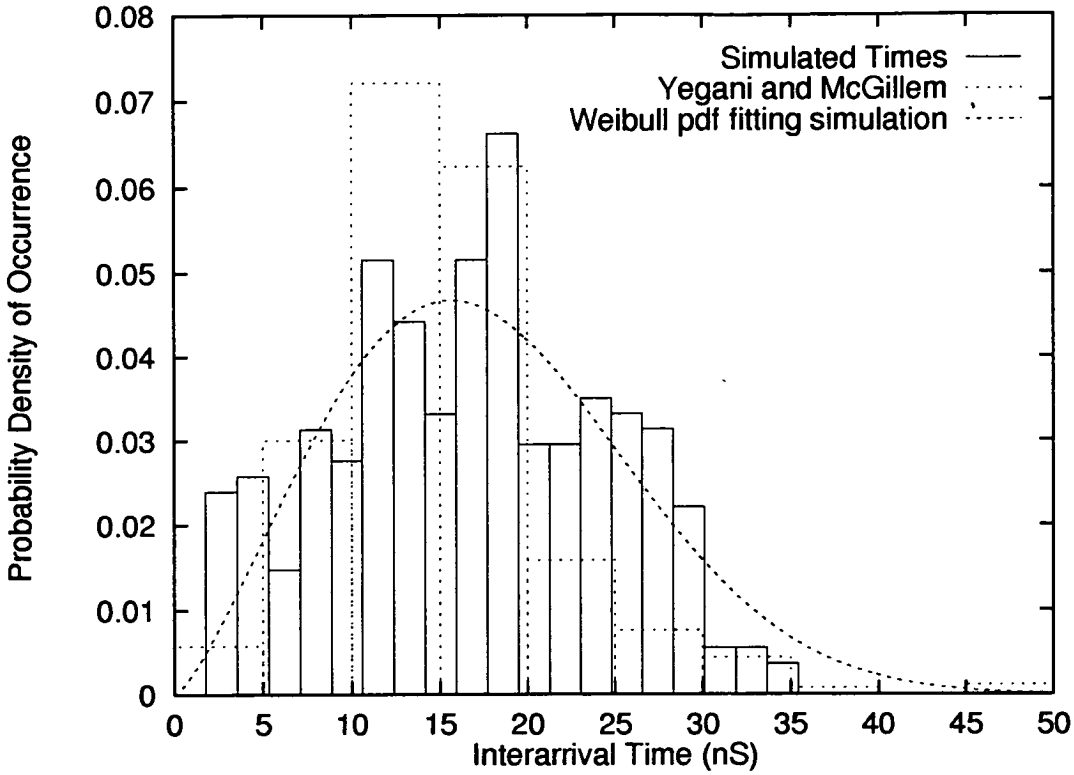

Figure 6–5: Adjusted simulated interarrival times for obstructed line of sight positions with results from [70]

objects (or clutter) in the environment and possibly to the distance between the transmitter and receiver during the measurement process.

Figure 6–5 shows that once the probability graph of Figure 6–2 has been adjusted to remove the strong component around the 1ns time delay the shape of the curve conforms with a reasonable match to both the data given in [70] and to a Weibull distribution. In this case the parameters of the Weibull distribution are $\alpha = 20$nS and $\beta = 2.28$. Such values of α and β correspond with values found by Yegani and McGillem for OBS environments with both light and heavy clutter at signal thresholds of -20dB. The environment within which the measurements were made has very light clutter and lower signal thresholds, the two effects appearing to cancel each other out giving approximately the same results as the physical measurements produced.

6.3 Joint probability function of signal strength and delay

Wideband channels can be characterised in a number of ways. The normal mechanism for simulating a wideband channel is to construct a tapped delay line with variable tap weights. On examining the general channel model, (2.4), the relationship between the signal amplitude and the delay of each multipath component can be seen. Using a physical modelling system, of which the ray tracing simulator already described is one example, the values for $A_i(t)$, $\phi_i(t)$ and $\tau_i(t)$ can be determined for each multipath component, and from this the overall received signal may be constructed. As has been discussed in Section 6.2, a physical measurement system cannot attain a resolution sufficient for determining such information about a radio channel, therefore a simulation system must be relied upon to obtain such details.

While a simulation system can determine the values of $A_i(t)$, $\phi_i(t)$ and $\tau_i(t)$ for each multipath component at every receiver and transmitter position for a given building, the information must be presented in a more compact form for analysis. Considering the variation of $\phi_i(t)$ as the transmitter, the receiver and other objects in the environment move, it is noted that the variable changes rapidly with small variation in path length. For this reason, it is commonly assumed that $\phi_i(t)$ can be treated as a random variable with a uniform distribution over the range $(-\pi, \pi)$ and does not provide much useful information to the channel characterisation.

Using the two remaining variables, $A_i(t)$ and $\tau_i(t)$, a joint probability distribution can be formed describing the channel in terms of the probabilities of multipath components arriving with certain amplitudes and time delays. The distribution function, $P_J(a, d)$, satisfies

$$0 \leq P_J(a, d) \leq 1, \quad \forall a, d \in \mathbb{R} \tag{6.3}$$

and

$$\iint P_J(a, d)\, da\, dd = 1\,, \tag{6.4}$$

where a is the amplitude d the delay of the multipath signals. For a discrete representation of $P_J(a, d)$, used to construct the two dimensional probability graph,

$$\sum_{i=0}^{M}\sum_{j=0}^{N} P_J(i,j) = 1 \,. \tag{6.5}$$

The function, $P_J(a, d)$, describes the probability of a multipath signal being present with a given amplitude at a given delay.

The amplitude of a signal arriving at the receiver is dependent not only on the reflections, transmissions and diffractions in the environment, but also on the length of path between the transmitter and the receiver, that is the delay. It is thus possible to factor out the free-space loss that would be experienced by a receiver the appropriate distance from the transmitter to experience the specific delay, with a correction factor included for diffracted signals because of the different rate of expansion. Once the free-space loss has been factored out, the axes of the probability graph are independent, and the detail at longer delays can more readily be observed.

The joint probability function, while providing detailed information on the probability of a signal with a specific amplitude and delay occurring, contains no information on the relationship between two multipath signals in a specific instance of the channel impulse response. For this reason it is possible to relate this function to the interarrival time results obtained in the previous section only through observing general trends.

6.3.1 Joint probability graph of LOS experiment at Site A

The experiment conducted in Section 6.2 was repeated for the LOS set of transmitter positions, and the joint probability graph described above determined. As the graph has two arguments the data can be represented pictorially by a three dimensional plot, or a contour plot. By the nature of the variables that are used to drive the probability function, a graph representing the results is sparse. In order to observe the detail contained within the function, the results for the experiment are shown in Figures 6–6 and 6–7 in the form of a

colour contour plot and a three dimensional wire frame plot. The banding exhibited in these figures is an artifact of the simulation process that relies on fixed reflection and transmission coefficients to determine the power of an electromagnetic wave.

From Figure 6–6 the dominance of the set of received signal amplitudes at a level of 0.45 (that is 45% of the transmitted signal amplitude) can be observed. With reference to Figure 6–7 the two main peaks of the multipath signals arriving with this amplitude can be seen, separated by approximately 60ns. The other strong feature evident on the joint probability function is the set of multipath signals of amplitude 0.3 centred around a delay of 110ns.

Comparing these results with those shown in Figure 6–1 the features contributing to the interarrival distribution can be identified. The distance between the two peaks of the most probable multipath signals occurring is approximately 60ns, and as the other multipath signals that occur in time between these peaks are not highly probable, it is suggested that this is the main contribution to the area of Figure 6–1 corresponding to the largest interarrival times centred around 55ns. The other section of Figure 6–1 identified as a concentration of interarrival times centred around 23ns can be related to the distance between the peak at the delay of 90ns for the signal amplitude of 0.45 and the other major peak at 110ns with the amplitude of 0.3.

The remaining features on the distribution, when signals are present at those positions indicated by the distribution, will contribute to the shorter interarrival delays as well as widening the distribution around the two concentrations identified in the interarrival time plot.

6.3.2 Joint probability graph of LOS experiment at Site B

Figures 6–8 and 6–9 show the joint probability graph that has been extracted from the full electromagnetic simulator, incorporating the effects of diffraction, for the experiment conducted at location 13, the narrowband simulation results of which are presented in Figure 5–1. Unlike the graphs shown in Figures 6–6 and 6–7, the results for this experiment exhibit a wide range of signal ampli-

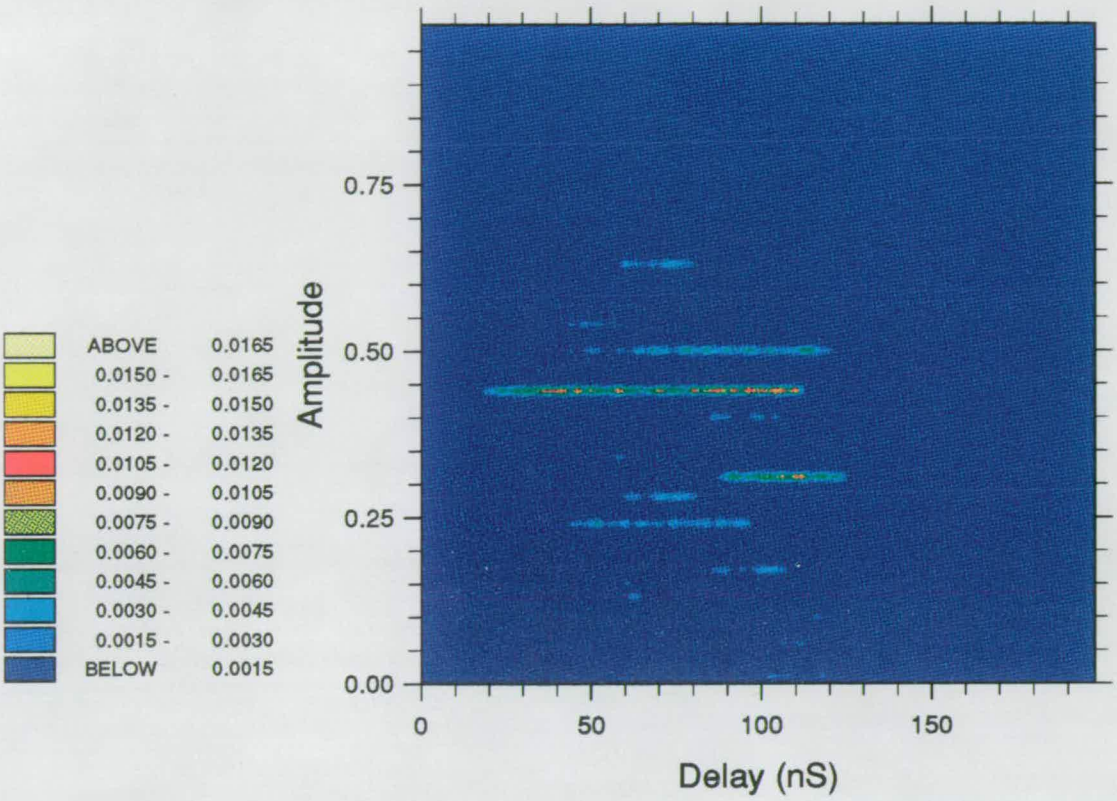

Figure 6–6: 2-D plot of joint probability function for LOS locations at Site A

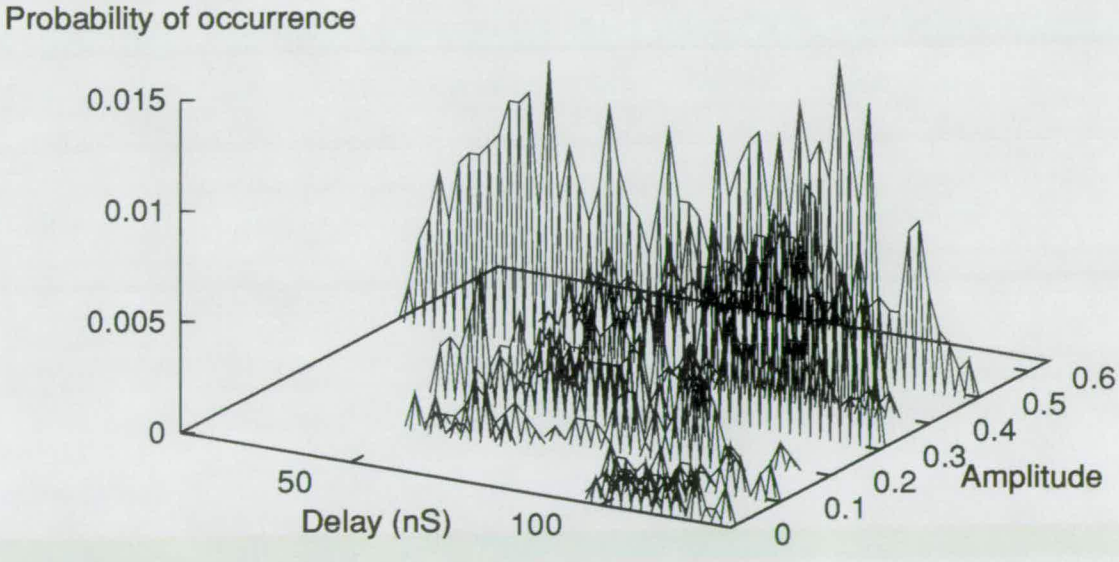

Figure 6–7: 3-D plot of joint probability function for LOS locations at Site A

tudes that are not grouped into discrete amplitude ranges. This is a result of the variable reflection and transmission coefficients that form an integral part of the complete electromagnetic simulation system, as opposed to the fixed coefficients used for the Site A simulations. The concentration of multipath signals at low signal amplitudes, compared to the results for Site A, is a consequence of the lower reflection coefficients in this simulation. This is a result of using the electromagnetic properties of concrete for their determination.

In Figure 6–8 a finite probability of a signal with an amplitude of over 0.5 at a delay of 22ns can be observed. This point on the graph represents the LOS component of the multipath signal, the other non-zero probabilities around the same delay being primary reflections of the LOS component. The difference in signal amplitude between the LOS component and the remaining components of the multipath signal, the next largest signal having an amplitude of 0.2 relative to the transmitter power, gives rise to a narrowband amplitude probability graph with a narrow range of amplitudes around a central peak as seen in Figures 5–6 and 5–7. As indicated in Section 5.2 for the results of experiments conducted at location 8, the narrow range of values results from lack of destructive interference of more than one large multipath component in the received signal.

In Chapter 4, the non-Rayleigh distributed nature of indoor channels was shown. One cause of this is that the multipath signals contributing to the overall received signal are not of equal magnitude. From the probability graphs presented for the two buildings this characteristic of the channel is evident. For those experimental locations where only one multipath component dominates the signal, the resulting distribution will be well modelled by a Ricean distribution. For other locations, the distribution is better modelled by a Nakagami distribution.

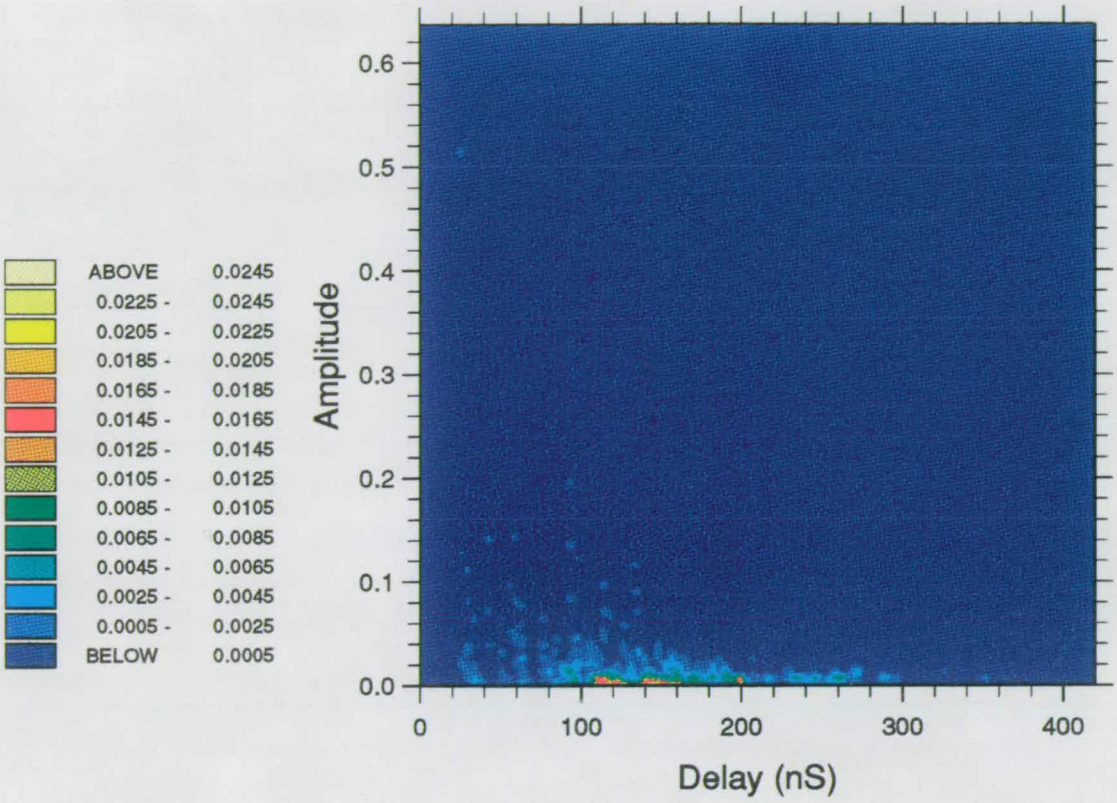

Figure 6–8: 2-D plot of joint probability function for LOS locations at Site B

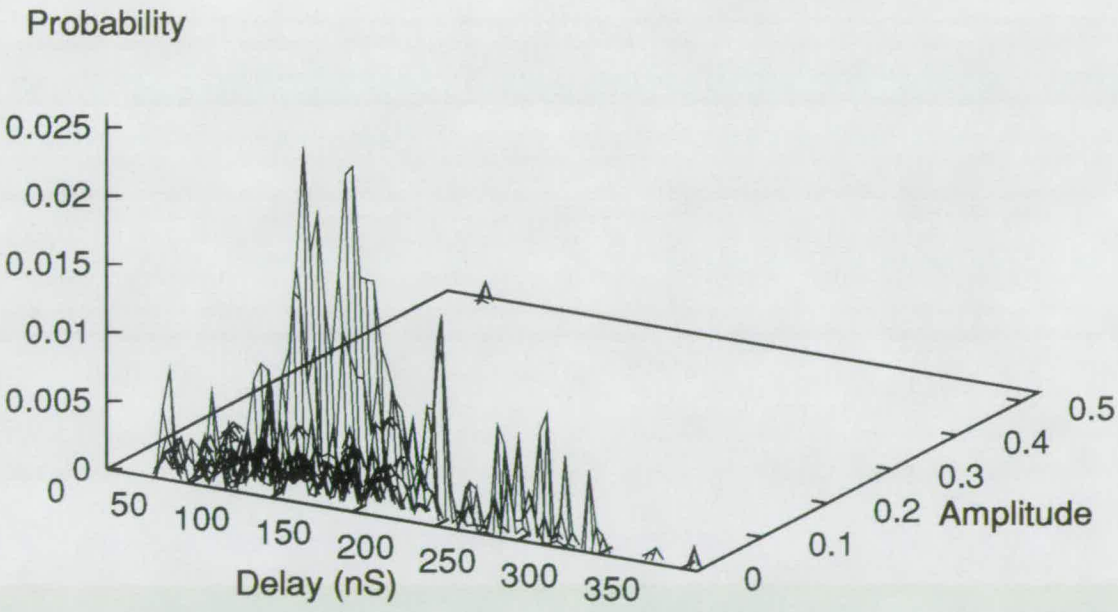

Figure 6–9: 3-D plot of joint probability function for LOS locations at Site B

6.4 Conclusions

This chapter has described the use of the simulation system to obtain wideband measurements for indoor channels. Due to the nature of a ray tracing simulation, more detailed information on the wideband nature of the channel can be obtained than a hardware measurement system could yield. This provides a unique tool for the investigation of multipath propagation mechanisms inside buildings.

The wideband results have been presented in terms of interarrival time distributions and joint probability graphs. A certain dependence between the two forms of information can be observed when the multipath components arriving at the receiver are clustered into discrete groups.

Chapter 7

Conclusions and Future Work

7.1 Conclusions

This thesis has shown that a physically based description of the channel impulse response is required not only for evaluation and development of indoor communication systems that attempt to use the limited available radio bandwidth to best effect, but also for investigation of the propagation mechanisms involved in indoor communications. A model based on ray tracing techniques, and the electromagnetic characteristics of the environment, has been presented and applied to two scenarios for which physical measurement results are available.

The channel model developed is based on ray tracing techniques, as used extensively in computer graphics applications, with extensions to describe propagation by diffraction. Electromagnetic theory describing the effect of a boundary between two media has been developed to produce a set of equations defining the reflection and transmission coefficients for structures such as walls, their derivations being presented in Appendix A. The coefficients are dependent on the electromagnetic properties of the wall, the wall thickness, the angle of incidence of the electric field, and the polarization of the field with respect to the surface. As the wall thickness was not known, a simplified set of equations were used in the simulation system to describe reflection and transmission.

In order to determine the significant factors in indoor radio propagation, a model of reduced complexity was constructed and the resulting channel obtained from this model compared with the measured one. Differences between

the measured and simulated results can be attributed, largely, to the lack of information on transmission and reflection coefficients, and therefore to selection of inappropriate values to describe them in the reduced model. In the complete electromagnetic model this lack of information also contributes to a marked difference between the simulated and measured channel statistics. In this latter case, it was found that the reflection coefficients arising from the choice of the electromagnetic properties for concrete as a model of the electromagnetic properties of walls was lower than experienced in the real environment, and that the transmission coefficients were greater than the values encountered in the practical environment. To remedy this situation, detailed measurements of reflection and transmission coefficients for various building structures are required. It is expected that such information will increase the accuracy of the model described in this thesis, resulting in a more accurate tool for channel investigation.

The significance of propagation by diffraction was evaluated for both the fixed reflection and transmission coefficients model, and the electromagnetic model with coefficients that vary according to the angle of incidence. It was found that, for both models, in certain circumstances propagation by diffraction was a minor contributor to the overall received signal. This was most notable in locations where a line of sight path, or a number of reflected paths, existed and the transmitter and receiver were far from diffracting corners. However, when no strong direct or reflected components are present in the multipath signal, and the transmitter and receiver are close to a diffracting corner, then the effects of diffraction are significant. For those locations where diffraction is not a major contributor, it serves only to increase the mean signal strength, and does not significantly alter the distribution around this mean.

In summary of the narrowband results, comparison of the results obtained from physical measurements, and from the simulation system, has shown the general applicability of the ray tracing technique. While the correspondence between the two sets of results is not favourable in terms of the mean signal amplitude and deviation around this mean, a relationship between the ray tracing

model, and the measurement results can be observed. In order to improve the correspondence more detailed information is required on the electromagnetic properties of typical building structures.

Wideband analysis of the simulation system was compared to results obtained from physical measurements for various multipath environments. It was found that the simulation system, with direct access to information on the various multipath components, could provide a wideband description of the environment with a greater degree of precision than could be hoped for from any measurement system. In addition, the wideband results obtained for the two sites for which narrowband simulations had been performed confirmed the analysis provided on the narrowband results showing that benefits of applying wideband results to analysis of narrowband channels. This is is clearly shown in the information that may be gleaned from the joint probability graph representations of the channel. The derivation of this new representation, and the application to the simulated channels have been presented in the previous chapter.

7.2 Further Work

A number of areas for future work on the model presented in this thesis have been identified. Namely,

- Determination of the electromagnetic properties of building structures
- Reduction in execution time of channel simulation
- Regeneration of a channel from statistical information
- Investigation of the phase relationships of multipath components

Determination of the electromagnetic properties of building structures

As has already been highlighted in the discussion of the work performed in this thesis, the need for more detailed information on the electromagnetic properties of walls, floors, ceilings and other structures found in the typical

office building is evident. For the purposes of channel modeling, this information can most usefully be presented in the form of reflection and transmission coefficients that depend on the angle of incidence, and polarization of the incident field. When this information is incorporated into the simulation model described, it is anticipated that the simulation results will approximate the measured results more closely, both in terms of mean signal power and in deviation around the mean.

Reduction in execution time of channel simulation

The computation process involved in creating the model for the electromagnetic simulation is prohibitively complex. Before further propagation mechanisms can be examined using this technique, a drastic reduction in the model complexity needs to be conducted. A number of techniques for performing this reduction are proposed in Appendix B. However, there is a fundamental limitation that the greater the degree of complexity in modelling, the longer will be the execution time of the simulation.

Regeneration of a channel from statistical information collected

The joint probability graph presented in Section 6.3 contains a great deal of information on the characteristics of the signals that constitute the total received signal for a particular experimental location. Using this information it should be possible to recreate a channel from this information, along with the number of multipath components that form part of the signal. Using a simple algorithm that selects multipath signals according to the probability distribution the narrowband results shown in Figure 7–1 are obtained.

Clearly, the regenerated narrowband response bears no resemblance to the simulated channel from which it was created. This is a result of an algorithm that allows more than one signal to be selected from a bin, even if in the practical situation such a case would not exist. Taking Figure 6–8, from which the recreated distribution was generated, a distinct point is observable at a delay of 25ns and an amplitude of over 0.5. This point corresponds to the

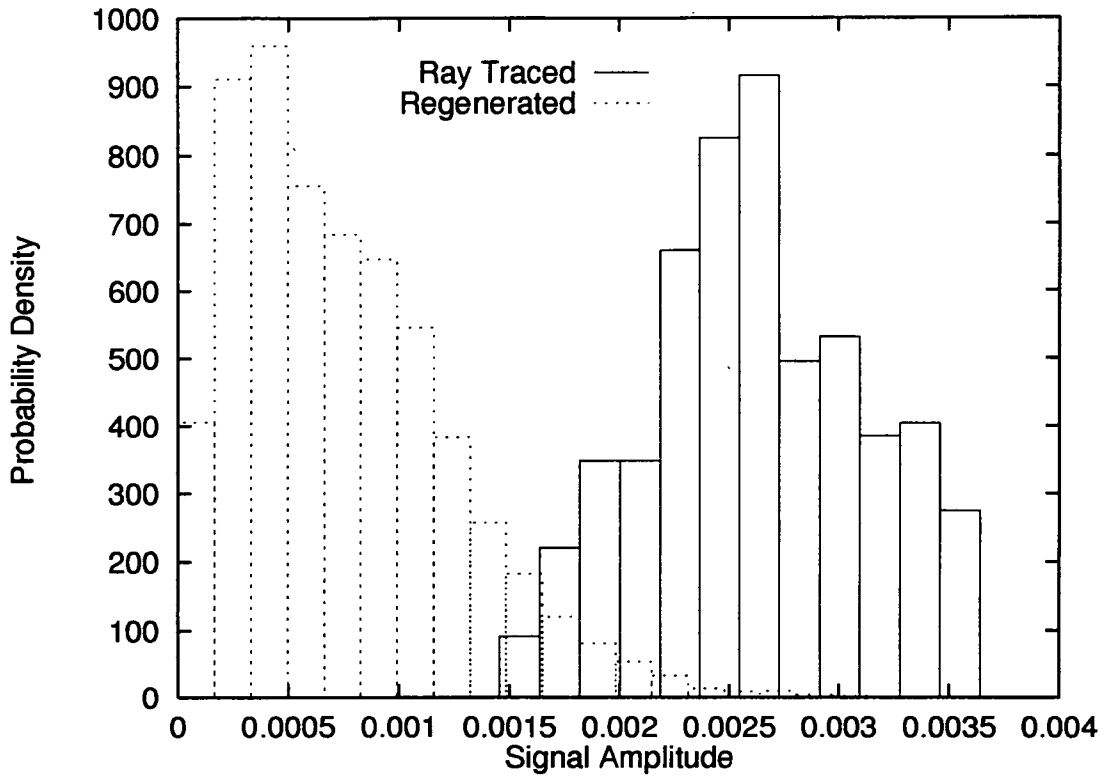

Figure 7–1: The results of using the joint probability graph information to regenerate a channel

LOS path, and occurs only once in each measurement made at this location. However, in the algorithm used to derive Figure 7–1 no such restrictions were placed on the choice of signal.

In order to generate a signal, then, from a statistical representation of the multipath nature of the channel, either more information must be obtained on the relationship between occupancy of the various points on the distribution, or some means of restricting the selection process in a logical manner must be evolved.

Investigation of the phase relationships of multipath components

Information on the phase relationship between the various multipath components that constitute a channel impulse have not been determined. While this is not readily determined in the practical environment, analysis of this may be performed by a simulation system.

Appendix A

Proof of Equations used in Section 3.3

Proof of (3.14) taken from [86]

For a horizontally polarized incident plane wave, the transmitted electric field, reflected electric field, and incident electric field are related by the relationship

$$\frac{\underline{E}_t}{\underline{E}_i} = 1 + \frac{\underline{E}_r}{\underline{E}_i} \Rightarrow \frac{\underline{E}_r}{\underline{E}_i} = \frac{\underline{E}_t}{\underline{E}_i} - 1 \tag{A.1}$$

given in (4.103) of [86]. A second relationship governing the electric fields which is true for all polarizations is given in (4.102) of [86] as

$$\frac{\underline{E}_r^2}{\underline{E}_i^2} = 1 - \frac{\eta_1}{\eta_2}\frac{\underline{E}_t^2}{\underline{E}_i^2}\frac{\cos\theta_t}{\cos\theta_i} \tag{A.2}$$

where η_1 and η_2 are the intrinsic impedances for the incident and transmission media respectively. Using Snell's law, we can relate θ_t to θ_i, and hence to ψ, the grazing angle of incidence, using the relationship

$$\cos\psi = \sin\theta_i = n' \sin\theta_t \tag{A.3}$$

where

$$n'^2 = \left(\frac{\eta_1}{\eta_2}\right)^2 . \tag{A.4}$$

Substituting (A.1) into (A.2) we get

$$\frac{\underline{E}_r^2}{\underline{E}_i^2}\left(1 + \frac{\eta_1}{\eta_2}\frac{\cos\theta_t}{\cos\theta_i}\right) + \frac{\underline{E}_r}{\underline{E}_i}\left(2\frac{\eta_1}{\eta_2}\frac{\cos\theta_t}{\cos\theta_i}\right) + \left(\frac{\eta_1}{\eta_2}\frac{\cos\theta_t}{\cos\theta_i} - 1\right) = 0 . \tag{A.5}$$

After factoring out

$$\frac{\underline{E}_r}{\underline{E}_t} = 1 \tag{A.6}$$

which is valid in the case of total reflection, the expression for (3.14) is obtained after substitution of (A.3) and (A.4) as

$$\frac{\underline{E}_r}{\underline{E}_t} = \frac{\sin\psi - \sqrt{n'^2 - \cos^2\psi}}{\sin\psi + \sqrt{n'^2 - \cos^2\psi}}. \tag{A.7}$$

Proof of (3.15) taken from [86]

For a vertically polarized incident plane wave, the transmitted electric field, reflected electric field, and incident electric field are related by the relationship

$$\frac{\underline{E}_t}{\underline{E}_i} = \left(1 - \frac{\underline{E}_r}{\underline{E}_i}\right)\frac{\cos\theta_i}{\cos\theta_t} \tag{A.8}$$

given in (4.107) of [86]. Substituting this into (A.2) we get

$$\frac{\underline{E}_r^2}{\underline{E}_i^2}\left(1 + \frac{\eta_1\cos\theta_t}{\eta_2\cos\theta_i}\right) + \frac{\underline{E}_r}{\underline{E}_i}\left(-2\frac{\eta_1\cos\theta_t}{\eta_2\cos\theta_i}\right) + \left(\frac{\eta_1\cos\theta_t}{\eta_2\cos\theta_i} - 1\right) = 0 \tag{A.9}$$

After factoring out

$$\frac{\underline{E}_r}{\underline{E}_t} = -1 \tag{A.10}$$

for the case of total reflection, the expression for (3.15) is obtained after substitution of (A.3) and (A.4) as

$$\frac{\underline{E}_r}{\underline{E}_t} = \frac{n'^2\sin\psi - \sqrt{n'^2 - \cos^2\psi}}{n'^2\sin\psi + \sqrt{n'^2 - \cos^2\psi}} \tag{A.11}$$

Proof of equations (3.16) and (3.17)

Using (A.1) and (3.14) it is possible to extend the equations given in [86] to describe the electric field that is transmitted into the second medium as well as the reflected field. Substituting (3.14) into (A.1) gives

$$\frac{\underline{E}_t}{\underline{E}_i} = \frac{2\sin\psi}{\sin\psi + \sqrt{n'^2 - \cos^2\psi}} \tag{A.12}$$

directly.

Burnside and Burgener [87] indicate that the transmission coefficient is related to the reflection coefficient by the relationship, $T = R - 1$ for both electric and magnetic fields. While this is true for horizontally polarized fields,

it is untrue for a vertically polarized ones. In order to deal with the electric field only, we can use (A.8) to derive the expression for a vertically polarized electric field. On substituting (3.15) into this equation we obtain

$$\frac{\underline{E}_t}{\underline{E}_i} = \left(\frac{2\sqrt{n'^2 - \cos^2\psi}}{n'^2 \sin\psi + \sqrt{n'^2 - \cos^2\psi}} \right) \frac{\cos\theta_i}{\cos\theta_t} \tag{A.13}$$

which after substituting in (A.3) we obtain

$$\frac{\underline{E}_t}{\underline{E}_i} = \frac{2n' \sin\psi}{n'^2 \sin\psi + \sqrt{n'^2 - \cos^2\psi}} . \tag{A.14}$$

Proof of equations (3.18) and (3.19)

We can calculate the transmission of $\underline{E}_t$ through the second skin of a wall by modifying the relationship given in (A.2) to

$$\frac{\underline{E}_{r_2}^2}{\underline{E}_t^2} = 1 - \frac{\eta_2}{\eta_1} \frac{\underline{E}_{t_2}^2}{\underline{E}_t^2} \frac{\cos\theta_i}{\cos\theta_t} . \tag{A.15}$$

Substituting a modified form of (A.1)

$$\frac{\underline{E}_{t_2}}{\underline{E}_t} = 1 + \frac{\underline{E}_{r_2}}{\underline{E}_t} \tag{A.16}$$

into (A.15) we can obtain the component $\underline{E}_{t_2}$ in terms of $\underline{E}_t$ as

$$\frac{\underline{E}_{t_2}}{\underline{E}_t} = \frac{2\sqrt{n'^2 - \cos^2\psi}}{\sin\psi + \sqrt{n'^2 - \cos^2\psi}} \tag{A.17}$$

and multiplying this by (3.16) gives (3.18) as

$$\frac{\underline{E}_{t_2}}{\underline{E}_i} = \frac{4 \sin\psi \sqrt{n'^2 - \cos^2\psi}}{\left(\sin\psi + \sqrt{n'^2 - \cos^2\psi}\right)^2} . \tag{A.18}$$

Similarly, substituting

$$\frac{\underline{E}_{t_2}}{\underline{E}_t} = \left(1 - \frac{\underline{E}_{r_2}}{\underline{E}_t}\right) \frac{\cos\theta_t}{\cos\theta_i} \tag{A.19}$$

into (A.15) gives

$$\frac{\underline{E}_{t_2}}{\underline{E}_t} = \frac{2\sqrt{n'^2 - \cos^2\psi}}{n' \sin\psi + \frac{1}{n'^2}\sqrt{n'^2 - \cos^2\psi}} \tag{A.20}$$

and hence (3.19),

$$\frac{\underline{E}_{t_2}}{\underline{E}_i} = \frac{4n'^2 \sin\psi \sqrt{n'^2 - \cos^2\psi}}{\left(n'^2 \sin\psi + \sqrt{n'^2 - \cos^2\psi}\right)^2} . \tag{A.21}$$

Proof of equations (3.20) and (3.21)

Using the relationship given in (A.16) for a horizontally polarized wave, and substituting (A.17) into this we obtain

$$\frac{\underline{E}_{r_2}}{\underline{E}_t} = -\frac{\sin\psi - \sqrt{n'^2 - \cos^2\psi}}{\sin\psi + \sqrt{n'^2 - \cos^2\psi}} \tag{A.22}$$

which describes the internally reflected electric field in terms of the internal incident field, giving rise to the general equation (3.20) as

$$\frac{\underline{E}_{r_{k+1}}}{\underline{E}_{r_k}} = (-1)\frac{\sin\psi - \sqrt{n'^2 - \cos^2\psi}}{\sin\psi + \sqrt{n'^2 - \cos^2\psi}} . \tag{A.23}$$

Similarly, substituting (A.20) into (A.19) we obtain

$$\frac{\underline{E}_{r_2}}{\underline{E}_t} = 1 - \left(\frac{2n'\sqrt{n'^2 - \cos^2\psi}\cos\theta_i}{\left(n'^2\sin\psi + \sqrt{n'^2 - \cos^2\psi}\right)\cos\theta_t} \right) . \tag{A.24}$$

After substituting in (A.3) we readily obtain (3.21) as

$$\frac{\underline{E}_{r_2}}{\underline{E}_t} = \frac{\underline{E}_{r_{k+1}}}{\underline{E}_{r_k}} = (-1)\frac{n'^2\sin\psi - \sqrt{n'^2 - \cos^2\psi}}{n'^2\sin\psi + \sqrt{n'^2 - \cos^2\psi}} . \tag{A.25}$$

Proof of equations (3.26) and (3.27)

From [87] we have the relationship that

$$R = R_1 + T_1T_2\sum_{n=2}^{\infty}(R_2)^{2n-3}(P_d)^{2n-2}(P_a)^{n-1} , \tag{A.26}$$

where $R_1 = -R_2$ for all polarizations, and P_d and P_a are phase delays. For a vertically polarized electromagnetic wave,

$$T_1 = (1 - R_1)\frac{\cos\theta_i}{\cos\theta_t} \tag{A.27}$$

and

$$T_2 = (1 - R_2)\frac{\cos\theta_i}{\cos\theta_t} = (1 + R_1)\frac{\cos\theta_i}{\cos\theta_t} . \tag{A.28}$$

Substituting this into (A.26) we obtain

$$R = R_1 + (1 - R_1^2)\frac{\cos^2\theta_i}{\cos^2\theta_t}\sum_{n=1}^{\infty}(-R_1)^{2n-1}(P_d)^{2n}(P_a)^n \tag{A.29}$$

and hence

$$R = R_1 \left[1 - (1 - R_1^2) \frac{\cos^2 \theta_i}{\cos^2 \theta_t} \frac{P_d^2 P_a}{1 - R_1^2 P_d^2 P_a} \right] . \tag{A.30}$$

Expanding this gives (3.26) as

$$R = R_1 \left[\frac{\cos^2 \theta_t - R_1^2 P_d^2 P_a \cos^2 \theta_t - P_d^2 P_a \sin^2 \psi + R_1^2 P_d^2 P_a \sin^2 \psi}{\cos^2 \theta_t \left(1 - R_1^2 P_d^2 P_a \right)} \right] . \tag{A.31}$$

A similar derivation for the transmission coefficient can be followed from the base equation

$$T = T_1 T_2 P_d P_t \sum_{n=0}^{\infty} (-R_1)^{2n} (P_d)^{2n} (P_a)^n \tag{A.32}$$

to give

$$T = \frac{T_1 T_2 P_d P_t}{1 - R_1^2 P_d^2 P_a} \tag{A.33}$$

and then (3.27) as

$$T = \frac{(1 - R_1^2) P_d P_t}{1 - R_1^2 P_d^2 P_a} \frac{n'^2 \sin^2 \psi}{n'^2 - \cos^2 \psi} . \tag{A.34}$$

Appendix B

Software

The software that has been developed during the course of the work for this thesis is partitioned into two sections. The first of these consists of the code for the ray tracing software to determine the received signal for a given building structure, and transmitter position. The software is designed to give access to various parameters of the propagation mechanisms, such as the number of multipaths that contribute to a given received signal, and present this information in the form of a probability distribution where appropriate or as a set of amplitudes and phases. The remainder of the software that has been developed, referred to as post processing software, is used for the processing of this information in order to make comparisons with measured data, and with statistical distributions. A certain degree of post processing is conducted in the ray tracing simulation software in order to reduce the storage requirements of the large quantity of data that the simulation can produce.

B.1 Ray Tracing Software

As described above, this software takes a representation of the building, within which the experiments are to be performed, and the location of a receiver and set of transmitter positions. For each of the transmitter positions, the effect of the transmitted signal on the receiver, its reflections off the walls and diffraction around corners is determined. Depending upon the type of information requested by the user, the result of this analysis may be output to

a file directly, or it may be stored internally for further analysis until the results for a set of transmitter positions have been determined.

B.1.1 Input and output data files

The input data to the programme consists of two files: one input file determines the building layout and construction as a series of walls and edges; and the other which determines the location of the receiver, the amount of noise to add to the system, the low signal threshold[1], the type of antenna to be used, the set of transmitter positions and the type of information to collect. This division of input information allows various experiments to be performed on the same building without duplication of the same information. A number of different types of information on the simulation run can be collected simultaneously, making more efficient use of computing resources. To run the programme, the user supplies the name of the second data file—which contains an explicit reference to the data file containing the description of the building—and the basename for the set of output files. The output files consist of one file with a human readable copy of the input information, which aids in identification of the data files later, and at least one other with the data from the simulation. Depending on the definition of the transmitter positions, multiple results files may be created.

B.1.2 Ray tracing software

The process of forming a ray tracing model of a particular environment is detailed in Section 3.7. The structure of this software is depicted in Figure B–1. In this figure each section of code is represented by a block. Blocks that are adjacent indicate that data is passed between the sections of code.

The operation of the simulation system is controlled by the input data files which influence the selection of the receiver and transmitter locations as well

---

[1]The low signal threshold is described in Section 3.7

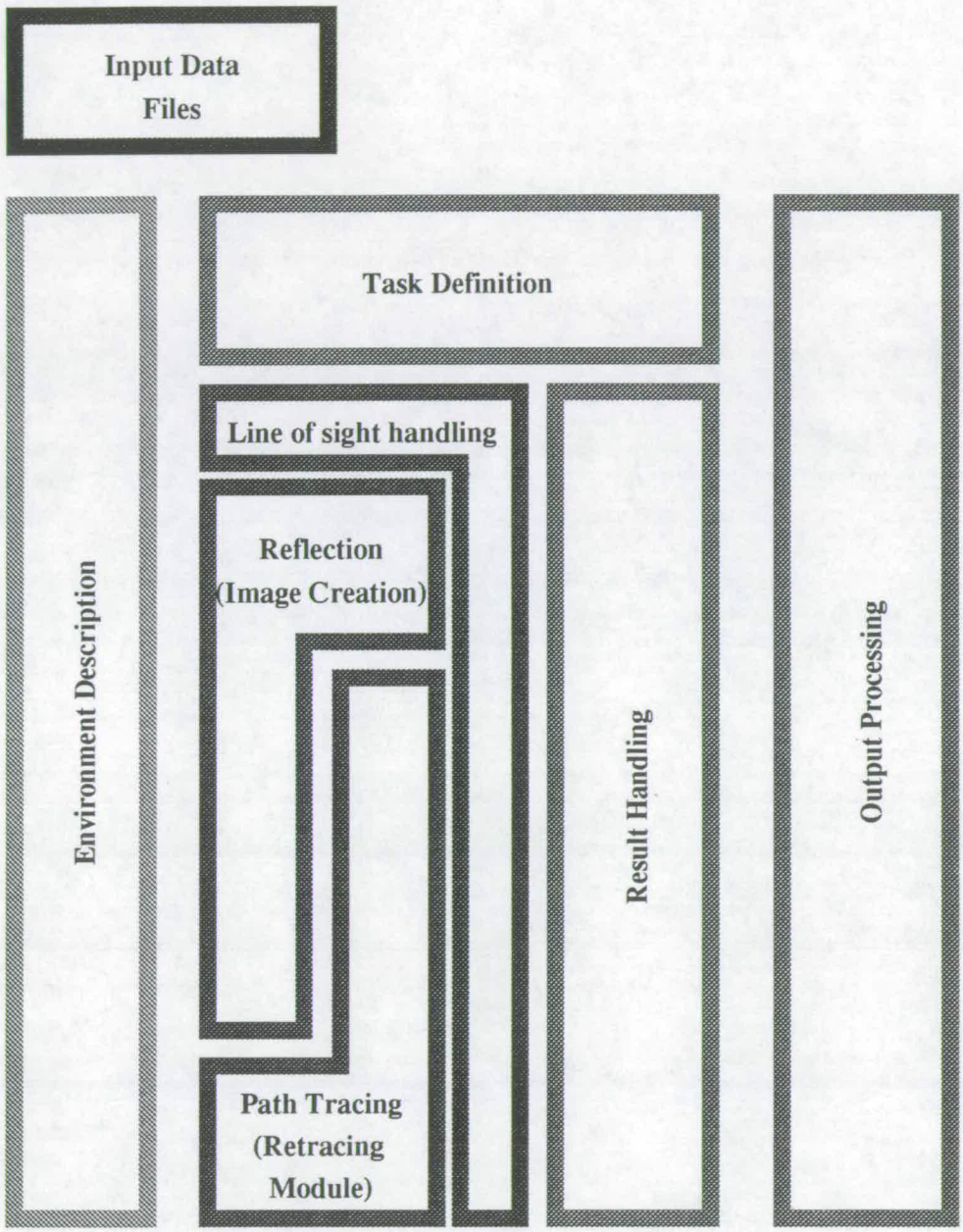

Figure B–1: Structure of the ray tracing software

as describing the environment. A description of the environment is derived from these files, and then used by the ray tracing functions of the software. The operation of the software is overseen by the task creation, or task definition, module which also passes accounting information to the result handler. The software deals with the line of sight path from the transmitter to the receiver initially, and then creates a set of images by a reflection process. These are operated on by a further module that traces out the path from the transmitter to receiver, via the reflections. The final segment of the transmitter to receiver path is treated in the same manner as the initial line of sight path by the same module. Finally, the result handling module collates the results which are then presented in a suitable format by the output processing module.

B.1.3 Possible speedup techniques to reduce computation time

The algorithm as it stands is not the most efficient mechanism for calculating a set of received signal values when the positions of the transmitter are close together. If a propagation path is considered for one transmitter position, and then the transmitter is moved to a location in close proximity to the first, the probability that the same surfaces are involved in the new propagation path is high. If it is determined that for two transmitter positions, within a reasonable distance of each other, the surfaces involved in the propagation paths are the same, then it is likely that for all transmitter positions in between these points the same is true. This allows the amount of computation involved in finding the propagation paths, which is the bulk of work in the above algorithm, to be reduced dramatically for a set of transmitter positions that are not randomly located around the building.

A second technique that doesn't make the above assumptions is to run the programme on a parallel machine. By doing so, a number of received signals may be computed simultaneously, and the programme is just as efficient for a random set of transmitter positions as it is for a set of positions in a regular pattern. However, as the transmitter positions may have different propagation trees, it is appropriate to run this algorithm on a multiple instruction, multi-

ple data (MIMD) machine—that is one with a set of independent processors. The disadvantage of this approach is that the communications overhead, and scheduling overhead of performing the first type of optimisation on such a machine make it impractical to implement efficiently. Therefore, a selection must be made between the two techniques as they are effectively mutually exclusive. The software written for the thesis uses the latter approach, implementing it on the Edinburgh Computing Surface provided by the Edinburgh Parallel Communications Centre.

The process of electromagnetic modelling, by its very nature, is an expensive task for computation, and the methods of reducing computation time described above do not address the basic problem of a task that increases rapidly as more information is incorporated into the modelling process. One remaining method exists to reduce the computation time for a given problem, and that is to simplify the description of the environment outwith the area of interest. For the Site B simulation, exact details of the building far from the areas of measurement are not critical to the simulation results as any signals that do propagate via these features will be attenuated greatly by the free-space propagation loss inherent in a point source transmission system. However, the error introduced by pursuing this technique may exceed the gain in accuracy of modelling the area of interest more completely.

B.2 Post Processing Software

The result of the ray tracing software is a set of signal values that represent the received signal for various positions within the environment, or may be a more detailed description of all of the propagating paths that contribute to the received signal for each position. In order to present the data in a more intelligible format, statistical processing may be performed, resulting in probability distributions. Such distributions may be used to compare the results of the simulation with measured results, or may be used to show that certain information is sufficient to recreate a particular type of channel model.

B.2.1 Probability Graphs

In essence a probability graph of a set of sampled data, whether the data is from a measurement experiment or from a simulation, is a histogram of the number of occurrences that a result was within a specific range centred around a notional mid-point of the histogram bin. The bin size may be irregular as in the case of data grouped in a logarithmic scale before being plotted on a linear one, in which case the mid-point is the mid-point of the logarithmic scale and is off-centre on a linear scale. A probability graph has the additional property that the sum of all the histogram bin values is 1, that is each bar indicates the number of times that a value fell within its specific range as a fraction of the total number of occurrences.

In order to compare with standard theoretical distributions which are generally in the form of probability density functions, it is necessary to scale the probability graph with respect to the range over which the graph is defined. For a probability graph with a regular bin size the scaling is uniform over the entire graph, but for a non-regular plot, each histogram bin must be scaled by the size of that bin. The result of the scaling operation is a probability density graph which is directly comparable to a probability density function.

On comparing a probability density graph with a probability density function it is necessary to have some measure of the closeness of the fit. One possible measure is the sum of square error (SE) values indicating the square of the difference between the probability density graph and the probability density function over that range. However, as each graph has a different range, it is difficult to compare the closeness of fit for a set of different measurements. A measure has been developed that overcomes this difficulty, and is called the modified mean square error (MoMSE). It is a value which is normalised to be independent of the area over which the distribution is fitted. It is calculated as

$$\mathrm{MoMSE} = \frac{\mathrm{samplesize}^2}{N} \sum (x_{\mathrm{samp}}(i) - x_{\mathrm{dist}}(i))^2 \qquad \text{(B.1)}$$

where $x_{\mathrm{samp}}(i)$ is the sample at point i, and $x_{\mathrm{dist}}(i)$ is the corresponding value of the distribution being fitted to the data. N is the number of samples being

used, and samplesize is the range of abscissal values over which the distribution is calculated. Using this method errors can be compared between different distributions, and different samples with different mean values.

The value of $x_{dist}(i)$ used in calculating the MoMSE should be determined from the cumulative distribution function of the theoretical distribution rather than the probability density function. The distinction is made as the probability density function value for a particular histogram bin centre point may not be the probability of a value occurring within that bin for the theoretical distributed variable. Instead, the cumulative distribution function values are calculated for each extreme of the histogram bin range, and the difference, when normalised by the size of the bin, can be compared with the probability density graph value. Clearly the normalisation process is the same one that was performed to generate the probability density graph from the probability graph, however using probability density graphs gives a useful visual aid in determining the closeness of a fit when the graph is superimposed with the probability density function on a plot. The cumulative distribution functions of the Nakagami, Ricean and Weibull distributions are given in Appendix C.

Appendix C

Probability Distributions

C.1 Nakagami Distribution

The Nakagami distribution [37] is defined by

$$p(R) = \frac{2m^m}{\Gamma(m)\Omega^m} R^{2m-1} \exp\left(-\frac{m}{\Omega}R^2\right) \quad R \geq 0 \tag{C.1}$$

where m is a shape parameter, and Ω controls the spread of the distribution. The distribution has a mean value defined by

$$E(R) = \frac{\Gamma(m+\frac{1}{2})}{\Gamma(m)}\left(\frac{\Omega}{m}\right)^{\frac{1}{2}} , \tag{C.2}$$

and a mean square value defined by

$$E(R^2) = \frac{\Gamma(m+1)}{\Gamma(m)}\left(\frac{\Omega}{m}\right) = \Omega \tag{C.3}$$

resulting in a variance

$$Var(R) = \Omega\left(1 - \frac{1}{m}\left(\frac{\Gamma(m+\frac{1}{2})}{\Gamma(m)}\right)^2\right) . \tag{C.4}$$

The cumulative distribution function can be defined by the expression

$$p(x) = \frac{2m^m}{\Gamma(m)\Omega^m}\int_0^x t^{2m-1}\exp\left(-\frac{m}{\Omega}t^2\right) dt . \tag{C.5}$$

Making the substitution of variable, $y = \frac{m}{\Omega}t^2$, we obtain the expression

$$p(x) = \frac{1}{\Gamma(m)}\int_0^{\frac{m}{\Omega}x^2} y^{m-1}\exp(-y)dy . \tag{C.6}$$

From [97, 3.381 (1)] we obtain

$$p(x) = \frac{1}{\Gamma(m)} \gamma\left(m, \frac{m}{\Omega} x^2\right) = P\left(m, \frac{m}{\Omega} x^2\right) , \tag{C.7}$$

the incomplete gamma function. Numerical solutions for this expression can be obtained using a series expression of $\gamma(a, x)$ or $\Gamma(a, x)$ selected according to which will give the fastest convergence [98, chapter 6].

C.2 Ricean Distribution

The Ricean distribution is defined by [2]

$$p(R) = \frac{R}{\sigma^2} \exp\left(-\frac{R^2 + s^2}{2\sigma^2}\right) I_0\left(\frac{Rs}{\sigma^2}\right) \quad R \geq 0 , \tag{C.8}$$

where s controls the mean of the distribution, σ its variance, and $I_0(\cdot)$ the modified Bessel function of the first kind, order zero. It has a mean value defined by

$$E(R) = \frac{\sqrt{\frac{\pi}{2}}\, \sigma^2\, L_{\frac{1}{2}}\left(-\frac{s^2}{2\sigma^2}\right)}{|\sigma|} , \tag{C.9}$$

where $L_n(x)$ is a Laguerre function satisfying the equation

$$x \frac{d^2y}{dx^2} + (1 - x) \frac{dy}{dx} + ny = 0 . \tag{C.10}$$

The mean square value of the distribution is given by

$$E(R^2) = s^2 + 2\sigma^2 . \tag{C.11}$$

The cumulative distribution function is defined by

$$p(x) = 1 - \exp\left(-\frac{s^2 + x^2}{2\sigma^2}\right) \sum_{k=0}^{\infty} \left(\frac{s}{r}\right)^k I_k\left(\frac{sx}{\sigma^2}\right) . \tag{C.12}$$

C.3 Weibull Distribution

The Weibull distribution is defined by three parameters, (α, β, ν) the location parameter, ν, being zero for positive random variables as encountered in radio channels. The reduced distribution is then defined by

$$p(R) = \frac{\beta}{\alpha}\left(\frac{R}{\alpha}\right)^{\beta-1} \exp\left[-\left(\frac{R}{\alpha}\right)^{\beta}\right] \quad R \geq 0 \tag{C.13}$$

where β is a shape parameter, and α controls the spread of the distribution. The distribution has a mean value defined by

$$E(R) = \alpha\Gamma\left(1 + \frac{1}{\beta}\right) , \tag{C.14}$$

and a mean square value defined by

$$E(R^2) = \alpha^2\Gamma\left(1 + \frac{2}{\beta}\right) \tag{C.15}$$

resulting in a variance

$$Var(R) = \alpha^2\left[\Gamma\left(1 + \frac{2}{\beta}\right) - \left(\Gamma\left(1 + \frac{1}{\beta}\right)\right)^2\right] . \tag{C.16}$$

The cumulative distribution function is defined by

$$p(x) = 1 - \exp\left[-\left(\frac{x}{\alpha}\right)^{\beta}\right] . \tag{C.17}$$

References

[1] R. H. Clarke. "A Statistical Theory of Mobile-Radio Reception". *Bell System Technical Journal*, 47(6):957–1000, July–August 1968.

[2] J. G. Proakis. *Digital Communications*. McGraw-Hill Series in Electrical Engineering. McGraw-Hill Book Company, second edition, 1989.

[3] I. S. Groves. "Personal Mobile Communications - a Vision of the Future". *British Telecom Technology Journal*, 8(1):7–11, January 1990.

[4] A. Lorenz. "Mercury plans mobile phone onslaught". In *The Sunday Times*, p 1, September 5 1993. Section 3.

[5] G. L. Turin. "Introduction to Spread-Spectrum Antimultipath Techniques and their Application to Urban Digital Radio". *Proceedings of the IEEE*, 68(3):328–353, March 1980.

[6] R. J. Bailey and G. R. Summers. "Radio channel characterisation for the digital European cordless telecommunications system". *British Telecom Technology Journal*, 8(1):25–30, January 1990.

[7] R. W. Lorenz and H.-J. Gelbrich. "Bit error distribution in digital mobile radiocommunication—Comparison between field measurements and fading simulation". *IEE Proceedings*, 132, part F(5):343–347, August 1985.

[8] D. C. Cox. "Delay Doppler Characteristics of Multipath Propagation at 910 MHz in a Suburban Mobile Radio Environment". *IEEE Transactions on Antennas and Propagation*, AP-20(5):625–635, September 1972.

[9] A. S. Bajawa and J. D. Parsons. "Small-area Characterisation of UHF urban and suburban mobile radio propagation". *IEE Proceedings*, 129, Part F(2):102–109, April 1982.

[10] J. D. Parsons and A. S. Bajawa. "Wideband Characterisation of Fading Mobile Radio Channels". *IEE Proceedings*, 129, Part F(2):95–101, April 1982.

[11] J. Van Rees. "Measurements of the Wide-Band Radio Channel Characteristics for Rural, Residential, and Suburban Areas". *IEEE Transactions on Vehicular Technology*, VT-36(1):2–6, Feburary 1987.

[12] S. H. Jamali and T. Le-Ngoc. "Bandwidth Efficient Communication via a Rayleigh Fading Channel Using RS Coded Multiphase Signaling". *IEEE Transactions on Communications*, 41(11):1594–1597, November 1993.

[13] B. Vucetic. "Bandwidth Efficient Concatenated Coding Schemes for Fading Channels". *IEEE Transactions on Communications*, 41(1), January 1993.

[14] K. H. Hofmann. "Bandwidth Efficient Multilevel Block 8-PSK Modulation Code for Rician Fading Chanels". *Electronic Letters*, 29(16):1493–1494, August 1993.

[15] W. T. Webb, L. Hanzo, and R. Steele. "Bandwidth efficient QAM schemes for Rayleigh fading channels". *IEE Proceedings*, 138, Part I(3):169–175, June 1991.

[16] W. Stallings. *Data and Computer Communications*. Macmillan Publishing Company, 866 Third Avenue, New York, New York 10022, second edition, 1988.

[17] J. Obuchowski. "Wireless Communications and Spectrum Conservation: Sending a Signal to Conserve". *IEEE Communications Magazine*, 29(2):26–29, February 1991.

[18] M. A. Stuchly. "Health Considerations for Portable Transceivers". In *Proceedings IEEE International Conference on Selected Topics in Wireless Communications*, pp 409–412, June 25–26 1992. Vancouver, BC.

[19] D. Molkdar. "Review on radio propagation into and within buildings". *IEE Proceedings*, 138, part H(1):61–73, February 1991.

[20] M. Lecours, J.-Y. Chouinard, G. Y. Delisle, and J. Roy. "Statistical Modeling of the Received Signal Envelope in a Mobile Radio Channel". *IEEE Transactions on Vehicular Technology*, 37(4):204–212, November 1988.

[21] A. M. D. Turkmani, J. D. Parsons, and D. G. Lewis. "Radio Propagation into Buildings at 441, 900 and 1400 MHz". In *Proceedings of the 4th International Conference on Land Mobile Radio*. IERE, December 1987. University of Warwick, Coventry.

[22] A. F. de Toledo and A. M. D. Turkmani. "Propagation into and within Buildings at 900, 1800 and 2300 MHz". In *Proceedings of the 42nd Vehicular Technology Conference*, pp 633–636, May 10–13 1992. Denver, Colorado.

[23] D. C. Cox, R. R. Murray, and A. W. Norris. "Measurements of 800–MHz Radio Transmission into Buildings with Metalic Walls". *The Bell System Technical Journal*, 62(9):2695–2717, November 1983.

[24] D. M. J. Devasirvatham, C. Banerjee, M. J. Krain, and D. A. Rappaport. "Multi-frequency Radiowave Propagation Measurements in the Portable Radio Environment". In *Conference Record of IEEE International Conference on Communications '90*. IEEE, April 16–19 1990. Volume 4.

[25] S. E. Alexander. "Radio Propagation within Buildings at 900 MHz". *Electronics Letters*, 18(21):913–914, October 14 1982.

[26] S. E. Alexander. "Characterising Buildings for Propagation at 900MHz". *Electronics Letters*, 19(20):860, September 29 1983.

[27] S. E. Alexander and G. Pugliese. "Cordless Communication Within Buildings: results of measurements at 900 MHz and 60 GHz". *British Telecom Technology Journal*, 1(1):99–105, July 1983.

[28] S. Y. Seidel and T. S. Rappaport. "900 MHz Path Loss Measurements and Prediction Techniques for In-Building Communication System Design". In *Proceedings of the 41st IEEE Vehicular Technology Conference*, pp 613–618, May 19–22 1991. St Louis, Missouri.

[29] F. C. Owen and C. D. Pudney. "In-building Propagation at 900MHz and 1650MHz for Digital Cordless Telephones". In *Sixth International Confer-*

ence on Antennas and Propagation, ICAP89, pp 276–280. IEE, April 4–7 1989. Volume 2:Propagation : University of Warwick, Coventry, U.K.

[30] S. R. Todd, M. S. El-Tanany, and S. A. Mahmoud. "Space and Frequency Diversity Measurements of the 1.7GHz Indoor Radio Channel using a Four-Branch Receiver". *IEEE Transactions on Vehicular Technology*, 41(3):312–320, August 1992.

[31] R. J. C. Bultitude. "Measurement, Characterization and Modeling of Indoor 800/900 MHz Radio Channels for Digital Communications". *IEEE Communications Magazine*, 25(6):5–12, June 1987.

[32] L. P. Rice. "Radio Transmission into Buildings at 35 and 150MHz". *The Bell System Technical Journal*, 38(1):197–210, January 1959.

[33] H. E. Dempsey. "A Standard Plane Earth Equation". In *Proceedings of Electronicom '85*. IEEE, October 7–9 1985. Toronto.

[34] T. S. Rappaport and C. D. McGillem. "UHF Fading in Factories". *IEEE Journal on Selected Areas in Communications*, 7(1):40–48, January 1989.

[35] A. J. Goldsmith and L. J. Greenstein. "An Empirical Model for Urban Microcells with Applications and Extensions". In *Proceedings of the 42nd Vehicular Technology Conference*, pp 419–422, May 10–13 1992. Denver, Colorado.

[36] H. Suzuki. "A Statistical Model for Urban Radio Propagation". *IEEE Transactions on Communications*, COM-25(7):673–680, July 1977.

[37] M. Nakagami. "The m-Distribution, a general formula of intensity of rapid fading". In W. G. Hoffman, editor, *Statistical Methods in Radio Wave Propagation: Proceedings of a Symposium held at the University of California*, pp 3–36. Permagon Press, 1960.

[38] M. Abdi. "RF Measurements for Indoor Radio Communications". Fourth Year Project, 94.497 : Department of Systems and Computer Engineering, Carleton University : Ottawa, Ontario, Canada.

[39] A. U. Sheikh, M. Handforth, and M. Abdi. "Indoor Mobile Radio Channel at 946MHz: Measurements and Modeling". In *Proceedings IEEE Vehicular Technology Conference*, pp 73–76, May 18–20 1993. Secaucus, NJ.

[40] N. C. Beaulieu and A. A. Abu-Dayya. "Analysis of Equal Gain Diversity on Nakagami Fading Channels". *IEEE Transactions on Communications*, 39(2):225–234, February 1991.

[41] N. C. Beaulieu and A. A. Abu-Dayya. "Correction to "Analysis of Equal Gain Diversity on Nakagami Fading Channels"". *IEEE Transactions on Communications*, 40(9):1553, September 1992.

[42] P. J. Crepeau. "Uncoded and Coded Performance of MFSK and DPSK in Nakagami Fading Channels". *IEEE Transactions on Communications*, 40(3):487–493, March 1992.

[43] W. C. Y. Lee. *Mobile Communications Engineering*. McGraw-Hill Book Company, 1221 Avenue of the Americas, New York, NY 10020, 1982.

[44] S. Kozono, T. Tsuruhara, and M. Sakamoto. "Base Station Polarization Diversity Reception for Mobile Radio". *IEEE Transactions on Vehicular Technology*, VT-33(4):301–306, November 1984.

[45] R. G. Vaughan. "Polarization Diversity in Mobile Communications". *IEEE Transactions on Vehicular Technology*, 39(3):177–186, August 1990.

[46] W. C.-Y. Lee and Y. S. Yeh. "Polarization Diversity System for Mobile Radio". *IEEE Transactions on Communications*, COM-20(5):912–923, October 1972.

[47] D. C. Cox, R. R. Murray, H. W. Arnold, A. W. Norris, and M. F. Wazowicz. "Cross-Polarization Coupling Measured for 800MHz Radio Transmission In and Around Houses and Large Buildings". *IEEE Transactions on Antennas and Propagation*, AP-34(1):83–87, January 1986.

[48] W. C. Y. Lee and Y. S. Yeh. "On the Estimation of the Second-Order Statistics of Log Normal Fading in Mobile Radio Environment". *IEEE Transactions on Communications*, COM-22(6):869–873, June 1974.

[49] S. Stein. "Fading Channel Issues in System Engineering". *IEEE Journal on Selected Areas in Communications*, SAC-5(2):68–89, February 1987.

[50] S. J. Howard and K. Pahlavan. "Doppler Spread Measurements of Indoor Radio Channel". *Electronic Letters*, 26(2):107–109, January 18 1990.

[51] G. A. Arredondo, W. H. Chriss, and E. H. Walker. "A Multipath Fading Simulator for Mobile Radio". *IEEE Transactions on Vehicular Technology*, VT-22(4):241–244, November 1973.

[52] J. I. Smith. "A Computer Generated Multipath Fading Simulation for Mobile Radio". *IEEE Transactions on Vehicular Technology*, VT-24(3):39–40, August 1975.

[53] E. Casas and C. Leung. "A Simple Digital Fading Simulator for Mobile Radio". *IEEE Transactions on Vehicular Technology*, 39(3):205–212, August 1990.

[54] J. R. Ball. "A real-time Fading Simulator for Mobile Radio". *The Radio and Electronic Engineer*, 52(10):475–478, October 1982.

[55] W. F. Bodtmann and H. W. Arnold. "Fade-Duration Statistics of a Rayleigh-Distributed Wave". *IEEE Transactions on Communications*, COM-30(3):549–553, March 1982.

[56] P. A. Bello. "Characterization of Randomly Time-Variant Linear Channels". *IEEE Transactions on Communications Systems*, CS-11(4):360–393, December 1963.

[57] E. N. Gilbert. "Energy Reception for Mobile Radio". *Bell System Technical Journal*, 44(8):1779–1803, October 1965.

[58] W. D. Rummler. "More on the Multipath Fading Channel Model". *IEEE Transactions on Communications*, COM-29(3):346–352, March 1981.

[59] A. A. M. Saleh and R. A. Valenzuela. "A Statistical Model for Indoor Multipath Propagation". *IEEE Journal on Selected Areas in Communications*, SAC-5(2):128–137, February 1987.

[60] R. Davies, M. Bensebti, M. A. Beach, and J. P. McGeehan. "Wireless Propagation Measurements in Indoor Multipath Environments at 1.7GHz

and 60GHz for Small Cell Systems". In *Proceedings of the 41st IEEE Vehicular Technology Conference*, pp 589–593, May 19–22 1991. St Louis, Missouri.

[61] D. Tholl, M. Fattouche, R. J. C. Bultitude, P. Melançon, and H. Zaghloul. "A Comparison of Two Radio Propagation Channel Impulse Response Determination Techniques". *IEEE Transactions on Antennas and Propagation*, 41(4):515–516, April 1993.

[62] E. Zollinger. "Measured Inhouse Radio Wave Propagation Characteristics for Wideband Communication Systems". In *Conference Proceedings on Area Communications of the 8th European Conference on Electrotechnics*, pp 314–317. IEEE, June 13–17 1988. Stockholm, Sweden.

[63] W. F. Walker. "Baseband Multipath Fading Simulator". *Radio Science*, 1(7):763–767, July 1966.

[64] P. A. Daniel, G. El Zein, M. Salehudin, and J. Citerne. "Etude et Réalisation d'un Simulateur de Canal Radiomobile à Large Bande". *L'Onde Electrique*, 68(2):82–89, Mars 1988.

[65] G. L. Turin, F. D. Clapp, T. L. Johnston, S. B. Fine, and D. Lavry. "A Statistical Model of Urban Multipath Propagation". *IEEE Transactions on Vehicular Technology*, VT-21(1):1–9, February 1972.

[66] H. Hashemi. "Simulation of the Urban Radio Propagation Channel". *IEEE Transactions on Vehicular Technology*, VT-28(3):213–225, August 1979.

[67] R. Ganesh and K. Pahlavan. "On Arrival of Paths in Fading Multipath Indoor Radio Channels". *Electronics Letters*, 25(12):763–765, June 8 1989.

[68] R. Ganesh and K. Pahlavan. "On the Modeling of Fading Multipath Indoor Radio Channels". In *Proceedings IEEE GLOBECOM '89*, pp 1346–1350. IEEE, 27–30 November 1989. Volume 3 : Dallas, Texas.

[69] R. Ganesh and K. Pahlavan. "Statistical Modelling and Computer Simultaion of Indoor Radio Channel". *IEE Proceedings*, 138, part I(3):153–161, June 1991.

[70] P. Yegani and C. D. McGillem. "A Statistical Model for the Factory Radio Channel". *IEEE Transactions on Communications*, 39(10):1445–1454, October 1991.

[71] K. Pahlavan and R. Ganesh. "Wideband Frequency and Time Domain Models for the Indoor Radio Channel". In *Proceedings IEEE GLOBECOM '91*, pp 32.4.1–6, 1991.

[72] S. J. Howard and K. Pahlavan. "Autoregressive Modeling of Wide-Band Indoor Radio Propagation". *IEEE Transactions on Communications*, 40(9):1540–1552, September 1992.

[73] W. H. Lau, J. Austin, A. Hewitt, E. Vilar, and L. Martin. "Analysis of the Time-Variant Structure of Microwave Line-of-Sight Multipath Phenomena". *IEEE Transactions on Communications*, 39(6):847–855, June 1991.

[74] K. J. Gladstone and J. P. McGeehan. "Computer Simulation of Multipath Fading in the Land Mobile Radio Environment". *IEE Proceedings*, 127, Part G(6):323–330, December 1980.

[75] K. J. Gladstone and J. P. McGeehan. "A Computer Simulation of the Effect of Fading on a Quasi-Synchronous Sideband Diversity AM Mobile Radio Scheme". *IEEE Journal on Selected Areas in Communications*, SAC-2(1):191–203, January 1984.

[76] M. Lebherz, W. Wiesbeck, and W. Krank. "A Versaitle Wave Propagation Model for the VHF/UHF Range Considering Three-Dimensional Terrain". *IEEE Transactions on Antennas and Propagation*, 40(10):1121–1131, October 1992.

[77] J. W. McKown and R. L. Hamilton, Jr. "Ray Tracing as a Design Tool for Radio Networks". *IEEE Network Magazine*, 5(4):27–30, November 1991.

[78] W. Honcharenko, H. L. Bertoni, J. L. Dailing, J. Qian, and H. D. Yee. "Mechanisms Governing UHF Propagation on Single Floors in Modern Office Buildings". *IEEE Transactions on Vehicular Technology*, 41(4):496–504, November 1992.

[79] K. Furutsu and T. Ishida. "On the Theory of Amplitude Distribution of Impulsive Random Noise". *Journal of Applied Physics*, 32(7):1206–1221, July 1961.

[80] K. L. Blackard, T. S. Rappaport, and C. W. Bostian. "Radio Frequency Noise Measurements and Models for Indoor Wireless Communications at 918MHz, 2.44GHz, and 4.0GHz". In *Conference Record of the International Conference on Communications, ICC '91*, pp 1.6.1–5. IEEE, 23–26 June 1991. Denver : Volume 1.

[81] G. R. Valenzuela. "Depolarization of EM Waves by Slightly Rough Surfaces". *IEEE Transactions on Antennas and Propagation*, AP-15(4):552–557, July 1967.

[82] V. Celli, A. A. Maradudin, A. M. Marvin, and A. R. McGurn. "Some Aspects of Light Scattering from a Randomly Rough Metal Surface". *Journal of the Optical Society of America A*, 2(12):2225–2239, December 1985.

[83] J. D. Kraus and K. R. Carver. *Electromagnetics*. McGraw-Hill, second edition, 1973.

[84] R. B. Adler, L. J. Chu, and R. M. Fano. *Electromagnetic energy transmission and radiation*. John Wiley & Sons, Inc., 1960.

[85] H. E. Dempsey. "Technical Opinion". *Mobile Radio Technology*, 4(7):21–22, July 1986.

[86] H. R. Reed and C. M. Russel. *Ultra High Frequency Propagation*. John Wiley & Sons, Inc., 1953.

[87] W. D. Burnside and K. W. Burgener. "High Frequency Scattering by a Thin Lossless Dielectric Slab". *IEEE Transactions on Antennas and Propagation*, AP-31(1):104–111, January 1983.

[88] J. B. Keller. "Diffraction by an Aperture". *Journal of Applied Physics*, 28(4):426–444, April 1957.

[89] R. G. Kouyoumjian and P. H. Pathak. "A Uniform Geometrical Theory of Diffraction for an Edge in a Perfectly Conducting Surface". *Proceedings of the IEEE*, 62(11):1448–1461, November 1974.

[90] M. C. Lawton and J. P. McGeehan. "The Application of GTD and Ray Launching Techniques to Channel Modelling for Cordless Radio Systems". In *Proceedings 42nd VTS Conference*, May 10–13 1992. Denver, Colorado : Volume 1.

[91] O. Landron, M. J. Feuerstein, and T. S. Rappaport. "In Situ Microwave Reflection Coefficient Measurements for Smooth and Rough Exterior Wall Surfaces". In *Proceedings IEEE Vehicular Technology Conference*, pp 77–80, May 18–20 1993. Secaucus, NJ.

[92] S. O. Rice. "Reflection of Electromagnetic Waves from Slightly Rough Surfaces". In *Communications on Pure and Applied Mathematics*, pp 351–378, 1951. Volume 4.

[93] P. Beckmann. "Scattering by Non-Gaussian Surfaces". *IEEE Transactions on Antennas and Propagation*, AP-21(2):169–175, March 1973.

[94] S. R. Saunders and F. R. Bonar. "Mobile Radio Propagation in Built-up Areas: a Numerical Model of Slow Fading". In *Proceedings of the 41st IEEE Vehicular Technology Conference*, pp 295–300, May 19–22 1991. St Louis, Missouri.

[95] J. G. Wilson. *The Electrical Properties of Concrete.* PhD thesis, The University of Edinburgh, Edinburgh, Scotland, 1986. Ph.D. Thesis.

[96] J. G. Wilson and H. W. Whittington. "Variations in the electrical properties of concrete with change in frequency". *IEE Proceedings*, 137, Part A(5):246–254, September 1990.

[97] I. S. Gradshteyn and I. M. Ryzhik. *Table of Integrals, Series, and Products.* Academic Press, corrected edition, 1980.

[98] W. H. Press, B. P. Flannery, S. A. Teukolsky, and W. T. Vetterling. *Numerical Recipies in Pascal.* Cambridge University Press, Cambridge, 1989.

Publications

- D. I. Laurenson, A. U. H. Sheikh and S. McLaughlin. "Characterisation of the Indoor Mobile Radio Channel Using a Ray Tracing Technique", in *Proceedings IEEE International Conference on Selected Topics in Wireless Communications*, pp 65–68, June 25–26, 1992. Vancouver, BC, CANADA.
- D. I. Laurenson, A. U. H. Sheikh and S. McLaughlin. "The use of Ray Tracing in Characterising the Indoor Mobile Radio Channel", in *Proceedings of the Canadian Conference on Electrical and Computer Envineering*, pp WM10.2.1–4, September 13–16, 1992. Toronto, ON, CANADA.
- D. I. Laurenson, S. McLaughlin and A. U. H. Sheikh. "A Ray Tracing Approach to Channel Modelling for the Indoor Environment", in *Proceedings IEEE Vehicular Technology Conference*, pp 246–249, May 18–20, 1993. Secacus, NJ, USA.
- D. I. Laurenson, S. McLaughlin and A. U. H. Sheikh. "Characterisation of the Indoor Mobile channel using a Ray Tracing Model", in *Proceedings of the Fifth Bangor Symposium on Communications*, pp 132-135, June 2–3, 1993. Bangor, WALES.
- D. I. Laurenson, S. McLauglin and A. U. H. Sheikh. "The Application of Ray Tracing and the Geometrical Theory of Diffraction to Indoor Channel Modelling", to be published in Proceedings IEEE GLOBECOM '93, November 29–December 2, 1993. Houston, TX, USA.

D. I. Laurenson, S. McLaughlin and A. U. H. Sheikh. "Characterisation of the Indoor Mobile channel using a Ray Tracing Model", in *Proceedings of the Fifth Bangor Symposium on Communications*, pp 132-135, June 2–3, 1993. Bangor, WALES.

Characterisation of the Indoor Mobile channel using a Ray Tracing Model

D. I. Laurenson* S. McLaughlin* A. U. H. Sheikh†

Abstract

A ray tracing model is constructed to investigate the propagation mechanisms underlying indoor radio communications. The model is used as the basis for a simulation of two buildings for which measured data is available. Characteristics of the channel distributions are determined using the simulation, and the role of diffraction in indoor propagation is also demonstrated.

1 Introduction

In recent years, the personal communications industry has witnessed a rapid growth in the number of communicating devices being used in the average office. With such an increase, the investigation into the use of radio based systems to connect these devices together becomes essential. Radio systems can not only reduce the amount of wiring, which reduces the cost of installing and updating a network of communicating devices, but also provide a flexibility not available in a wired network. As the radio bandwidth in the indoor environment is already overcrowded, a rationalisation of the various communication techniques must be performed. To perform this task efficiently detailed models of the channel must be developed, and the results used to design efficient coding and interconnection strategies.

The indoor environment is characterised by a large number of propagation paths from the transmitter to the receiver resulting in a multipath environment. Unlike the outdoor mobile environment where one of the communicating entities is sited above building height, the indoor environment has both the communicating entities in close proximity to each other, and to reflecting and diffracting objects. In relation to channel models, the indoor environment differs from its outdoor counterpart in that the effects of a floor and ceiling necessitate the examination of the problem in three dimensions. To date, much of the work on indoor channel characterisation has concentrated on experimental work, and attempts to model these results for various types of environment.

By examining the physical mechanism of the radio propagation that occurs in the indoor environment, it should be possible to derive one unified model that is flexible enough to incorporate the various types of channel encountered by a radio communication system. One approach to this problem is to use a ray tracing technique to model the propagated wave in terms of the constituent parts of the fields that arrive at the receiver via various reflections and diffractions that occur because of objects and partitions in the building. Such a technique leads to the determination of the physical basis behind various statistical models that are found to describe the indoor environment such as the Nakagami model.

A simulation of the ray tracing model is applied to two buildings that have been previously characterised by measurements. The measurement results are compared, as are the simulation results for the same locations. From this comparison, characteristics of the environment important in determining the resulting channel are derived. Investigation into the effects of diffraction for one of the sites is also conducted by incorporating the Geometrical Theory of Diffraction[1] into the simulation system.

2 Ray Tracing Model

A ray tracing model of electromagnetic propagation is based on the principles of optics with extensions to incorporate additional mechanisms that apply to radio propagation. The source of the electromagnetic wave is treated as the source of a number of directed rays that are normal to the surfaces of equal electric potential. On striking a surface, an additional, or reflected ray, is generated with a phase and power at the surface determined by the type of surface causing the reflection as well as the wavelength of the incident wave, the angle of incidence and the polarisation of the wave. Along the length of a ray, the power diminishes according to the freespace power loss. A signal may be reflected multiple times and still be a significant contributor, so multiple order reflections of the transmitted and the diffracted electromagnetic signals have to be considered.

Surfaces can be considered as smooth when the surface irregularities are below a specific height. In general the commonly assumed height is $\frac{\lambda}{8}$, but can be more stringent for rays whose grazing angle is less than $\frac{\pi}{6}$[2]. For purposes of simulation at frequencies around 1GHz it is assumed that the size of irregularities in walls is not sufficiently great to cause a large degree of scattering, so surfaces are treated as perfectly smooth objects.

The total electromagnetic field can be determined

*Department of Electrical Engineering, The University of Edinburgh

†Department of Systems and Computer Engineering, Carleton University, Ottawa, Canada

at an observation point as the superposition of all the incident reflected and diffracted rays as well as the direct line of sight path between the transmitter and the observation point. As the path lengths of each of the contributions vary, multiple copies of any transmitted signal are received with various time delays.

3 Simulation Results

A simulation of the ray tracing model was applied to two different scenarios for which measured results are available. The first scenario, known as site A, is one floor of an open plan office building that is devoid of furnishings save for one sectioned off area containing metallic equipment. A lift shaft, with some adjoining offices, is located at the centre of the building. A schematic layout of the floor is shown in figure 1. The second building to be modelled (site B) is one floor of a University building containing furniture, and a large number of partitions. A schematic showing the room partitions for this site is shown in figure 2. As a result of using different transmitter frequencies, the dimensions of the two buildings are approximately the same when measured in terms of transmitter wavelengths, each building being approximately 200 wavelengths wide. They are shown to the same scale in figures 1 and 2.

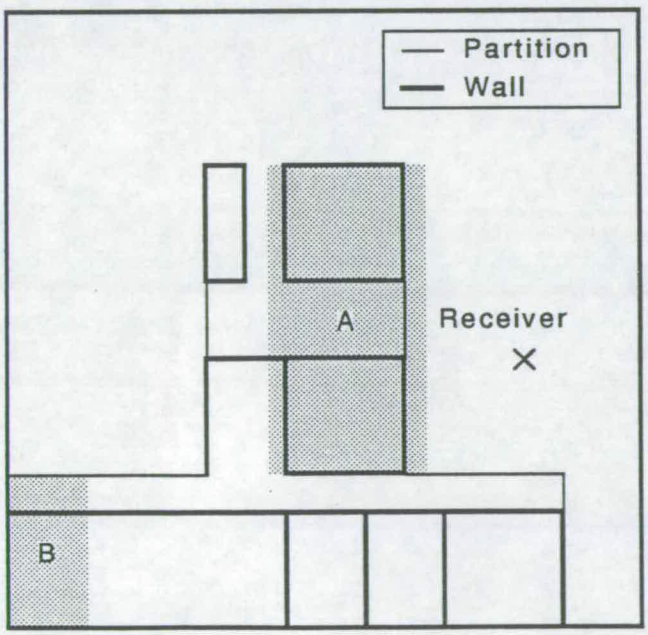

Figure 1: Schematic of site A

At site A, the receiver is located at ceiling height close to the centre of the building while the transmitter is free to roam over the floor area being carried by the person conducting the measurements. The floor area is divided up into 64 cells of size 8m × 8m each with measurement runs of 60 seconds being conducted over each area. The transmitter is operating at 945MHz with a sampling frequency of 60Hz. Results for the shaded areas A and B were not obtainable due to obstructions that impeded the experimental process.

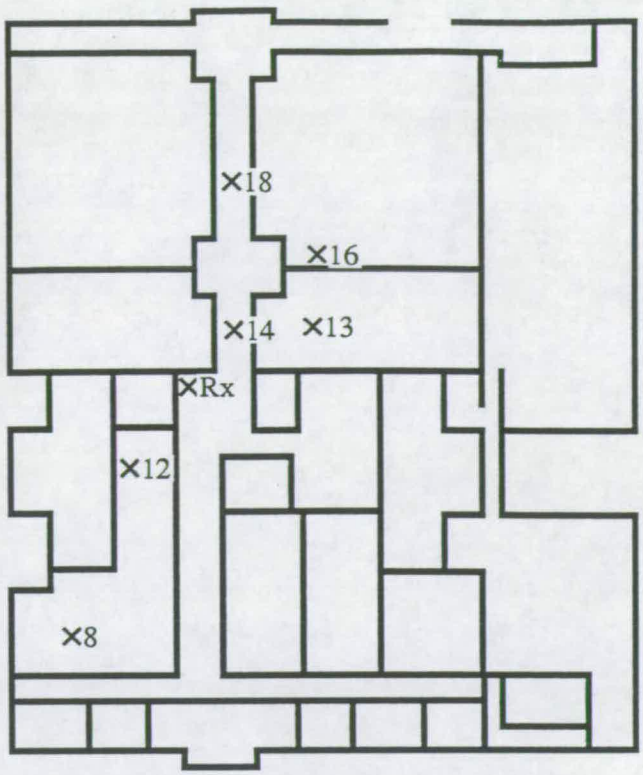

Figure 2: Schematic of site B

The measurement procedure for site B is documented by Todd *et al.*[3]The receiver is again located centrally in the building (marked Rx on the schematic), and test sites are located at various positions in the building. The experimental procedure consists of moving the transmitting antenna around a prescribed circle of circumference 1m using a wooden assembly. Measurements are conducted on a continuous wave (CW) transmission centred at 1.75GHz.

3.1 Signal amplitude distributions

For both sites, probability density functions are created from both the measured and the simulated results, modelling the experimental procedure as closely as possible. It is found that the probability functions are modelled well, in both the simulations and the measurement experiments, by a Nakagami distribution. This distribution incorporates the Rayleigh distribution as a special case, can approximate the Ricean distribution. The Nakagami distribution is a two parameter distribution defined by[4]

$$p(x) = \frac{2m^m x^{2m-1}}{\Gamma(m)\Omega^m} \exp\left(-\frac{m}{\Omega}x^2\right) \qquad (1)$$

with mean value $\overline{X} = \frac{\Gamma(m+\frac{1}{2})}{\Gamma(m)}\left(\frac{\Omega}{m}\right)^{\frac{1}{2}}$ and variance $\overline{X^2} = \frac{\Gamma(m+1)}{\Gamma(m)}\left(\frac{\Omega}{m}\right)$. m controls the overall shape of the distribution, and Ω the spread and mean value.

A sample result for site A showing the measured and the simulated results as well as a Nakagami distribution that models the measured results well is shown in figure 3. A similar comparison is made for location 8 of site B in figure 4. For these figures, the simulated results are based solely on reflectors in the environment, the effects of diffraction initially being neglected.

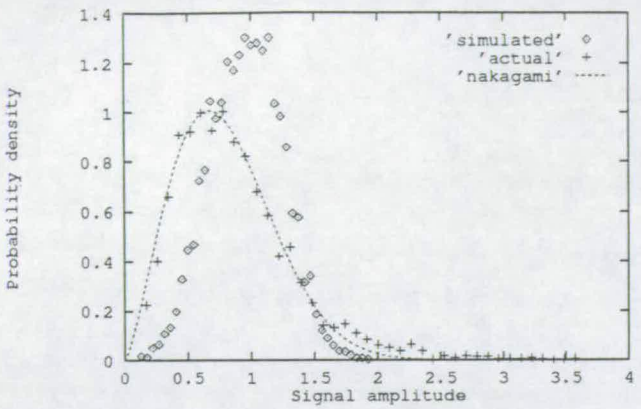

Figure 3: Simulated and Actual pdf with closest fit Nakagami curve for site A

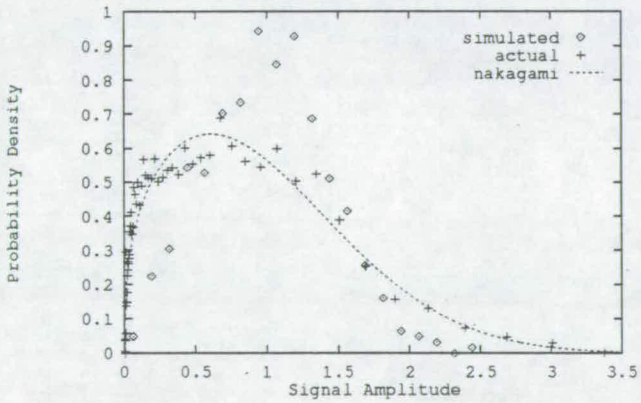

Figure 4: Simulated and Actual pdf with closest fit Nakagami curve for site B

In order to analyse these results it is convenient to use the best fitting Nakagami curve to determine the shapes of the distributions. The best fitting curve is defined as one which results in the lowest Modified Mean Square Error (MoMSE) value between the distribution and the results to be modelled. MoMSE is a normalised error that can be compared between distributions, and is independent of the mean value of the distribution. It is defined as

$$\text{MoMSE} = \frac{samplesize^2}{N} \sum (x_{samp}(i) - x_{dist}(i))^2 \quad (2)$$

where *samplesize* is the range of abscissal values over which the distribution is calculated, N is the number of samples being considered, $x_{samp}(i)$ is the sample at point i, and $x_{dist}(i)$ its corresponding theoretical distribution value.

From these results differences between the distributions are evident. The Nakagami distribution describing the measured results at the test location of site A has a shape parameter of $m = 1.15$, with a MoMSE value of 0.0178, which is close to the Rayleigh value of $m = 1$. This is for a location that is separated from the transmitter by a single partition. The simulated results for this location are described by a Nakagami distribution of shape $m = 2.86$. For the site B data for which the receiver is also separated from the transmitter by a single partition, the results show that the measured data is modelled well by a Nakagami distribution of shape $m = 0.68$ with a MoMSE of 0.0529, while the simulation gives an m value of 1.47.

The data from the two sites exhibit distinct variations in form, those from site B having a greater concentration of received signal amplitudes close to zero. This can be accounted for by the different number of reflectors that are present in the two sites. For site A with only a few reflectors, and a lack of furnishings, only a small number of multipath components are received at the fixed location. This accounts for a small number of low signal components, and fewer multipath signals combining destructively. For site B, however, there are a large number of reflecting objects, both structural walls and office furniture, with the addition of a number of absorbing bodies as personnel move around the site. In this instance, the receiver is subjected to a larger number of multipath signals, with a greater number of low signal contributions as well as more interference from multipath signals.

The simulation results, although not very close to the measured results, do show a similar trend with the value of m being significantly lower for site B than the corresponding value for site A. The simulation results at these sites are based solely on reflections for this comparison, indicating that the shape of the curve is primarily determined by the number of multipath components, and the strength of those components. It can be shown that the summation of a number of multipath components that have equal magnitudes but random phase results in a Rayleigh distribution. However, the simulation results, as do the measured results, indicate that the indoor channel is not well modelled by a Rayleigh distribution, but rather that the strength of the multipath components is crucial in determining the final signal strength distribution. Using the simulation it is possible to extract the signal strengths and time delays of each multipath contribution in the form of a joint probability distribution, and from that information alone be able to regenerate the signal strength distributions[5].

3.2 Effects of Diffraction

The electromagnetic propagation from a transmitter to a receiver in the indoor environment involves not

only reflections of the transmitted wave off surfaces, and the multiple reflections that occur, but also involves diffraction effects off edges in the environment. In order to determine the effects of diffraction on the final channel distribution, the simulation model was reapplied to site B with the effects of diffraction being incorporated. The results of this experiment are shown in figure 5.

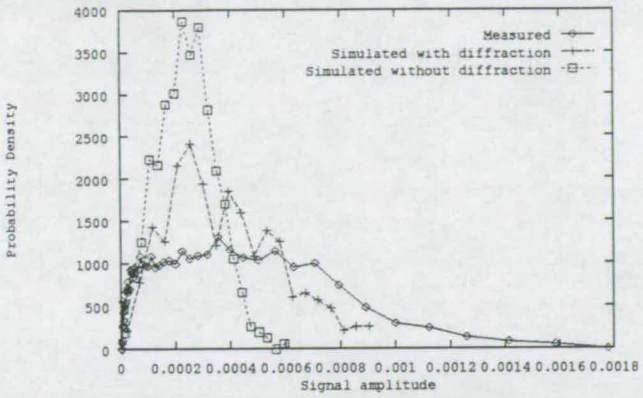

Figure 5: Probability density functions for site B

The Nakagami m parameter that best fits the simulation with diffraction is 0.913 with a MoMSE of 0.050 which is closer to the measured m value of 0.676 than the simulation results that ignore the effects of diffraction. It is therefore clear that diffraction is a significant component of the electromagnetic propagation for the indoor environment.

The differences between the measured and the simulated distributions can be accounted for partly by the modelling simplifications such as ignoring the effects of furniture and personnel moving around the building, and partly by lack of information pertaining to the electromagnetic properties of the construction materials, and the scattering effects of such surfaces. However, with current computing resources it is impractical to include information on furniture, and on scattering for all but the simplest of rooms. The simulated model of site B currently requires 2000 hours of processor time on a transputer based Meiko to calculate the received signal for 500 points on one circular path.

4 Discussion

It is clear that the simulation of the indoor channels, although not being accurate with respect to the measured data, is useful in determining the important characteristics of electromagnetic propagation. In order to obtain a more accurate model of the environment it is necessary to obtain more detailed information regarding the electromagnetic properties of materials used to construct buildings, as well as the effects of surface scattering. Such detailed information is not readily available for these materials, so estimated values for these parameters need to be used.

Increasing the complexity of the simulation model of a particular indoor environment by incorporating more reflecting surfaces, or considering the effects of scattering may be impractical without making simplifications to other aspects of the model. The current simulation environment is reaching the limit of practical system sizes as the execution time increases rapidly when additional propagation mechanisms are incorporated.

Acknowledgements

This work was carried out with the assistance of the Science and Engineering Research Council (UK), the Athlone Vanier Fellowships Scheme administered by the Fellowship of Engineering, the Carleton/Edinburgh exchange programme, and the Royal Society. Special thanks is given to the Mitel Corporation for access to the measured data for site A, and to S. Todd, Professor Mahmoud and the Telecommunications Research Institute of Ontario (TRIO) for access to the measured data for site B. Thanks is also given to the Edinburgh Parallel Computing Centre (EPCC) for the use of a parallel machine.

References

[1] Jospeh B. Keller. Geometrical Theory of Diffraction. *Journal of the Optical Society of America*, 52(2):116–130, February 1962.

[2] Henry R. Reed and Carl M. Russel. *Ultra High Frequency Propagation.* John Wiley & Sons, Inc., 1953.

[3] Stephen R. Todd, Mohammed S. El-Tanany, and Samy A. Mahmoud. Space and Frequency Diversity Measurements of the 1.7GHz Indoor Radio Channel using a Four-Branch Receiver. *IEEE Transactions on Vehicular Technology*, 41(3):312–320, August 1992.

[4] M. Nakagami. The m-Distribution, a general formula of intensity of rapid fading. In W. G. Hoffman, editor, *Statistical Methods in Radio Wave Propagation: Proceedings of a Symposium held at the University of California*, pages 3–36. Permagon Press, 1960.

[5] D. I. Laurenson, S. McLaughlin, and A. U. H. Sheikh. A Ray Tracing Approach to Channel Modelling for the Indoor Environment. In *Proceedings IEEE Vehicular Technology Conference*, May 18-20 1993. Secaucus, NJ.

D. I. Laurenson, S. McLauglin and A. U. H. Sheikh. "The Application of Ray Tracing and the Geometrical Theory of Diffraction to Indoor Channel Modelling", to be published in Proceedings IEEE GLOBECOM '93, November 29–December 2, 1993. Houston, TX, USA.

The Application of Ray Tracing and the Geometrical Theory of Diffraction to Indoor Channel Modelling

D.I. Laurenson S. McLaughlin A.U.H. Sheikh

D.I. Laurenson, postgraduate student, Department of Electrical Engineering, The University of Edinburgh, Scotland. EH9 3JL
S. McLaughlin, research fellow, Department of Electrical Engineering, The University of Edinburgh, Scotland. EH9 3JL
A.U.H. Sheikh, professor, Department of Systems and Computer Engineering, Carleton University, Ottawa, Canada. K1S 5B6

Abstract

Ray tracing and the Geometrical Theory of Diffraction are applied to a simulation of the radio channel experienced by equipment communicating inside buildings. Comparisons are made between the simulated results and electromagnetic measurements through the use of probability distributions fitted to the data. System parameters are determined from the simulation, and used to recreate the channel in a statistical manner, demonstrating that a limited set of information on the channel is sufficient to model the channel.

1 Introduction

Increased demand on the radio spectrum from high bandwidth communicating devices, especially within the indoor environment, has prompted detailed examination of the environments within which these devices operate. The purpose of this examination is to make efficient use of the multipath channel through a better understanding of how the environment affects communication. A more detailed knowledge of the channel leads to the exploitation of the potential bandwidth that has yet to be realised through more efficient calculation of reuse distance for a cellular system, and through the application of signal processing techniques.

A multipath channel such as that encountered in indoor communications is particularly suited to the use of a ray tracing technique which, by its nature, accommodates fading and delay of the multipath components. The model uses the physical construction of the environment to determine the signal experienced by a receiver at any particular point in space. The combined effect of the features in the environment is determined through the use of superposition. A model based solely on ray tracing does not take account of the effects of diffraction around corners in the environment. To extend the model to take account of these effects, the Geometrical Theory of Diffraction (GTD) is incorporated into the model. The effect of this propagation mechanism on the statistical result is determined.

A detailed model of the environment, such as that obtained through the use of ray tracing and the GTD, gives access to channel information that would otherwise be difficult to obtain. Data on the amplitude and arrival times of the multipath components of a signal can most usefully be derived from the model in the form of a joint probability density function. Using this information in conjunction with the number of contributing multipath signals it is possible to regenerate the statistics of a non-Rayleigh channel. This information can be used to find the physical basis for non-Rayleigh and non-Ricean distributions that often occur in channel models. It is found that one particular distribution, the Nakagami distribution, models the indoor environment particularly well. Whilst the physical basis for the Rayleigh and Ricean channels is well understood, the physical basis for the Nakagami model is not. Using the ray tracing model, a more detailed view of the construction of this channel can be obtained, and the causes of the particular characteristics be determined.

The remainder of this paper describes the simulation model that is developed from ray tracing theory and GTD. This model is applied to a simplified layout of a building at Carleton University in Ottawa, and the results are compared with data obtained through physical measurements. Results from this comparison are presented, and conclusions are drawn.

2 Simulation Model

Channel modelling has, in many cases, been performed using a simple tapped delay line with Gaussian tap weights well suited to modelling a Rayleigh channel, or a Ricean channel if non-zero mean weights are used. While this model is suitable for general purpose simulation, a more detailed model may be required for the evaluation of signal processing techniques used to increase the usable channel capacity. The approach taken in this paper is to construct a ray tracing model of the environment.

The ray tracing model constructs the received signal amplitude and phase from superposition of contributions from direct line of sight between the transmitter and receiver, from reflections off walls, and from diffraction around corners of the transmitted signal. A signal may be reflected multiple times and still be a significant contributor, so multiple order reflections of the transmitted and the diffracted electromagnetic signals are considered. The model is constructed from a number of rays defined as vectors that are normal to surfaces of equal field strength. These rays emanate from the receiver and any reflecting or diffracting object. For a simple reflector the normal rules of optics apply; that is the angle of reflection is equal to the angle of incidence. The type of surface determines the power and phase of the reflected signal.

Surfaces can be considered as smooth when the surface irregularities are below a specific height. In general the commonly assumed height is $\frac{\lambda}{8}$, but can be more stringent for rays whose grazing angle is less than $\frac{\pi}{6}$[1]. For purposes of simulation at frequencies around 1GHz it is assumed that the size of irregularities in walls is not sufficiently great to cause a large degree of scattering, so surfaces are treated as perfectly smooth objects.

Associated with each surface in the simulation are a reflection

coefficient and a transmission coefficient. These determine the percentage of a signal that impinges on the surface that is reflected and transmitted respectively. As surfaces are assumed to be infinitely thin, transmitted signals are not subject to the effects of refraction.

Corners within the environment result in diffraction occurring, which can be modelled using the Geometrical Theory of Diffraction [2]. For a right angled corner, as most frequently found in buildings, the diffraction coefficient can be defined by

$$D = -\frac{e^{j\frac{\pi}{4}}}{\sqrt{3}\,(2\pi k)^{\frac{1}{2}}\sin\beta}\left[\left(\frac{1}{2}+\cos\left(\frac{2(\theta-\alpha)}{3}\right)\right)^{-1} \mp \left(\frac{1}{2}+\cos\left(\frac{2(\theta+\alpha+\pi)}{3}\right)\right)^{-1}\right], \quad (1)$$

where α, β, and θ are defined by Figure 1. The diffracted field of an incident ray is a cone of rays emanating from the point of incidence. If α or θ are in the range $-\frac{\pi}{2}$ to $-\pi$ then the diffraction coefficient is defined as being zero. The upper sign is used for the boundary condition that on the edge the field is horizontally polarised, and the lower sign for the vertical polarisation case. In the former case the field described by the equation is the electric field, and in the latter it describes the magnetic field. The resulting diffracted field, u_e, is given by

$$u_e = D u_i r^{\frac{1}{2}} e^{jkr}, \quad (2)$$

where u_i is the incident field, and r is the distance of the observation point from the diffracting edge.

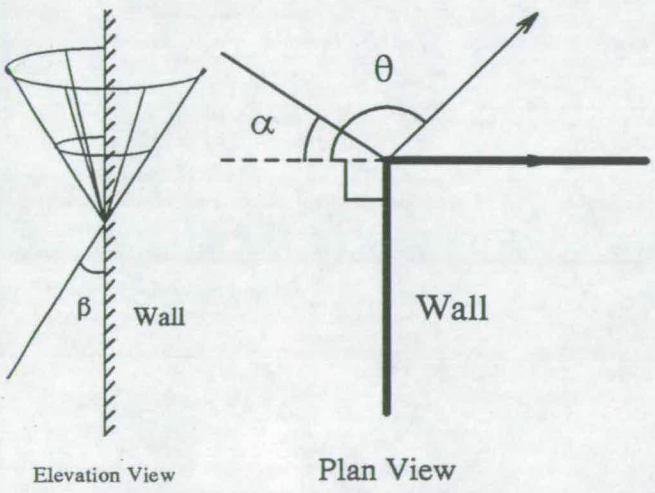

Figure 1: Diffraction around a right angled corner

3 Simulation Results

The simulation model was applied to a representation of one floor of an office complex at Carleton University (Figure 2). The building is 30m×45m in size with plasterboard dividing walls, a concrete floor, and a false ceiling with a corrugated steel roof. A number of measurements were made at this site by Todd *et al.* [3]. The experimental measurements were made at a centre frequency of 1.75GHz using a transmitter mounted on a wooden frame that allowed the transmitter to move through a circular path of radius 15.9cm (0.9λ) at a fixed height of 1.6m. The receiver was located at a central position in the building, and measurements made for various transmitter locations.

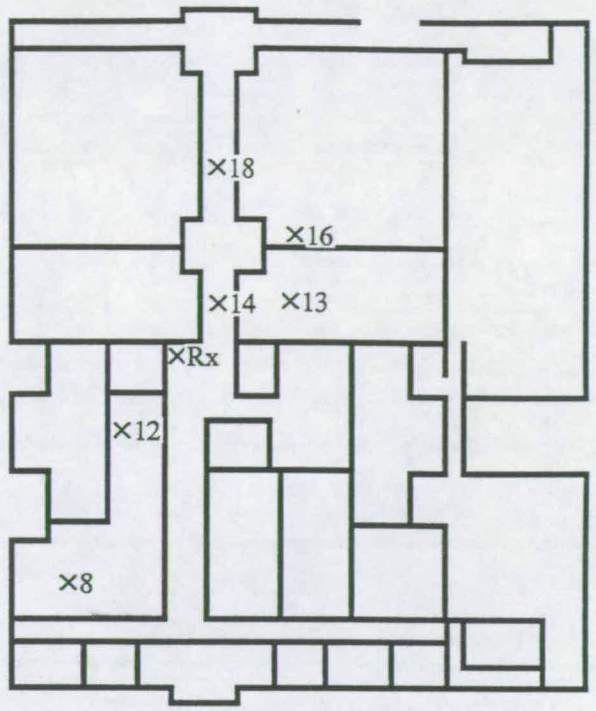

Figure 2: Schematic of Carleton University annex

A subset of the measurement experiments were repeated using the simulator with the transmitter and receiver locations indicated on the diagram. The path that the transmitter is moved through is simulated with measurements made at various positions. In the simulation, no account is taken of people moving, or of other changes to the environment. The received signal is combined with additive white Gaussian noise (AWGN) to simulate the effects of thermal noise at the receiving antenna. All powers are calculated with reference to the transmission power.

For the transmitter site number 8, Figure 3 shows the probability density function (pdf) of signal amplitude received at the central location with reference to a 0dB transmitter power. The transmitter is located in a classroom populated with desks and chairs. The area of the room closest to the receiver site is partitioned off from the remainder of the room and used as an office. The partition is constructed out of metallic lockers and a cloth blind. The figure shows the results of the physical measurements made at this site as well as the simulated results for the same location. The simulated data is given in the form of two sets of points; one which ignores the effects of the diffraction propagation mechanism, and the second which takes this into account.

The figure shows that the simulation results are almost identical, whether or not the effects of diffraction are included in the model. This would indicate that diffraction may not be a significant propagation mechanism for indoor communications. In order to examine this information in more detail, the three curves were

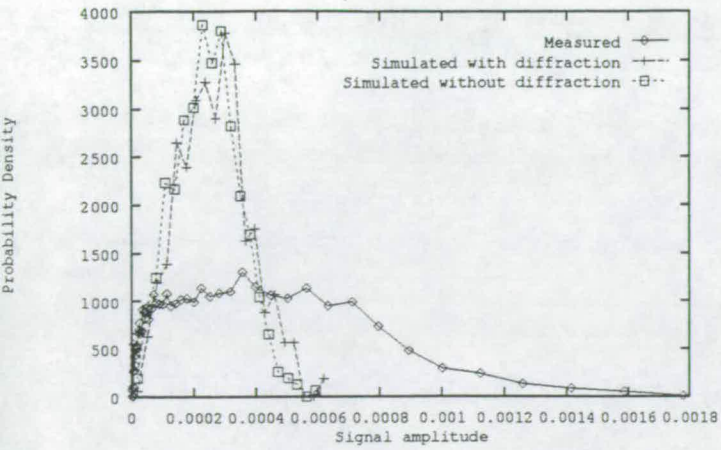

Figure 3: Probability Density Functions for site 8

fitted to a Nakagami distribution that is known to model indoor channels well. The Nakagami distribution[4] is defined by

$$p(x) = \frac{2m^m x^{2m-1}}{\Gamma(m)\Omega^m} \exp\left(-\frac{m}{\Omega}x^2\right). \quad (3)$$

The mean and variance are given by $\overline{X} = \frac{\Gamma(m+\frac{1}{2})}{\Gamma(m)}\left(\frac{\Omega}{m}\right)^{\frac{1}{2}}$ and $\overline{X^2} = \frac{\Gamma(m+1)}{\Gamma(m)}\left(\frac{\Omega}{m}\right)$ respectively. Table 1 shows the results of this comparison. It can be seen that the values of m, the shape parameter of the Nakagami distribution, for the simulations are close, and that the value for the simulation incorporating diffraction is marginally further away from the measured case than when diffraction is not incorporated into the model. The Ω parameter of the distribution is directly related to the variance of the distribution. The Modified Mean Square Error (MoMSE) of the fitting of the distribution is displayed in the final column. It is a measure of the fit of a theoretical distribution with measured or simulated data. It is normalised to be independent of the area over which the distribution is fitted. It is calculated as

$$\text{MoMSE} = \frac{samplesize^2}{N}\sum\left(x_{samp}(i) - x_{dist}(i)\right)^2 \quad (4)$$

where $x_{samp}(i)$ is the sample at point i, and $x_{dist}(i)$ is the corresponding value of the distribution being fitted to the data. N is the number of samples being used, and $samplesize$ is the range of abscissal values over which the distribution is calculated. Using this method errors can be compared between different distributions, and different samples with different mean values.

The difference in the distributions can be partly accounted for by the simplifications required by the model to make the computation tractable, and partly from the lack of information concerning the electromagnetic characteristics of the building materials used. The simulation results consistently show lower measures of signal amplitude than expected. The likely cause of this is an underestimation of the coefficients of reflection and transmission. With more detailed information on the building materials it is hoped that results that are closer to the absolute measures can be obtained. Unfortunately very little information relating to this topic is available in the literature. Information

	m	Ω	MoMSE
Measured data	0.676	3.880×10^{-7}	0.0529
Simulated with diffraction	1.509	8.959×10^{-8}	0.0457
Simulated without diffraction	1.492	7.721×10^{-8}	0.0273

Table 1: Fit of Nakagami distribution to site 8 results

on the electrical characteristics of concrete can be found in [5] and [6], however this information is collected for the purpose of non-destructive testing, and is only available for a limited frequency range. The office environment contains a multiplicity of construction material types many of which have not been characterised for their electromagnetic properties, and so these values are not available in the literature.

Other simplifications that may contribute to the difference between the measured results and the simulated values include the effects of scattering from surfaces. The simulation used assumes that scattering is not a significant mode of propagation, however this assumption may, in the light of the results, be invalid. A second source of difference between the simulated and measured results is a determination of the thermal noise power that is seen by the reciever. The simulation fixes this at -80dB, and uses this as a threshold for determining significant contributions to the overall received signal. Any contribution that has a power level lower than -80dB is deemed to be below the noise floor, and therefore does not contribute significantly to the received signal. These signals then take no further part in the model and act as the terminating cases where the signal reaches the receiever after multiple reflections.

The data sets from the above computations were normalised to have the same average signal amplitude. The results of fitting a Nakagami distribution to the curves is shown in Table 2. The shape parameter, m, is identical to the non-normalised case demonstrating the insensitivity of m to the average power of the data. In Figure 4 the similarity of the three results can be seen, along with the best fit Nakagami curve for the measured data. From the figure, the similarity and differences in shape of distribution between the simulation and the measured results can be seen clearly. The measured results have more energy concentrated at low signal amplitudes than the simulated results.

	m	Ω	MoMSE
Measured data	0.676	1.3976	0.0529
Simulated with Diffraction	1.509	1.2474	0.0457
Simulated without Diffraction	1.492	1.2969	0.0273

Table 2: Fit of Nakagami distribution to normalised data

The same experiment was repeated with receiver location 13, the results being shown in Figure 5 and Table 3. This location is a study office that contains a number of soft partitions to isolate desks from each other. The transmitter is located at an

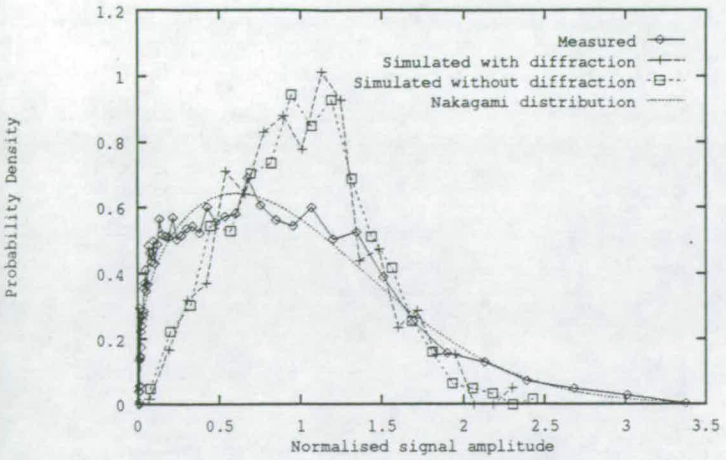

Figure 4: Normalised distributions for site 8

open area near to the door. Again it is seen that the simulations are insensitive to diffraction although the best fitting m values are different between the simulated distributions. One possible explanation for the apparent insignificance of diffraction is that it is a mode of propagation that causes the field incident on the edge to expand. This expansion causes the effects of the diffraction to be significant only at small distances from the diffracting edge.

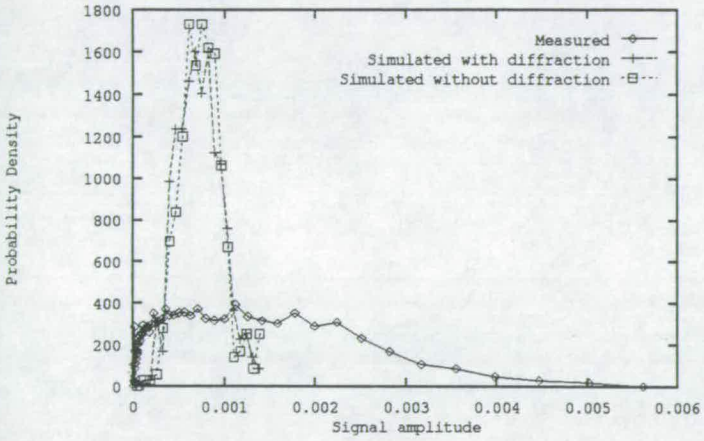

Figure 5: Probability Density Functions for site 13

	m	Ω	MoMSE
Measured data	0.653	3.959×10^{-6}	0.0693
Simulated with diffraction	2.285	5.902×10^{-7}	0.0277
Simulated without diffraction	3.006	6.083×10^{-7}	0.0333

Table 3: Fit of Nakagami distribution to site 13 results

A summary of the comparison between the measured and simulated results for all of the locations is given in Table 4. The table shows that the simulated results obtained for sites 14 and 18 in particular have shape and mean values that vary considerably from the measured results. Neither site is located such that diffraction plays an important role as a primary source of received signal. This would indicate that the coefficients for transmission and in particular for reflection that have been chosen are too low. This can be deduced from the data given as the reflection coefficient that is involved in the propagation of a diffracted ray to site 14 is critical in calculating the received power. The simulation results for sites 8 and 16 where power is mainly from transmitted rays and diffracted rays the results are closer to the measured results. The simulation results for site 12 are significantly different from the measured results. In addition to the lack of information on transmissivity and reflectivity of the building structure, one possible source of error is the effect of the metallic locker structure that partitions the room into two. The reflection and transmission characteristics of this locker are unknown.

(m,Ω)	Measured	Simulated
Site 8	$(0.676,3.88 \times 10^{-7})$	$(1.509,1.25 \times 10^{-7})$
Site 12	$(0.636,2.59 \times 10^{-5})$	$(2.450,1.73 \times 10^{-6})$
Site 13	$(0.653,3.96 \times 10^{-6})$	$(2.285,5.90 \times 10^{-7})$
Site 14	$(0.628,8.27 \times 10^{-5})$	$(1.242,1.89 \times 10^{-6})$
Site 16	$(0.664,2.39 \times 10^{-6})$	$(1.043,6.16 \times 10^{-8})$
Site 18	$(0.665,4.19 \times 10^{-6})$	$(1.844,3.00 \times 10^{-7})$

Table 4: Comparison of parameters for all sites

In order to achieve a better match between the measured results and the simulated results more information needs to be incorporated into the model. Such additional information includes the layout and composition of furnishings in each room, and the types of surfaces that are encountered. The latter is particularly important for higher frequency propagation where surface features become significant scatterers. However, incorporating such information into a simulation model increases complexity of the model. The simulation that has been conducted for the Carleton University building requires an hour of computation time on a transputer to calculate the received signal at one receiver position. A typical run of 500 positions is not uncommon, such simulations being performed on a parallel machine running the simulation on 50 processors simultaneously. Thus increasing the complexity of the model much further makes the computation no longer feasible.

Multipath signals can be characterised by their signal amplitude and the delay with which they arrive. In a simulation environment, the delays and amplitudes of each multipath signal can be resolved exactly. This information can be represented as a joint probability distribution of power and delay. For a continous distribution the probability function, $P_J(a,d)$ satisfies

$$0 \leq P_J(a,d) \leq 1, \quad \forall a,d \in \mathbb{R} \tag{5}$$

and

$$\int\int P_J(a,d)\, da\, dd = 1\,, \tag{6}$$

where a is the amplitude and d is the delay of a multipath signal. For a discrete representation of P_J,

$$\sum_{i=0}^{M}\sum_{j=0}^{N} P_J(i,j) = 1. \quad (7)$$

The simulator was used to construct a joint probability distribution of this form for transmitter site 13. Amplitude information is modified by removing the free-space loss, however this information is also present in the delay characteristic of the multipath component. A three dimensional plot of this probability function is shown in Figure 6. Using this probability function, and information on the number of multipath components that are significant at the receiver, the results of the ray-tracing simulation can be recreated with reasonable conformance from this restricted set of information. The results of this experiment are shown in Figure 7 This indicates that the amplitude and delay information on the multipath components is sufficient to reconstruct a channel, and therefore contains the necessary information for characterising a channel.

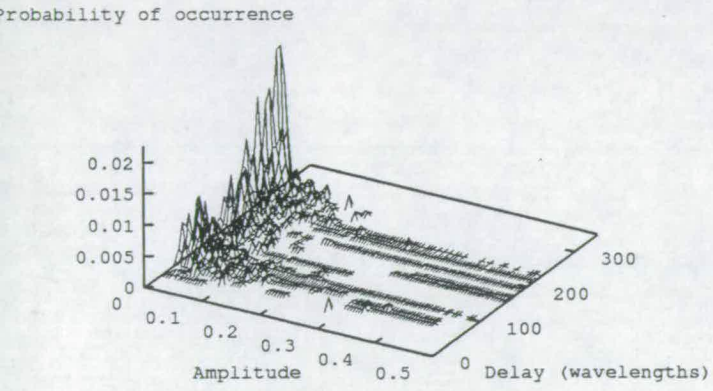

Figure 6: Joint probability function for site 13

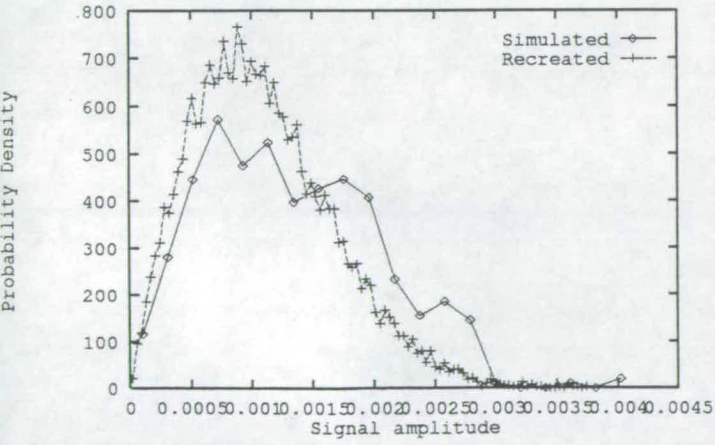

Figure 7: Simulated and Recreated pdfs

4 Conclusions

A ray tracing simulator based on the physical construction of the environment has been shown to be a useful tool in gaining an understanding of a communications environment. The comparison between measured and simulated results has shown that more detailed information is required on the electromagnetic characteristics of the construction materials used. In order to use a similar simulation environment to characterise a particular building, a large amount of information is required, and a very large computation resource to handle the complexity. A ray tracing model can be used to characterise types of buildings and building structures on a small scale, the information being useful in characterising the layout of a building with respect to efficient radio communication.

Acknowledgements

This work was carried out with the assistance of the Science and Engineering Research Council (UK), the Athlone Vanier Fellowships Scheme administered by the Fellowship of Engineering, the Carleton/Edinburgh exchange programme, and the Royal Society. Special thanks is given to S. Todd, Professor Mahmoud and the Telecommunications Research Institute of Ontario (TRIO) for access to the measured data. Thanks is also given to the Edinburgh Parallel Computing Centre (EPCC) for the use of a parallel machine.

References

[1] Henry R. Reed and Carl M. Russel. *Ultra High Frequency Propagation*. John Wiley & Sons, Inc., 1953.

[2] Jospeh B. Keller. Geometrical Theory of Diffraction. *Journal of the Optical Society of America*, 52(2):116–130, February 1962.

[3] Stephen R. Todd, Mohammed S. El-Tanany, and Samy A. Mahmoud. Space and Frequency Diversity Measurements of the 1.7GHz Indoor Radio Channel using a Four-Branch Receiver. *IEEE Transactions on Vehicular Technology*, 41(3):312–320, August 1992.

[4] M. Nakagami. The m-Distribution, a general formula of intensity of rapid fading. In W. G. Hoffman, editor, *Statistical Methods in Radio Wave Propagation: Proceedings of a Symposium held at the University of California*, pages 3–36. Permagon Press, 1960.

[5] John G. Wilson. *The Electrical Properties of Concrete*. PhD thesis, The University of Edinburgh, Edinburgh, Scotland, 1986. Ph.D. Thesis.

[6] J. G. Wilson and H. W. Whittington. Variations in the electrical properties of concrete with change in frequency. *IEE Proceedings*, 137, Part A(5):246–254, September 1990.